



DISSERTATION

Titel der Dissertation

QCM Sensors for Safety Applications: Artificial
Recognition Materials from Nanoparticles to Mo-
lecularly Imprinted Polymers targeting VOC, For-
maldehyde and Ephedrine

Verfasserin

Mag. Kira Kotova

angestrebter akademischer Grad

Doktorin der Naturwissenschaften (Dr. rer.nat.)

Wien, 2013

Studienkennzahl lt. Studienblatt: A >791 419<

Dissertationsgebiet lt. Studienblatt: Chemie

Betreuerin / Betreuer: Univ.-Prof. Dr. Peter Lieberzeit

Preface

This work has been done in the group of Chemical Sensors and Rapid Analysis from March 2010 until December 2013 under the supervision of Univ. Prof. Dr. Peter A. Lieberzeit at the Department of Analytical Chemistry, University of Vienna, Währinger Strasse 38, 1090 Vienna, Austria.

Dedicated To My Parents

Acknowledgements

First, I am grateful to my research supervisor Univ. Prof. Dr. Peter A. Lieberzeit for his help and patience. Also I am thankful for the opportunity to work in this group and to gain insight into molecular imprinting and sensors. Furthermore his care extended also to problems beyond scientific questions if necessary.

Very importantly, I thank my fellow colleagues for their kindness and their support during experimental problems, especially Dr. Ghulam Mustafa and Dr. Munawar Hussain.

Also I want to express my gratitude towards my parents for their love, sacrifices and support: especially my mother for motivating me wisely during all my education and for her willingness to give me absolute freedom in my choices. Also I am thankful to my uncle Sergey Afanasiev and his mother Zinaida, who always believed in me. Finally, I am indebted to my friends from Vienna, who helped me a lot during settling here and thus made my stay in Vienna possible.

Last, but not least, I also thank the European Commission for their financial support within two projects, namely FP6-IP-NMP3-CT-2007-026549 (Nanosecure) and FP7-NMP-2010-LARGE-4-263382 (Photosens).

Table of contents

Preface	1
Table of contents	4
1. Introduction	6
1.1 Chemical Sensors.....	6
1.2 Main Components of Chemical Sensors.....	7
1.3 Important Features of Chemical Sensors.....	8
1.4 Mass-sensitive Sensors	10
1.4.1 Quartz Crystal Microbalance (QCM)	11
1.4.2 Operational principle of the QCM.....	12
1.4.3 Receptor Layers.....	15
1.4.4 Molecular Imprinting.....	16
2. Titania and silica nanoparticles and their composites for gas sensing.....	21
2.1 Introduction	21
2.2 Experimental	23
2.2.1 Materials	23
2.2.2 Preparation of QCM and Coating.....	24
Sieves	24
2.2.3 Synthesis of nanoparticles	27
TiO ₂ NPs.....	27
SiO ₂ NPs.....	27
2.2.4 Synthesis of molecularly imprinted polyurethane	28
2.2.5 Atomic Force Microscopy (AFM).....	29
2.2.6 Coating	30
2.2.7 Apparatus	31
2.3 Results and Discussion.....	33
2.3.1 Nanoparticle Characterization.....	33
TiO ₂ Selectivity	46
Molecularly imprinted polyurethane	47
MIP selectivity	50
PUR+TiO ₂ Nanocomposite material.....	51
PUR (non-imprinted) +TiO ₂ Nanocomposite material	53
SiO ₂ NPs	55
3 Formaldehyde Sensing with MIP Nanoparticles	59
3.1 Introduction	59
3.1.1 Toxicity.....	61
3.1.2 Formaldehyde Sensing: few examples	62
3.2 Experimental	65
3.2.1 Materials	65
3.2.2 Synthesis of Molecularly Imprinted Polymer	65
3.2.3 Optimization of formalin measurements.....	66

3.3 Results and Discussion.....	70
3.3.1 Nanoparticle Characterization.....	70
3.3.2 Mass sensitive measurements.....	70
Polymer thin film	70
Nanoparticles	72
4. Ephedrine MIP	77
4.1 Introduction	77
4.2 Experimental strategies and polymer screening	82
4.2.1 Materials	82
4.2.2. Selection of polymer system and optimization	83
4.2.3 FT-IR Screening.....	87
Template removal	88
Result.....	88
Re-inclusion	88
Result.....	89
4.2.4 Synthesis of the final ephedrine MIP for sensor coatings.	89
4.2.5 Synthesis of MIP nanoparticle and coatings	90
4.2.6 Nanoparticles Characterization	91
Results.....	92
4.2.7 Sensing Apparatus.....	92
4.2.8 QCM Sensor results and Discussion	93
Polymer films	93
Nanoparticles	96
Nanoparticles: selectivity	99
Preliminary tests in a real-life matrix	102
4.2.9 Conclusion	104
Abstract (English)	106
Zusammenfassung (Deutsch).....	108
Literature List	110
Curriculum Vitae	120

1. Introduction

This thesis explores a range of recognition strategies for sensors that aim at detecting safety-related analytes both in gas phase and in liquid phase that have the potential for mass manufacturing. First of all, they include exploiting the interaction properties of oxide nanoparticles as affinity materials for interacting with volatile organic compounds (VOC) as well as carrying that approach further to design composite materials for these analytes consisting of a molecularly imprinted polymer and such nanoparticles.

Furthermore, the thesis also deals with developing molecularly imprinted polymers (MIP) for sensing safety-related analytes in both gas and liquid phase. The analytes in these parts are formaldehyde – an indoor pollutant - as well as ephedrine. Most measurements are based on quartz crystal microbalances (QCM) as the transducer. Such a sensor strategy requires a multidisciplinary approach including analytical chemistry, polymer chemistry, measuring sciences and electronics.

This introductory chapter gives a brief overview of the recent history of chemical sensors, their development and characteristics.

1.1 Chemical Sensors

It is becoming more and more difficult to ignore the essential role of chemical sensors in modern life, which increasingly demands from us on-site and instantaneous methods of analysis. [1] Some examples for this are the needs for analytical tools to e.g. continuously control the degree of water and air pollution or to avoid related health issues. [2] They can also be an essential part of industrial processes. Compared to other analytical instruments they are usually small and can be used for remote measurements. [3] Such systems have to be easy to transport to the place of analysis, i.e. they have to be robust, accurate and inexpensive. Also they should be straight-

forward to operate and should not demand highly trained staff. [4] Because of their dimensions, several chemical sensors can inherently be combined to one multi-analysis-device. Although vast numbers of chemical sensors have been discovered and are continuously being published, still only a limited number are robust enough for harsh real-life conditions.[5] These rare examples of such application are presented in sensing of yeast cells [6], bacteria [7], viruses [8], pesticides such as atrazine [9, 10] or monitoring engine oil degradation. [11, 12]

Looking into history, the glass electrode developed by F. Haber and Z. Klemensiewicz in Germany in the beginning of the 20th century [13] can be regarded as the starting point for designing chemical sensors in general and ion-selective electrodes (ISE) in special. This system is still in use for pH-measurements routinely and worldwide.

There are many definitions of sensors depending on their respective construction and purpose of use. The probably most general one is the one by IUPAC which reads: “A chemical sensor is a device that transforms chemical information, ranging from the concentration of a specific sample component to total composition analysis, into an analytically useful signal.”[14] Generally speaking sensors can be classified into two main categories: physical sensors which record physical parameters and chemical sensors that detect chemical phenomena.

1.2 Main Components of Chemical Sensors

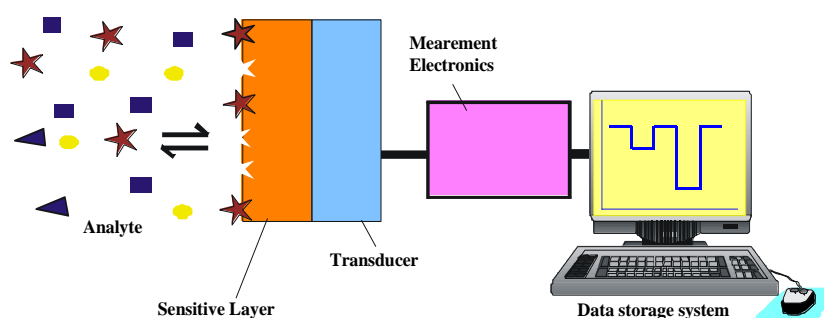


Figure 1 Schematic setup of Chemical Sensor

A chemical sensor usually consists of three basic components as demonstrated in **Figure 1**. The arrangement usually consists of sensitive layer, transducer and electronics. [15] The sensitive layer or molecular (analyte) recognition system is responsible for selectivity and also sensitivity of the sensor; the layer must be able to interact highly selectively with the analyte of interest in the presence of other species. [16, 17] When considering an ideal sensor, its layer should not interact with any species but the target analyte. The nature of this process varies: for example, if the analyte is a bacteria species, it is recognized on the basis of its size and shape. However, also the exact surface chemistry plays an important role. In this case and also if the sensor addresses molecules, it requires recognition equilibrium depending on the shape and functionality of the respective target species. Also the fact where the process takes place (confined to the surface of the respective recognition layer or also within in the entire matrix of the layer) plays a relevant role. Generally speaking chemical sensors have to fulfil the same standards as any other analytical technique. However, a few additional features have to be taken into account, which will be summarized in the following section.

1.3 Important Features of Chemical Sensors

Basically, chemical sensors have to fulfil the standards of chemical analysis. However, their potential applications and the necessity to keep them simple in usability also bring some additional aspects into focus. This section summarizes these main requirements towards a good chemical sensor:

First of all, **selectivity** is the ability of a sensor to yield a signal in the presence of the target analyte and to “ignore” other molecules even when they have a similar structure. Selectivity is of course – not exclusively – introduced by the respective receptor layer. The selectivity factors in sensing generally have to be rather high: whereas e.g. in chromatography a column

can offer tens or even hundreds of thousands of theoretical plates, a sensor system relies on a single equilibrium state between the receptor and its surroundings.

Sensitivity describes the magnitude of the sensor response towards a given analyte concentration in liquid media or in gas phase. Sensitivity depends on many parameters of the system, such as the transducer, the receptor, design of the cell, density and temperature of the media etc. [18] The sensitivity of quartz crystal microbalances (QCM) first of all depends on the respective fundamental frequency.

Noise is closely related to sensitivity. In the case of QCM it is e.g. directly related to damping (impedance of the device) and therefore to the electronic quality of the system. At low analyte concentrations the noise can of course exceed the sensor response.

Reversibility describes the ability of the sensor to return to its initial state, i.e. fundamental frequency in the case of QCM, after contact with the analyte when the latter is removed from the sensing environment. If the analyte remains bound in the matrix of the receptor material, it means that the sensor is not reversible and hence rather a dosimeter than a sensor. Especially if long-term remote operation of a sensor system is required, reversibility is of utmost importance.

Finally, also **ruggedness** is an essential characteristic for chemical sensors, [19] and especially for mass sensors in liquid phase. This refers to tolerating different experimental conditions: Ideal sensors perform constantly when exposed to pressure and vibration, temperature, humidity and viscosity changes.

Reversibility, sensitivity and selectivity are often related to one another: the more sensitive and the more selective a sensor, the less reversible it is on an average.

1.4 Mass-sensitive Sensors

The simple fact that every analyte has a mass can be exploited for chemical sensing by so-called mass-sensitive or acoustic devices. This is an especially intriguing approach, because mass of course is one of the most fundamental material properties.

Selectivity in mass-sensitive sensors is equilibrium-based. This type of sensors finds its application in numerous sensing situations, such as sensing of biological and chemical species, also because they are especially suitable for detecting neutral species. The second large class of sensors relies on kinetic selectivity. The most well-known class is enzyme-based sensors. [20, 21]

Acoustic sensors usually are based on the piezoelectric effect, which was discovered by Pierre and Jacques Curie in 1880 [22] and occurs in a range of crystalline materials, such as quartz. Basically, it says that in piezoelectric materials any deformation will cause charge separation on the surfaces of the crystal and vice versa. Quartz is the most frequently used piezoelectric material due to low cost and ruggedness. However, also other matrices such as e.g. lithium niobate or barium titanate are used for sensor purposes. Generally speaking, there are two mainly different types of mass-sensitive resonators: bulk acoustic wave and surface acoustic wave devices. Surface acoustic wave devices – which have not been used during the experiments in this thesis - in principle consist of a piezoelectric substrate onto which interdigitated microelectrode patterns are deposited. Known in electronics as narrow bandwidth frequency filters, they are applied in chemical sensing for detecting a wide variety of analytes with very appreciable sensitivity.[23] However, focusing on the topics within this work, only bulk acoustic wave devices will be discussed in more detail here. Quartz Crystal Microbalances (QCM) – sometimes also referred to as Thickness Shear Mode (TSM) resonators - is the most frequent example for a bulk acoustic wave device. They

represent the “transducer backbone” of this thesis and hence shall be discussed in some more detail.

1.4.1 Quartz Crystal Microbalance (QCM)



Figure 2 Image of a 10 MHz quartz crystal microbalance as applied in this thesis

Quartz Crystal Microbalances are small, robust, sensitive and comparably straightforward devices.^[24] **Figure 2** shows a typical QCM applied within this thesis. It consists of a thin, AT-cut, quartz plate with 15.5mm in diameter. The AT cut is characterized by a cutting angle of roughly 35 degrees with respect to the crystallographic asymmetry axis and leads to devices that show minimum temperature effects at around room temperature.

It is patterned on both faces with circular metal electrodes. Frequently used metals for this purpose are gold and aluminum (although Al is hardly used in chemical sensing due to its higher reactivity compared to gold). The exact electrode geometry depends on the analyte of interest and the sensing medium. If the device is to be operated in aqueous solution, the following

setup has proven optimal: on the side facing the liquid, the electrodes are larger in diameter than on the opposite side to avoid undesired conductivity effects, and they sometimes are connected. As during measurements in liquid phase the electrodes facing towards the solution are usually grounded, this apparent short circuit does not lead to any problems. When sensing in gas phase, the electrodes are not connected and all have the same diameter.

1.4.2 Operational principle of the QCM

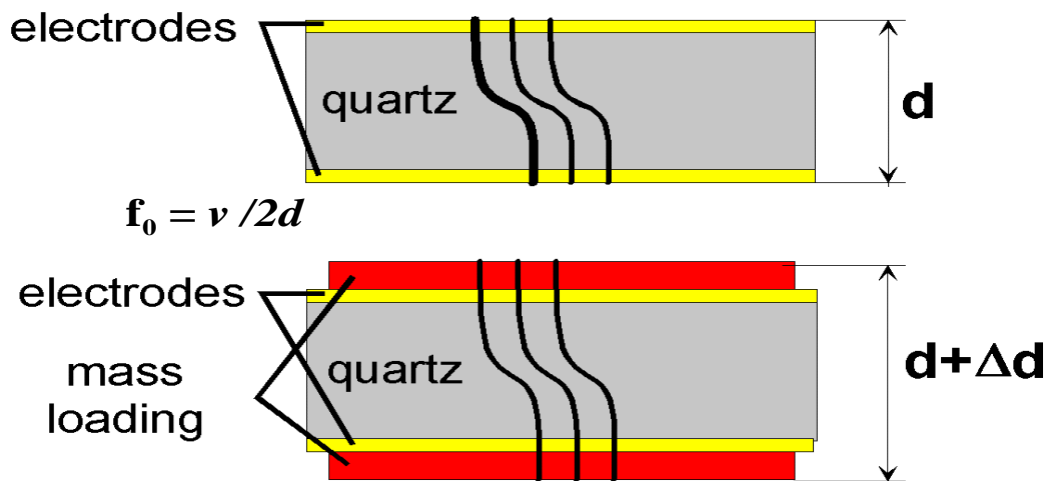


Figure 3 QCM principle

Figure 3 shows the side view of a QCM with the two electrodes on the top and the bottom. Following the inverse piezo effect, applying voltage to the electrodes in this case leads to shear motion of the two faces against one another. The concrete way of deformation of course depends on the cut, so AT cuts show this type of motion. When changing to an alternating voltage, the two faces will of course start to oscillate against one another. For physical reasons a resonance phenomenon occurs when half a wavelength

of the excitation voltage fits between the two electrodes. QCM used during this thesis – 168µm thick – lead to a frequency of 10 MHz. When operating on the fundamental frequency (and thus not on one of the higher harmonics) typical frequencies are in the range of 5-30 MHz. Above that frequency, devices become too thin to be mechanically stable. Therefore at the resonance frequency the device transforms electrical energy into mechanical one (almost) without resistance. However these facts do not yet explain the mass sensitivity of the device. This gap has been bridged by G. Sauerbrey in 1959 with his groundbreaking article on QCM responses in gas phase. He established the equation now bearing his name to describe the behavior of quartz oscillators when exposed to volatile compounds in their respective surroundings that can adsorb on the electrode surface. He observed that such adsorption shifts the frequency of the device towards lower values. The Sauerbrey equation [25] in its Initial form is given in Eq. 1:

$$\Delta f = -f_o^2 \frac{2}{A_{cr} (\rho_m C_q)^{1/2}} \Delta m \quad (1)$$

where

Δf - Frequency change (Hz)

Δm - mass change (g)

ρ_m - the chemical film density

C_q - the quartz crystal shear modulus

f_o - the crystal fundamental resonance frequency (Hz)

A_{cr} - piezoelectrically active crystal area (electrode area, cm²)

The Sauerbrey equation thus quantifies the dependency of the frequency change from the mass change on the electrode, taking into consideration material parameters such as the quartz crystal shear modulus, the density of the film, the fundamental resonance frequency and the electrode area. Furthermore, it assumes that the increasing mass change resulting from the deposited material is considered a part of the initial quartz plate. The second essential assumption is that the deposited film is ideally rigid.

Obviously, the frequency change Δf depends on the mass change Δm , caused by analyte molecules absorbed from the gas phase by the sensing material or directly onto the electrodes. Furthermore, it also depends on the fundamental frequency of the device in a quadratic manner. This explains why higher frequencies are desirable: sensitivity increases by the second power, system noise only by the first. Hence better limits of detection (LoD) can be reached with higher frequencies. This is of course counteracted by the reduced mechanical stability of thinner devices. The Sauerbrey equation of course does not take into consideration any selectivity: the devices as such react to any compound adsorbed. The task of chemistry is to provide suitable recognition materials on the respective surface to achieve the desired sensor properties.

In the early days of mass-sensitive QCM sensing liquid phase measurements were believed difficult. In addition to the effects in gas phase, the viscosity of the surrounding liquid was believed to strongly damp QCM oscillation. When operating QCM in liquid phase, not only mass adsorption onto the electrode faces plays an important role, but also parameters of the liquid medium, mainly density and viscosity. Kanazawa and Gordon [26] therefore expanded the original Sauerbrey equation to account for the properties of the liquid phase. Hence, the outcome looks somewhat more complex than for gas phase:

$$\Delta f = -f_o^2 \frac{2}{(\rho_m C_q)^{1/2}} \sqrt{\frac{\rho_l \eta_l}{4\pi f_o}} \quad (2)$$

where

Δf - Frequency change (Hz)

ρ_m - the chemical film density

C_q - the quartz crystal shear modulus

f_o - the crystal fundamental resonance frequency (Hz)

ρ_l - liquid density

η_l - liquid viscosity

1.4.3 Receptor Layers

Being surrounded by numerous biological and chemical species, living organisms have to cope with them. This would not be possible without high sensing abilities, based on shape and functionality recognition, created by nature. Here antibodies should be mentioned as perfect bio-recognition material (species). Antibodies are serum proteins produced by the immune system that are highly selective towards exactly defined antigens. They have in principle defensive function, detecting viruses and other foreign species. Playing such essential role in living organisms, antibodies and fragments of antibodies can also be applied as sensitive materials in artificial systems, leading to so-called biosensors, or immunosensors. One such application is e.g. a pregnancy home test [27], detecting HCG (human chorionic gonadotropin) hormone in urine. Applying antibody fragments can be useful when smaller size of the recognition material is desired that nonetheless preserves the original bio-activity.

Although the use of biological species, namely antibodies and enzymes, has yielded very good results, novel sensor surfaces implied designing fully artificial sensitive materials by mimicking the concept of biological shape recognition. In this way chemists took their inspiration from nature and combined it with synthesis strategies to replace bio-species. This gave birth to new approaches, such as self-assembled monolayers and molecularly imprinted polymers (MIP). One example for the former is depicted in **Figure 4** showing immobilizing N-acetyl glucosamine on a transducer surface followed by binding of WGA lectin onto this immobilized ligand, [28] which is a beautiful example of how such effects can even be visualized by modern analytical imaging techniques.

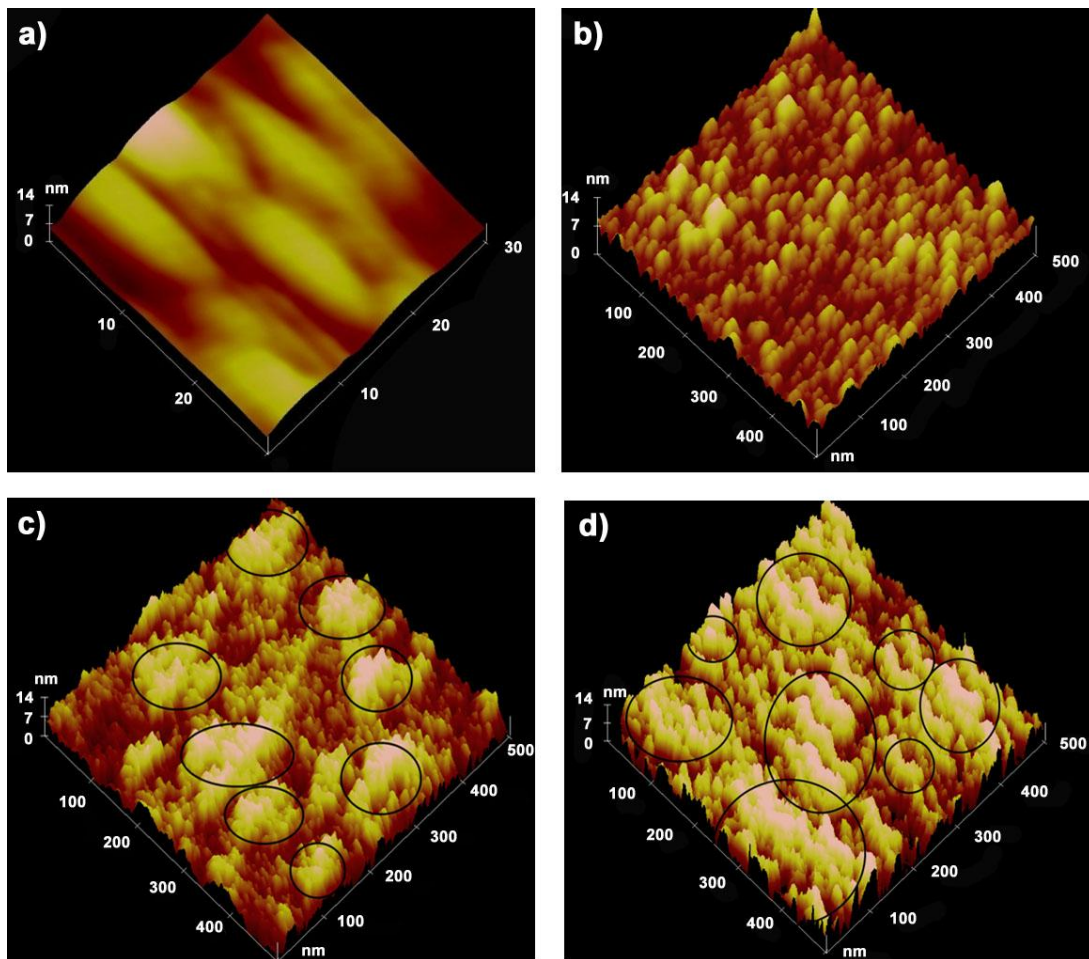


Figure 4 Scanning tunneling microscopy images of **a** gold (30 nm*30 nm), **b** immobilized ligand selfassembled monolayer (SAM) (500 nm*500 nm), **c** ligand SAM (500 nm*500 nm) surface exposed to 10 µg/ml wheat germ agglutinin (WGA), and **d** ligand SAM (500 nm*500 nm) surface exposed to 80 µg/ml WGA. Voltage bias 500 mV, current setpoint at 67 pA. Some parts with bound WGA are marked with dark circles. © Springer Verlag, reproduced with permission from [28]

1.4.4 Molecular Imprinting

The initial concept of MIP came from observing naturally occurring receptors, for example highly selective enzymes.[29, 30] The challenging task for material scientists has been to reveal the principle of bio-recognition and to adopt this strategy to artificial materials, which have their own numerous

advantageous characteristics over natural matrices, namely e.g. robustness, ruggedness, thermal stability, low cost among others. [31]

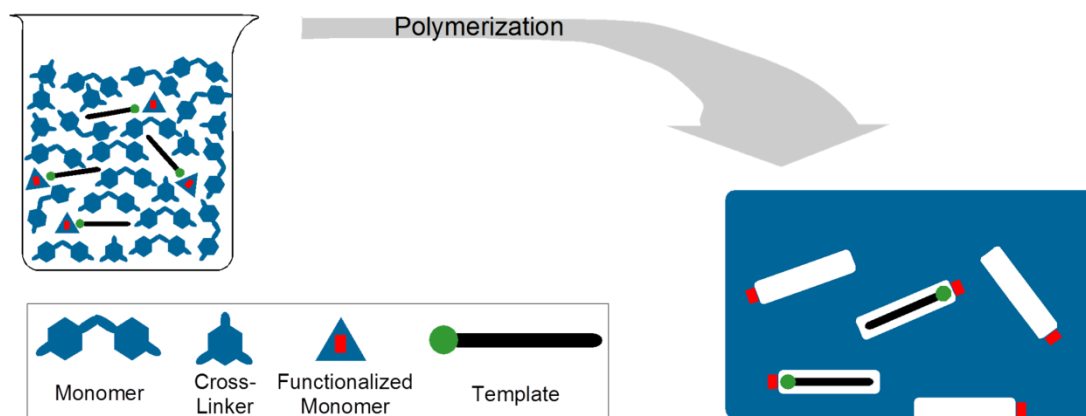


Figure 5 MIP preparation

Molecular Imprinting generates highly selective membranes for chemical sensors based on macromolecular matrices. Molecularly imprinted polymers and nanoparticles in combination with mass-sensitive transducers result in sensors, which can be easily miniaturized. One of the essential advantages of the MIP technique is that the analyte for MIP does not have to be a pure compound: imprinting is also possible with substance mixtures. Also the structure of the analyte does not necessarily have to be known. [32]

Molecular Imprinting consists of three steps: preparing the template - monomer complex or adduct, polymerization and removing of template molecules. The procedure of preparing MIP polymer is presented in **Figure 5**. Generally speaking, there are two main strategies in Molecular Imprinting, namely covalent and non-covalent imprinting.

The covalent approach was first reported by G. Wulff [33] and requires a covalent bond between the template and the functional monomer before polymerization (**Figure 6**). In order to remove the template molecule from the polymeric matrix, this initial covalent bond needs to be broken: if

there is a chemical way to do so, it is therefore possible to extract the analyte and to form highly selective cavities within the polymer matrix. [34]

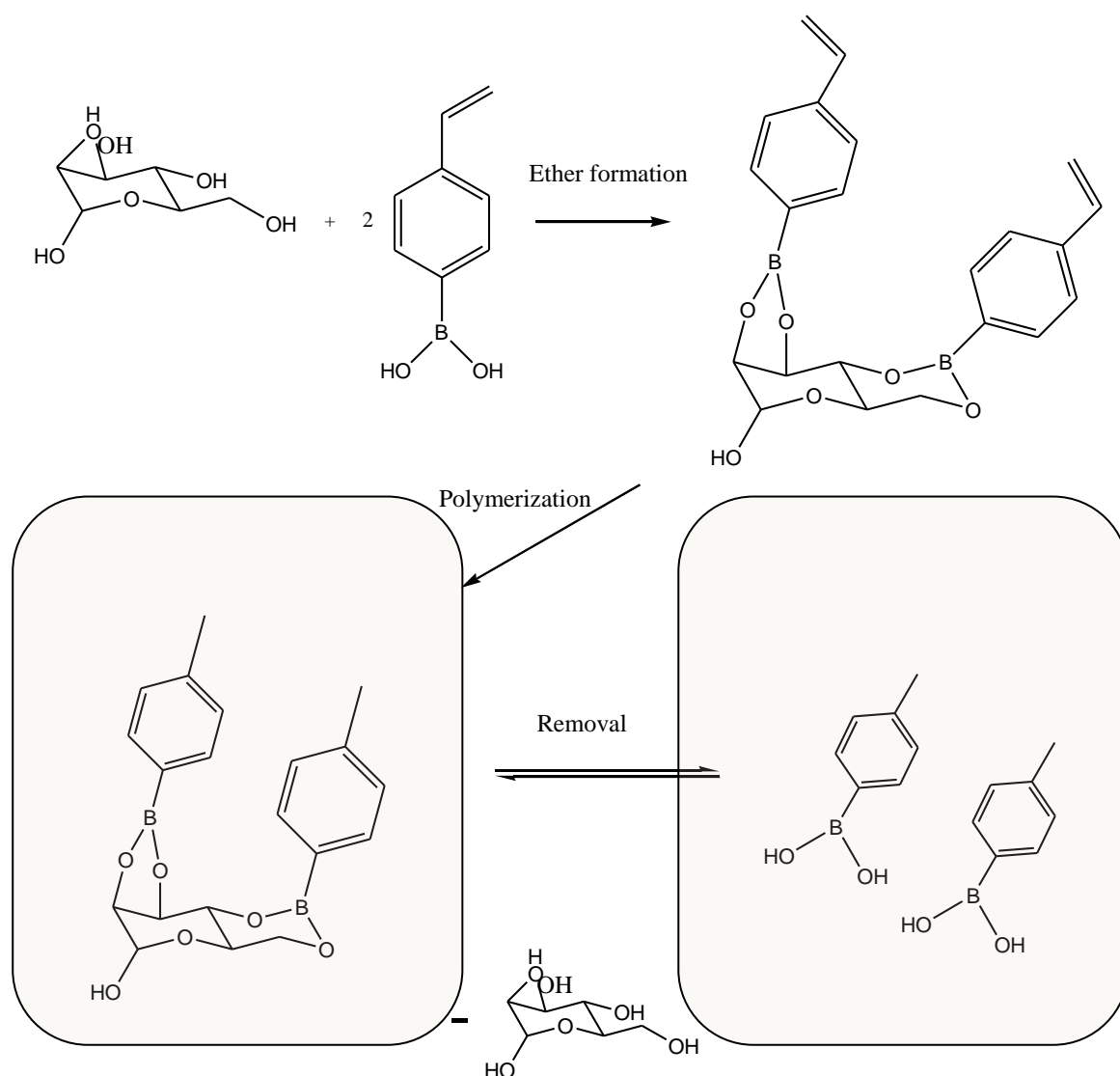


Figure 6 Covalent imprinting, adapted from [31]

Non-covalent imprinting as the other main MIP strategy was mainly developed by Klaus Mosbach. [35] This approach relies on the fact that the monomers are polymerized in the presence of template molecules. Functional monomers and the respective templates are expected to self-assemble in solution to form a pre-organized adduct. During polymerization, the positions of the respective monomer molecules are “frozen” by cross-

linking them with one another and the forming polymer matrix (**Figure 7**). As a consequence of the non-covalent nature of bonds between the respective binding partners, extracting the template compounds usually is a less tedious task, than in covalent Imprinting. It can straightforwardly happen by the means of washing with a porogenic solvent or even evaporation. [36]

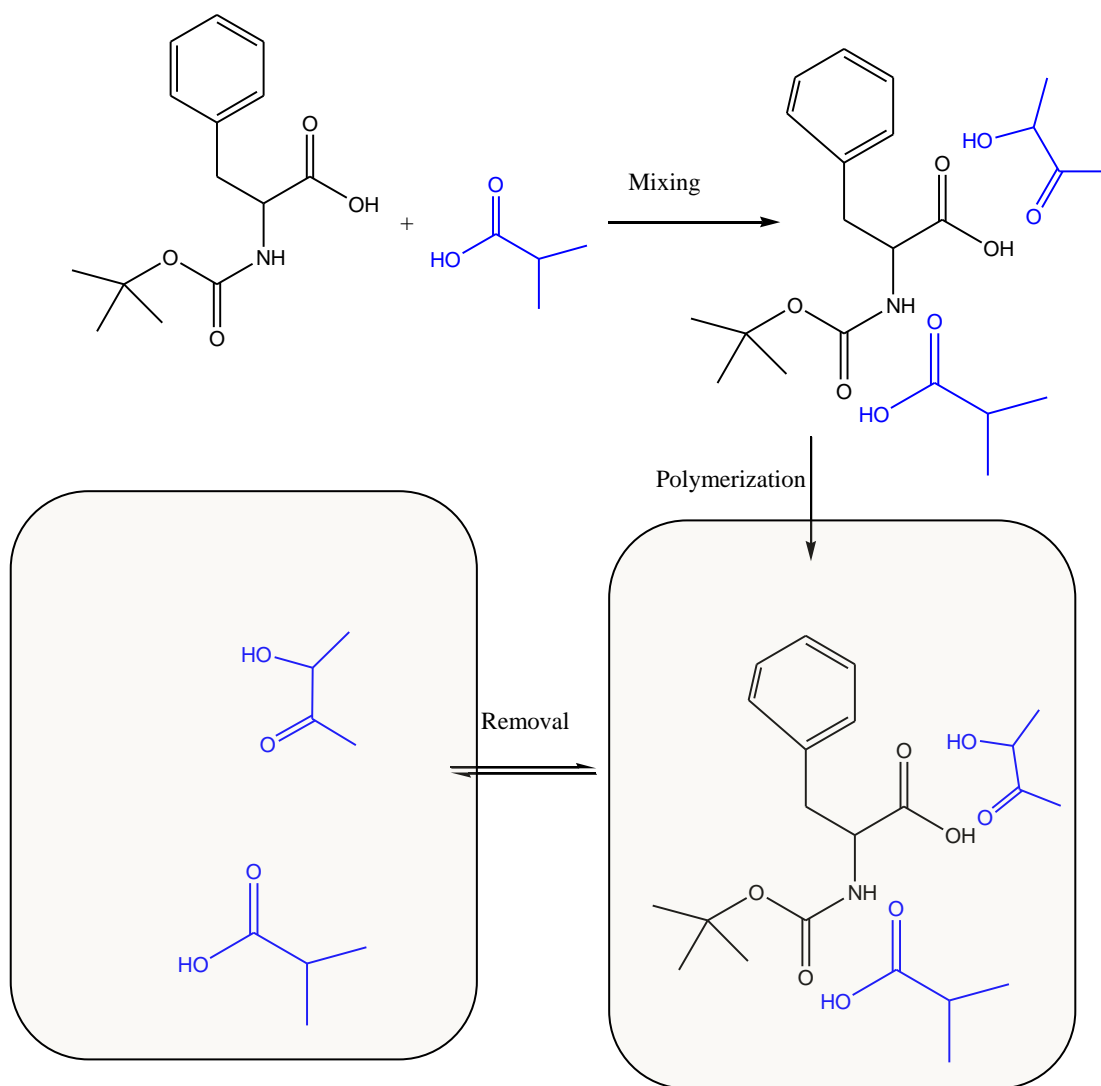


Figure 7 Non-covalent imprinting, adapted from [31]

It is an interesting fact that the first report of what is now Molecular Imprinting was based on silica systems. [37] Application of organic polymers came later gaining special popularity in chromatographic separations [38] and solid phase extraction. [39]

2. Titania and silica nanoparticles and their composites for gas sensing

2.1 Introduction

Nanoparticles are usually defined as particles with a diameter from 1 to 100 nanometers. [40] One of the most investigated types of metal oxide nanoparticles is the main topic of this chapter regarding the potential use as sensing material, namely titanium dioxide nanoparticles. Titania (with chemical formula TiO_2) is a non-expensive and chemically stable mineral, which is especially well-known for its application as white pigment. [41] Titania is present in nature in three different modifications: rutile, brookite and anatase [42] of which anatase and rutile are the most widespread forms. [43]

Further application scenarios include health, cosmetics and sunscreen products, paints and tooth paste. [44] Its uses in sunscreen and cosmetics are based on the ability of nanoparticles to absorb harmful UV radiation. Furthermore, one should not forget about their use as photocatalysts due to the oxidizing abilities of titania. [45] As a consequence of the widespread application, titania-based nanoparticles were among the first to be synthesized in huge amounts for commercial purposes. Only in the period from 2006 till 2010 approximately 5000 metric tons of titania nanoparticles were produced annually. [46] In 2006 the annual production of titania including microparticles and larger structures in the USA aggregated to 40.000 tons. Following a prognosis the production of titania NPs will 2.5 million tons per year by 2025. [47] (**Figure 8**)

Within this part of the thesis titania nanoparticles (NP) are tested for their potential in chemical sensing together with their nanocomposites with molecularly imprinted polyurethanes, followed by silica NPs.

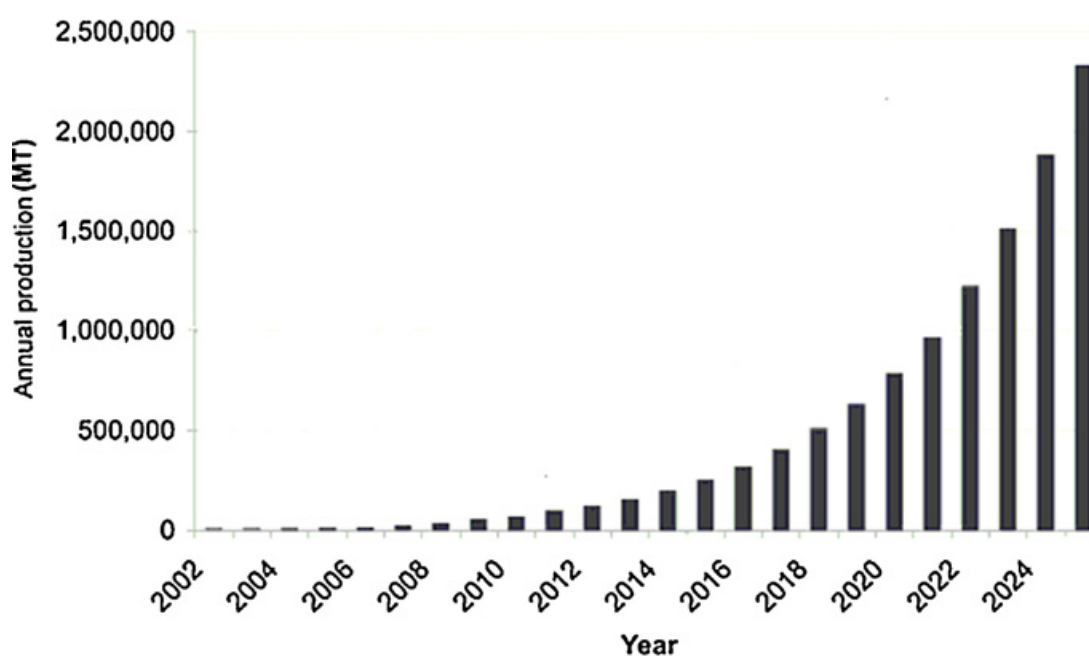


Figure 8 Forecast of TNP production in the U.S. (MT = metric tons). Reproduced with permission from [47] - © Elsevier B.V.

Silica is the second material tested with regard to its sensor properties within this work. In the same way as titanium dioxide, silica (with chemical formula SiO_2) is a chemically stable material and comparably non-expensive due to rather straightforward synthesis methods. Silica nanoparticles find their application in separation, adsorption and catalysis. One of the interesting features of these nanoparticles is that they are optically transparent. [48] Furthermore, biocompatible and water soluble silica nanoparticles are also applied for biomolecule immobilization and biological analysis. [49]

Globular, monodisperse silica nanoparticles can be obtained by the stirring tetraethyl orthosilicate (TEOS) in aqueous solution of ethanol, in which ammonia is used as a catalyst. This synthesis is also known as Stöber method. [48]

All sensor approaches discussed here have in common that they use metal oxide nanoparticles for gas sensors. [50] Summarizing the coating strategies described in this chapter, there were two ways to apply metal oxide nanoparticles as a sensing material, as summarized in **Figure 9**: the

electrodes of QCM were coated either with pure nanoparticles, or nanoparticle-polymer composites.

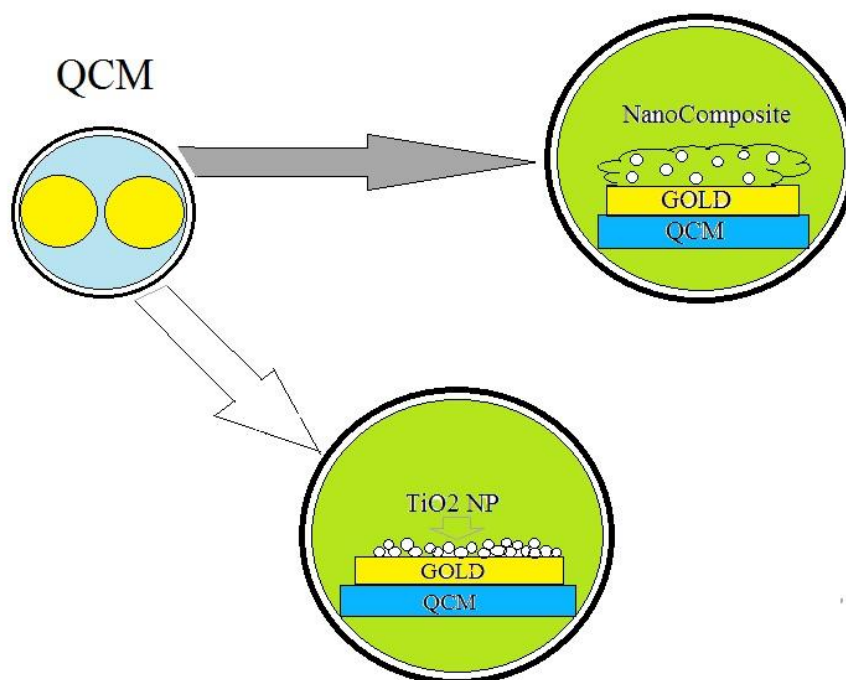


Figure 9 QCM working electrodes, coated with either pure titania nanoparticles or nanoparticle-polymer composites

2.2 Experimental

2.2.1 Materials

Quartz crystal sheets with a thickness of 168 μm (resulting in a fundamental frequency of 10 MHz) and a diameter of 15.5 mm were purchased from Zhejiang, China. The brilliant gold paste for screen printing of electrode structures was purchased from Heraeus GmbH, Germany.

Titanium tetrachloride, carbon tetrachloride, ethanol, tetraethyl orthosilicate (TEOS), ammonium hydroxide, 1-butanol, n-octane, 1-octanol, acetic acid, ethylenediamine and triethylamine were purchased from Fluka, Merck and Aldrich in highest available purity. All chemicals were used as received.

2.2.2 Preparation of QCM and Coating

First we deposited dual electrode structures on the front and on the rear face of the quartz crystal sheets by screen-printing. The respective front side electrodes have a diameter of 5 mm and are not connected with each other (electrode design for QCM in gas phase). The electrodes on the rear side are also not electrically connected with one another, because they are coupled to the phase sides of the oscillator circuit, respectively.

Sieves

Sieves for screen printing, shown in **Figure 10**, were prepared as follows: commercially available 36 μm mesh sized fabric was stretched and glued on a metal framework. Then we coated the sieves with UV photo-resist lacquer (Azocol poly-plus S from KIWO) and kept them in the dark for one hour to block mesh pores.

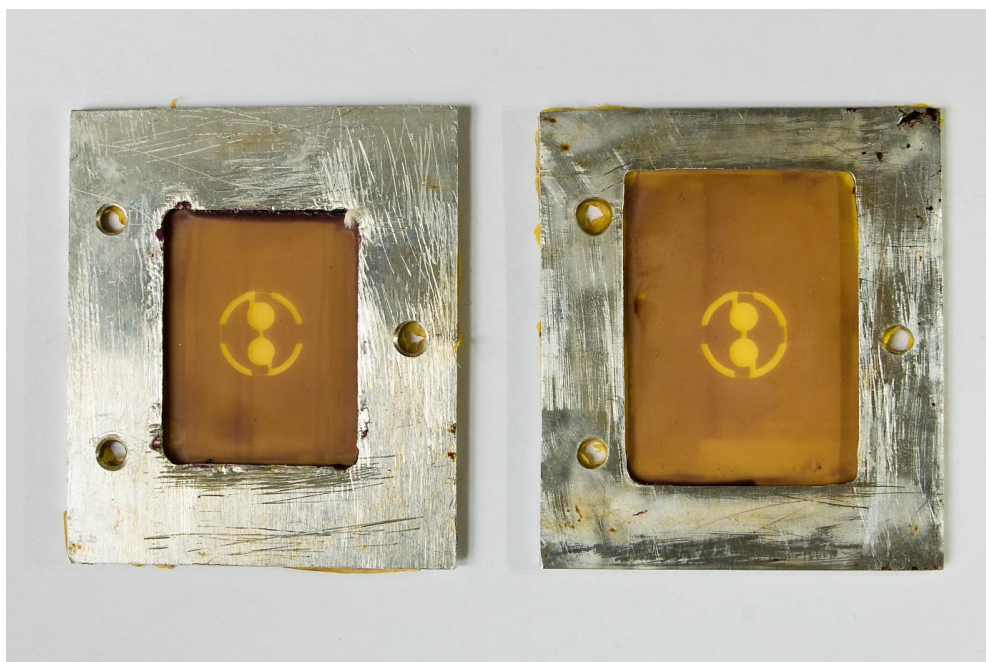


Figure 10 Sieves

We transferred the desired electrode structure onto the coated sieves coated photolithographically: A transparent sheet with the final electrode de-

sign printed in black color was fixed on the surface of a UV illumination chamber (UV-Belichtungsgerät 1, 220V, isel-automation, Germany). The sieve was aligned in a way that the electrode design was in the middle of the fabricated sieve, which was then exposed to UV light for 30 seconds in the closed chamber. To remove unhardened polymer in the areas not exposed to UV, the sieve was washed with hot water. For actual screen printing, we placed the quartz sheet on to a Teflon block and used vacuum to fix it there. In the next step the sieve was aligned with the quartz. Brilliant gold paste was spread smoothly over the sieve, which was then carefully removed from the quartz surface. The most challenging part of this task was to produce gold layers of uniform thickness. The readily prepared quartzes were burnt in an oven at 400⁰C for 4 hours to remove the organic residues from the gold paste. Electrodes on the opposite side were screen-printed exactly the same way by paying special attention to the alignment of front and back electrodes.



Figure 11 QCMs

After heating and cooling down, QCMs (**Figure 11**) were cleaned with acetone and utilized for mass sensitive measurements. Prior to that, the frequency spectra of both electrodes were checked (**Figure 12**) by the means of a network analyzer (**Figure 13**; Agilent E5062A). The electrode with less

damping was usually chosen for depositing NPs, MIP thin films and nanocomposite thin films, respectively, constituting the measuring electrode, whereas the other one was chosen as a reference.

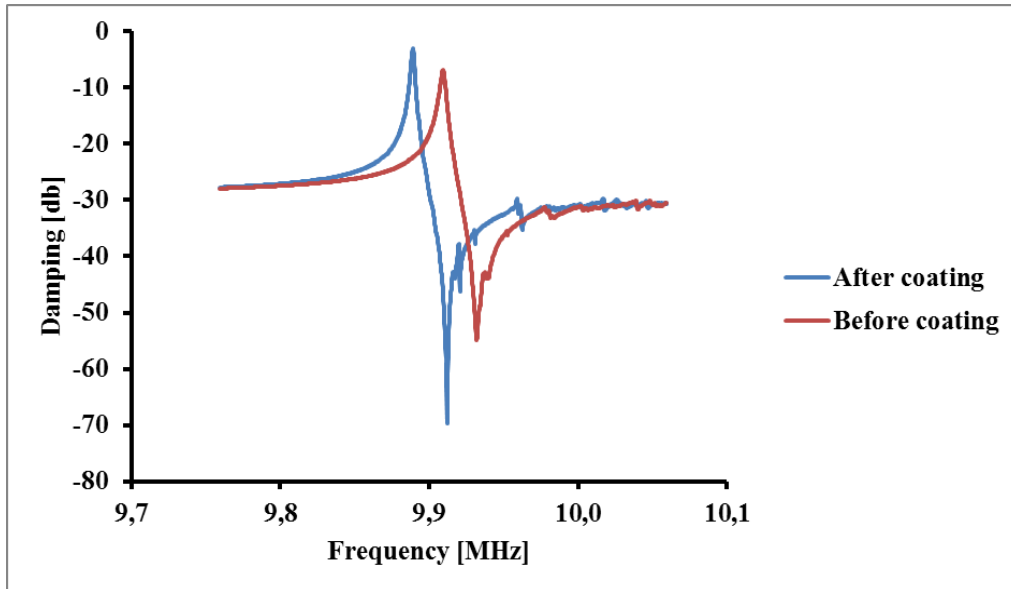


Figure 12 Typical damping spectra of 10 MHz QCM for sensing before and after coating (span is 300 kHz)

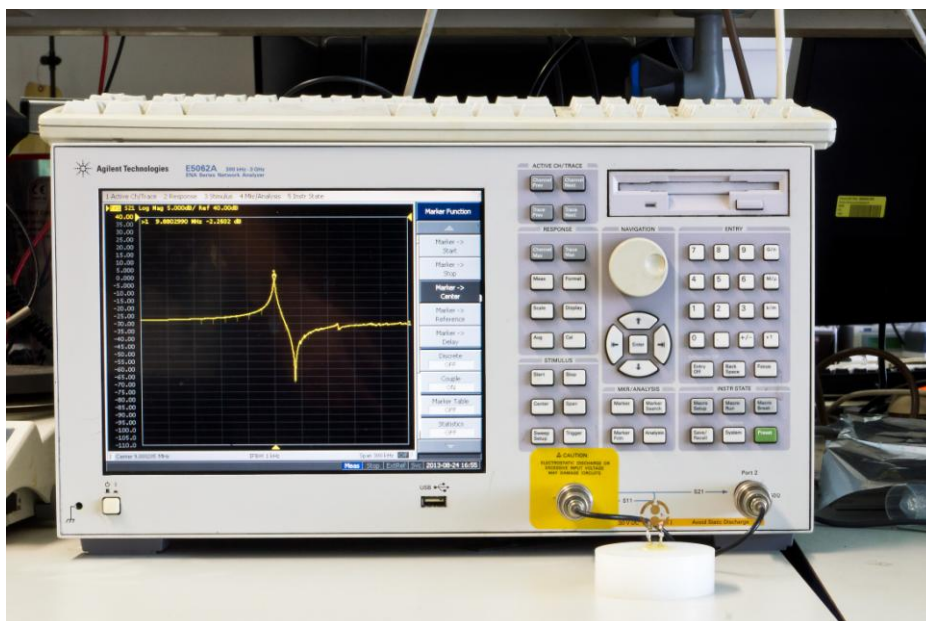


Figure 13 Network analyzer

2.2.3 Synthesis of nanoparticles

TiO₂ NPs

Titania nanoparticles were synthesized from titanium tetrachloride and water in carbon tetrachloride. 178 μL of titanium tetrachloride were dissolved in 6.5 mL carbon tetrachloride. For half an hour the mixture was polymerized at 60⁰C. Afterwards 63 μL of water were added. In order to precipitate titania nanoparticles the solution was vigorously stirred. The resulting TiO₂ particles were washed by centrifugation, removal of the supernatant solution, resuspension in water, followed by centrifugation and drying at 110 degrees centigrade. The scheme of the synthesis is shown in **Figure 14**.

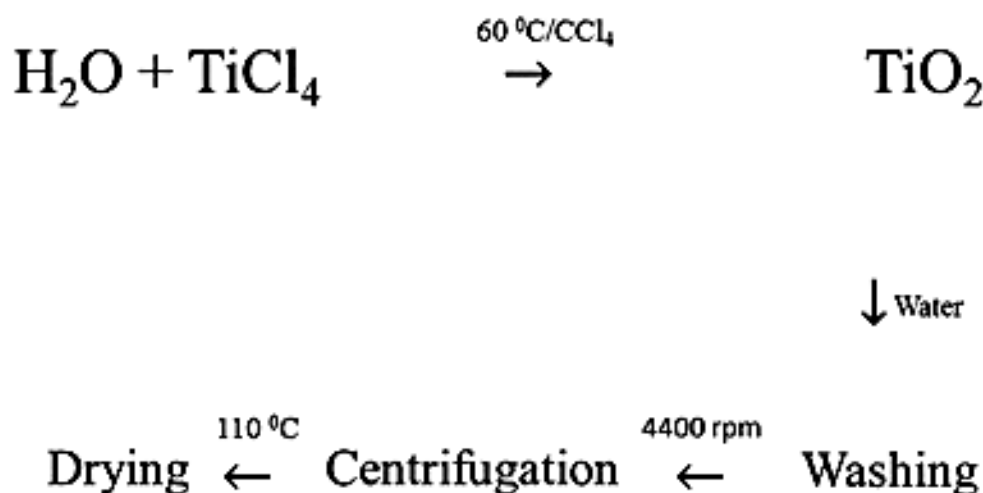


Figure 14 Schematic TiO₂ NP synthesis pathway

SiO₂ NPs

We prepared silica nanoparticles by sol-gel synthesis [48] in an ultrasonic bath using tetraethyl orthosilicate (TEOS) as a precursor. The scheme of the synthesis is shown in **Figure 15**. First 2 mL of ethanol were sonicated for about 10 min. After that, we added a 200 μL of tetraethyl orthosilicate (TEOS) and continued sonication. After 20 min 200 μL of a catalyst (28% ammonium hydroxide in water) was added in order to support the condensa-

tion reaction. The reaction mixture was sonicated at room temperature for further 60 min until a turbid suspension occurred. The resulting silica nanoparticles were obtained from the turbid solution by centrifugation, removing of the supernatant solution and re-suspension in water. Finally they were again subjected to centrifugation and dried at 100 degrees centigrade.

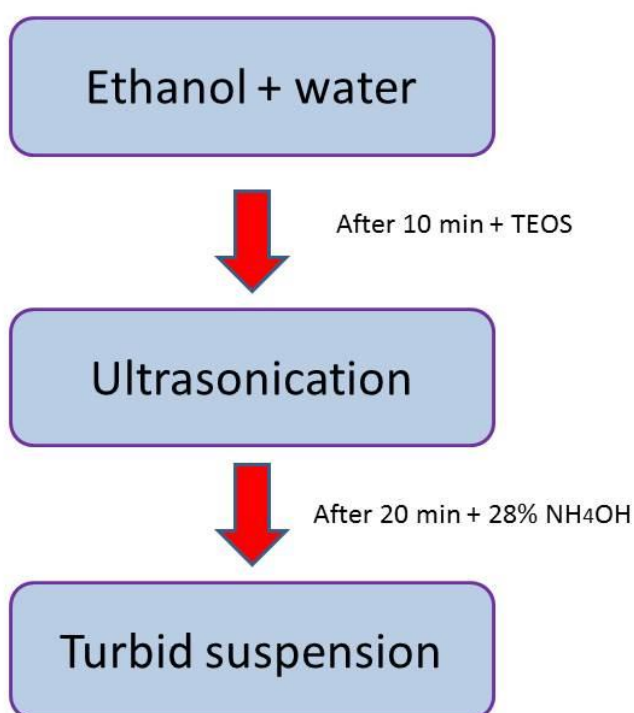


Figure 15 Scheme of SiO₂ NP synthesis

2.2.4 Synthesis of molecularly imprinted polyurethane

1g of diisocyanato-diphenylmethane (DPDI) was mixed with 1.97 g of bisphenol A (BPA), 0.22 g of phloroglucinol and 2 ml of tetrahydrofuran (THF). Pre-polymerization was performed at 60 degree centigrade for 45 minutes. [51] We added 30 μ l of pre-reacted polymer solution to 970 μ l of 1-butanol (the template and analyte-to-be). For spin-coating the pre-polymer mixture was further diluted 1+30 with 1-butanol. The same procedure was applied for NIP synthesis except for adding 1-butanol.

2.2.5 Atomic Force Microscopy (AFM)

AFM is an imaging technique (**Figure 16**), where a sharp tip mounted on a cantilever is scanned over a surface. When moving the tip close to the surface of interest, the cantilever is deflected according to the forces between tip and surface. By measuring these deflections as a function of xy position on the surface, it is possible to collect morphology information with a lateral resolution of a few nanometers. [52] The fundamental advantage of AFM over Scanning Tunneling Microscopy (STM) is that it is also suitable for non-conductive surfaces.

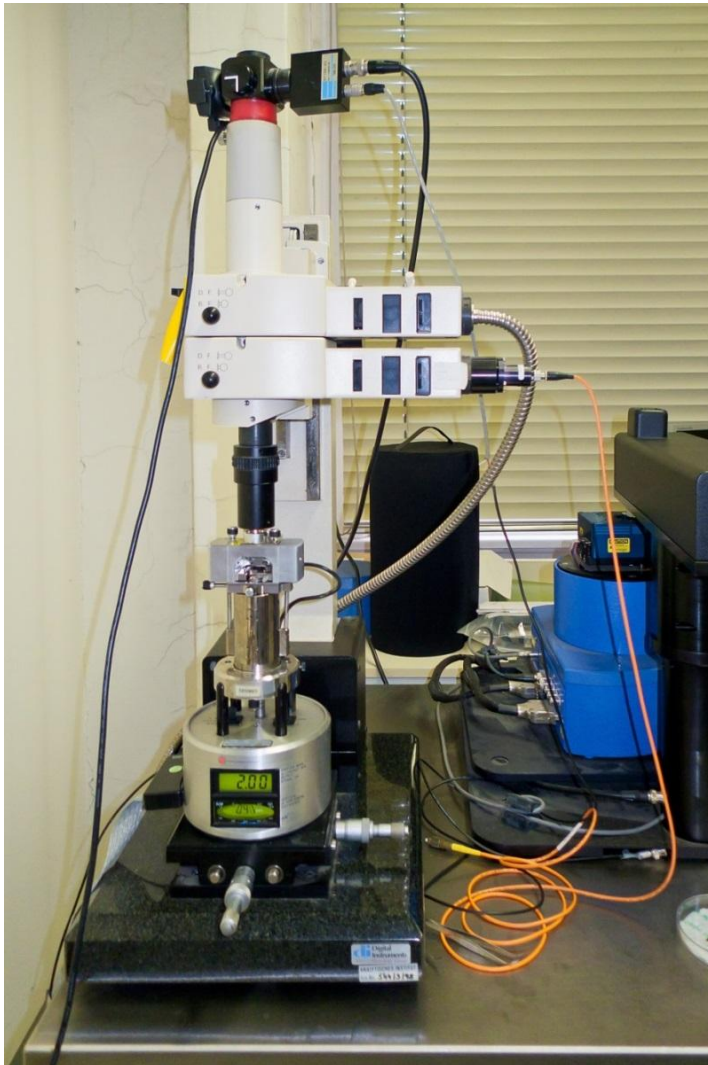


Figure 16 AFM setup

In both cases we used 7 μl of aqueous nanoparticles suspension; spin coated onto glass substrates at 1600 rpm to obtain AFM images. The resulting samples were analyzed with contact mode scanning on a Veeco NanoScope IVa using SNL-10 silicon tips.

2.2.6 Coating

For generating actual sensors, we coated the working electrode with NPs (later with polymer and nanocomposite thin films) on both sides of the respective QCM, which is usual when working in gas phase (both sides of each electrode are thus exposed to the gas stream containing the analyte during measurements). Spin-coating makes sure that both thin films and nanoparticle coatings on the QCM electrodes are homogeneous. On dual electrode QCM this of course requires suitable masks. For this purpose we applied adhesive foils that can be removed from the device surface without leaving behind any residues. In this way only the electrode to be coated is exposed to the nanoparticles or oligomer solution. Furthermore this allows mounting the QCM on the spin-coater in a way that the electrode of interest is placed exactly in the center of the coater (**Figure 17**). For coating we used nanoparticle suspensions in ethylenediamine, as this solvent resulted in the most homogeneous layers: 5 mg of titania NP were added to 500 μl ethylenediamine. Then 7 μl of resulting suspension were used for coating one side of QCM electrode. After turning on the spinner, 7 μl of NPs suspension was dropped onto the exposed electrode at 2000 rpm followed by spinning for two minutes. The resulting layer height was from usually 50 nm. After coating QCMs were dried for an hour at room temperature. Then the mask was carefully removed without affecting the layer. To complete the process we transferred QCM into an oven, where they were dried overnight at 70^oC.

The same procedure was undertaken in order to coat the other side of the respective electrode without affecting the hardened layer. The new layer

height was also about 50 nm, so in result there was a overall polymer layer height about 100 nm.



Figure 17 Spin coater with QCM mounted together with mask to coat one electrode

When also coating the reference electrode (like in the cases of polymer and nanocomposite thin layers), we had to mask the already coated working electrode, avoiding contamination. Usually on the following day the cooled QCM were characterized on the network analyzer (Agilent Technologies E5062A) for damping of the coated working electrode. Then the QCM were placed in the measuring cell, connected to the gas mixing apparatus. Before exposing the QCM to organic solvent vapors, the QCM was left to stabilize at least 1 hour in dry air.

2.2.7 Apparatus

A dual channel frequency counter (Agilent Technologies 53131A) was used to perform QCM frequency measurements in a custom-made oscillator

circuit (**Figure 18**) containing the respective sensor as the frequency-determining element. A customized Lab View Routine was used to read out the data and transfer it to a computer. Gas samples were produced by a gas mixing apparatus consisting of mass flow valves (type RS-485) addressed by a Brooks Instruments SLA5850 S controller. The setup for gas measurements is shown in **Figure 19**.



Figure 18 QCM mounted onto the custom-made oscillator circuit



Figure 19 Setup for gas measurements

2.3 Results and Discussion

2.3.1 Nanoparticle Characterization

Before bringing synthesized nanoparticles onto the electrode surfaces, they were characterized via AFM. Both images show homogeneous distribution of particles, although in the case of titania (**Figure 20**), a larger amount of particles can be found deposited on the surface. The size distribution in both cases seems homogenous showing a mean diameter of 200 nm. Neither in the case of titania, nor in the case of silica (

Figure 21), substantial clusters can be found. This very clearly shows the ability of the chosen procedure to achieve optimal NP coatings.

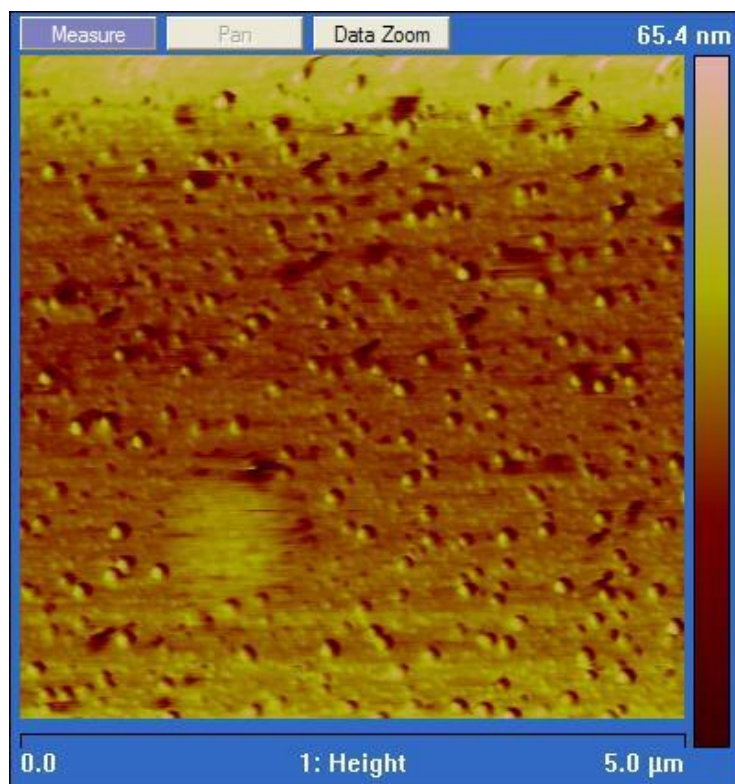


Figure 20 AFM image of TiO_2 nanoparticles on glass substrate

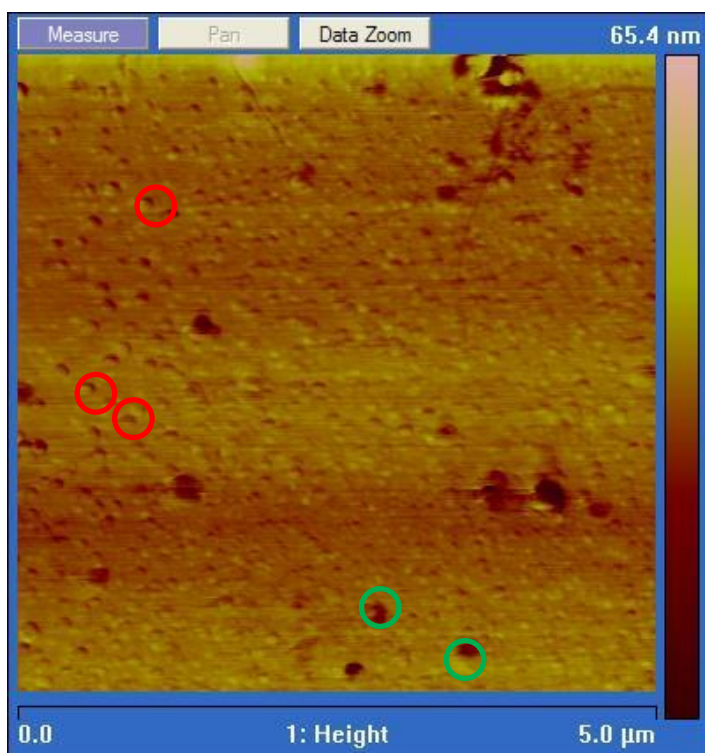


Figure 21 AFM image of SiO₂ nanoparticles on glass substrate. Red circles show some areas, where particles are present, green circles mark some of the clusters

2.3.2 Mass sensitive measurements

TiO₂ NPs

For gas phase measurements the respective QCM was mounted in measuring cell containing an oscillator circuit. The measuring cell is connected to a gas mixing apparatus by Teflon® tubes. The gas mixing device can regulate 8 mass-flow channels which allows generating exactly defined mixtures of dry and humid air as well as solvent vapors. The results presented in this chapter were obtained by using two channels for air and analyte vapors. One electrode of QCM was coated with sensing material (TiO₂) and the reference one was left uncoated. (**Figure 22**)

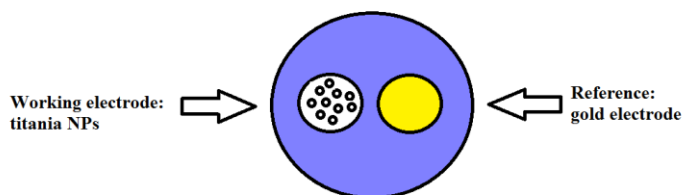


Figure 22 QCM TiO₂ nanoparticles

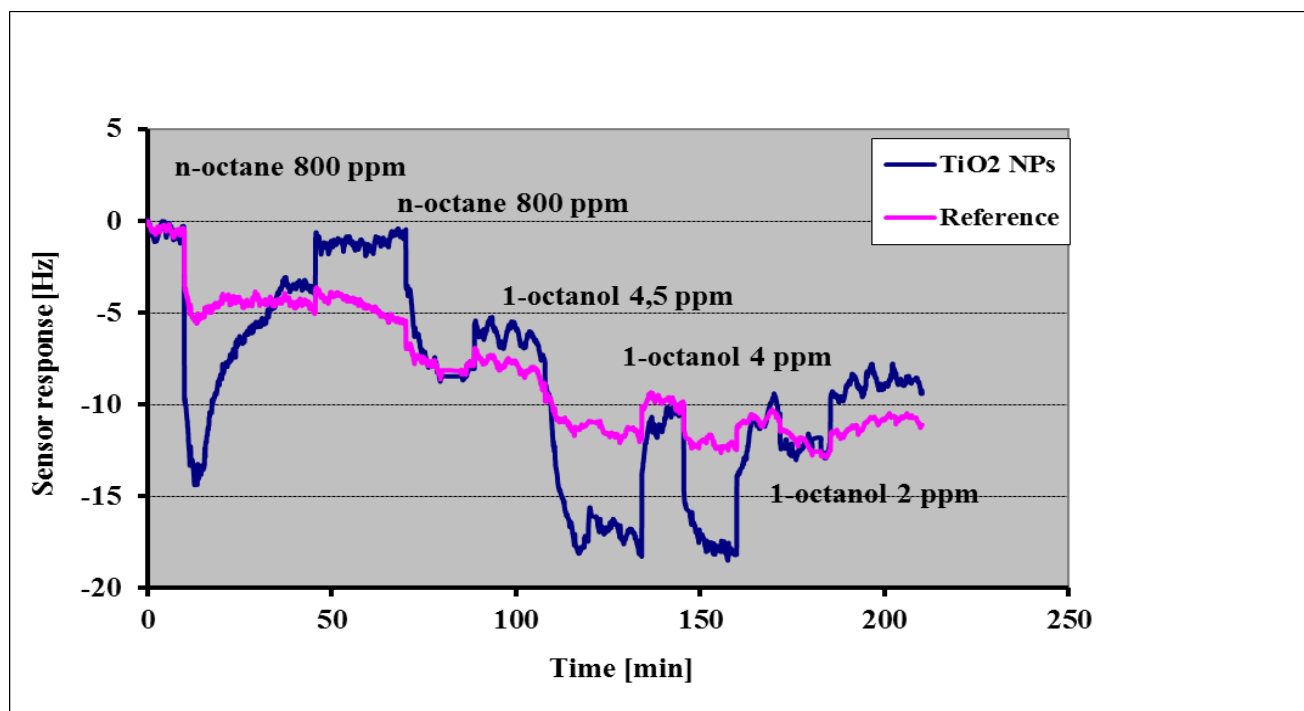


Figure 23 Sensor response of TiO₂ nanoparticles towards n-octane and 1-octanol.

Figure 23 shows an early trial measurement with titania nanoparticles, where the blue curve represents the frequency shifts obtained by the nanoparticles and the magenta one those of non-coated channel. At the beginning one can see the constant signal in dry air. This frequency is used as the reference point and thus set to zero. By exposing the nanoparticle sen-

sensor to organic compounds with the same carbon chain length but with different functional groups (800 ppm of n-octane and 2.4 and 4.5 ppm of 1-octanol, respectively), it should be possible to assess acid-base behavior of TiO₂ NP.

Despite unstable base line (if it is at zero Hz at the beginning of the measurement, at the end we find it at -9 Hz), the compounds yield sensor effects that are partly reversible (the first sensor response is towards 800 ppm of n-octane, the following responses towards 4 ppm and 2 ppm of 1-octanol). Despite its shortcomings, this experiment contains substantial information on the system: approximately calculating and comparing the respective sensor responses (sensor response towards n-octane is approximately 0.0109 Hz/ppm, and sensor response towards 1-octanol is 1.216 Hz/ppm, which is 111 times larger than for n-octane), one can observe significantly different behavior of the sensor towards the two analytes and can suppose somewhat hydrophilic character of the sensor material. This can be deduced from the fact that both analytes share the same amount of carbon atoms and only differ by one oxygen.

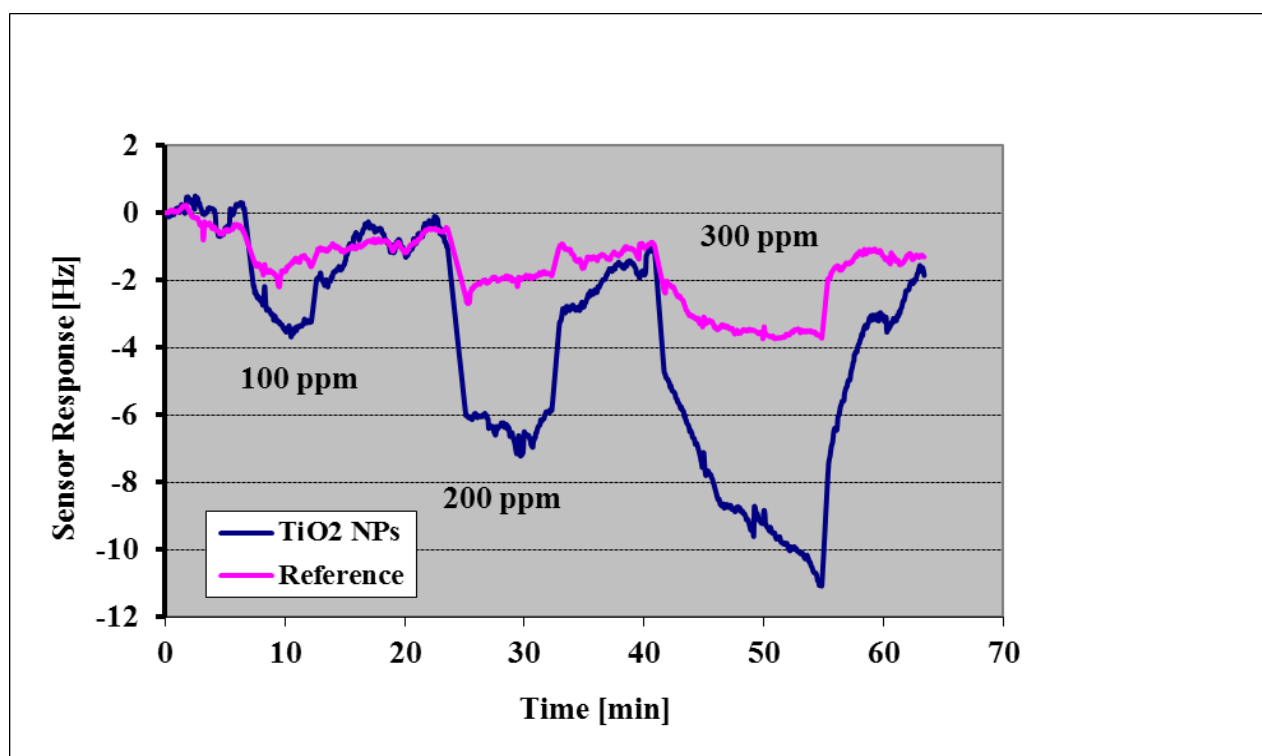


Figure 24 TiO₂ nanoparticles response against 1-butanol

Without additional selectivity, the sensor responses towards both compounds should only differ by around 12%, which corresponds to the mass contributed by the oxygen atom. This opens the way for further studies assessing the recognition properties of the of titania NP. The first analyte tested has been 1-butanol, which yields frequency responses such as the ones shown in **Figure 24**. The reference point again is the frequency obtained in dry air. When exposed to 100, 200 and 300 ppm 1-butanol vapor in air, respectively, the frequency decreases on both channels. However, the channel coated with particles yields substantially larger responses. This clearly indicates that particles undergo affinity interaction with the 1-butanol. Furthermore, the sensor signal is almost reversible and its magnitude depends on vapor concentration. Comparing this outcome with the previous results the first main difference is the quality of the baseline. It hardly shows any drift lying within the 0 and -2 Hz range over more than an hour of measuring time. Speaking of the outcome of the experiment, one can conclude that the responses of 1-butanol are appreciable (0.024 Hz/ppm) but lower, than for 1-octanol (more exactly, 50 times lower).

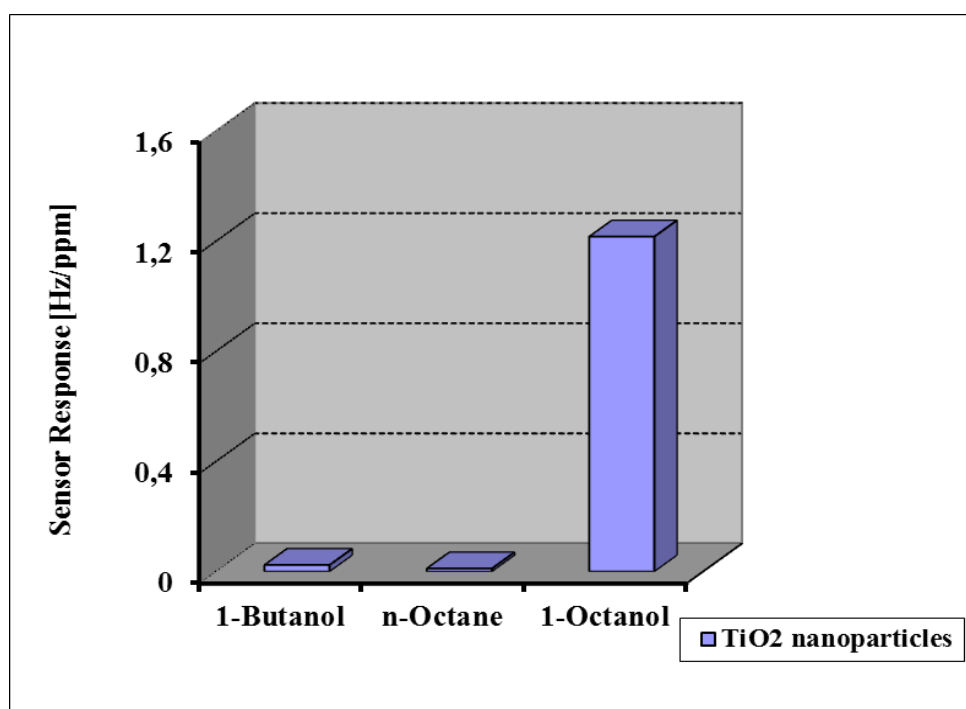


Figure 25 Selectivity pattern of TiO_2 nanoparticles

To summarize measurements performed on the same QCM,

Figure 25 collects the data for all three analytes: here, 1-octanol stands out significantly against the two other analytes: 1-butanol and n-octane.

From the table below containing molar mass, boiling point and vapor pressure for three analytes, one can clearly see that 1-octanol (the analyte with the highest sensor response) possesses the lowest vapor pressure which in addition to the interaction with the OH group also means that it shows stronger tendency to “condensate” on the particle surfaces.

	1-butanol	N-octane	1-octanol
Molar mass, g/mol	74.12	114.23	130,23
Boiling point, °C	117.7	126	195
Vapor pressure, mmHg (20°C)	5.5	11	0.14

For further experiments, the first batch of QCM with optimized noise performance was generated. To ensure that all the results are fully comparable, both the previous analytes (1-butanol, 1-octanol and n-octane) and additional compounds were tested, namely acetic acid, triethylamine and ethylenediamine

Measurements with 1-butanol, 1-octanol and n-octane on the new QCM were repeated, as one can see in **Figure 26**, **Figure 27** and **Figure 28**.

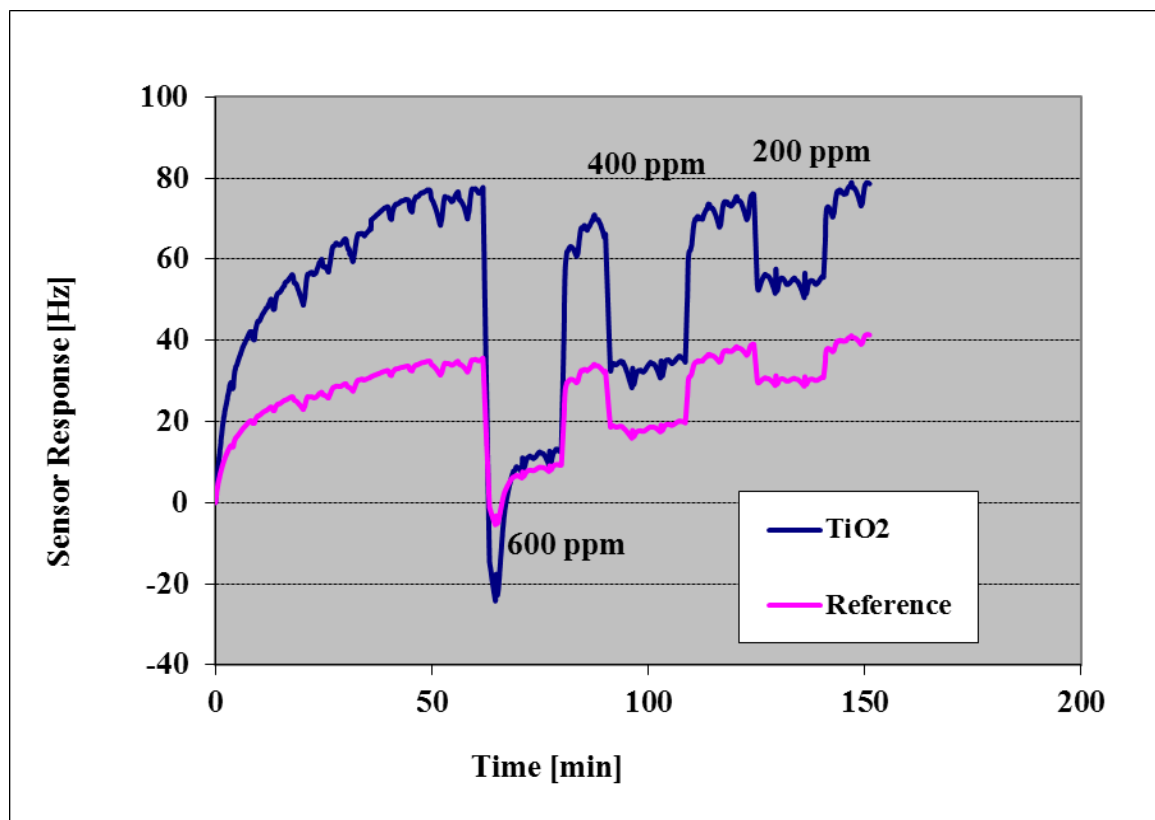


Figure 26 Sensor signal of TiO₂ nanoparticles layer against 1-butanol

The sensor shown in **Figure 26** was exposed to the following concentrations of 1-butanol: 200, 400 and 600 ppm analyte vapor in air, respectively. After having achieved stable baseline the frequency decreases on both channels upon exposure to the analyte. Again, the sensor signals both depend on analyte concentration and are reversible. The working electrode with titania particles shows substantially larger responses than the reference electrode. Reversible signals strongly indicate that the nanoparticles indeed show suitable affinity and can therefore inherently be used for sensing purposes: the results prove interactions between sensor material and 1-butanol and give reliable quantitative information.

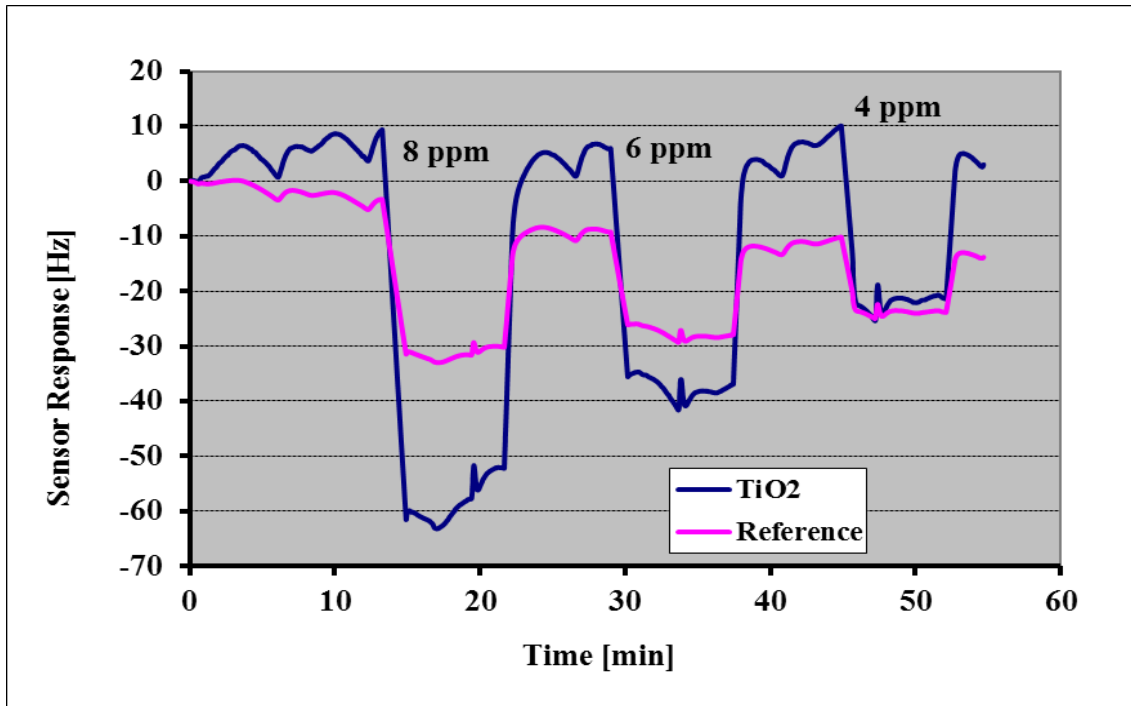


Figure 27 TiO₂ nanoparticles response towards 1-octanol

Figure 27 summarizes the sensor responses of the same system when exposed to 8, 6 and 4 ppm 1-octanol vapor, respectively in air.

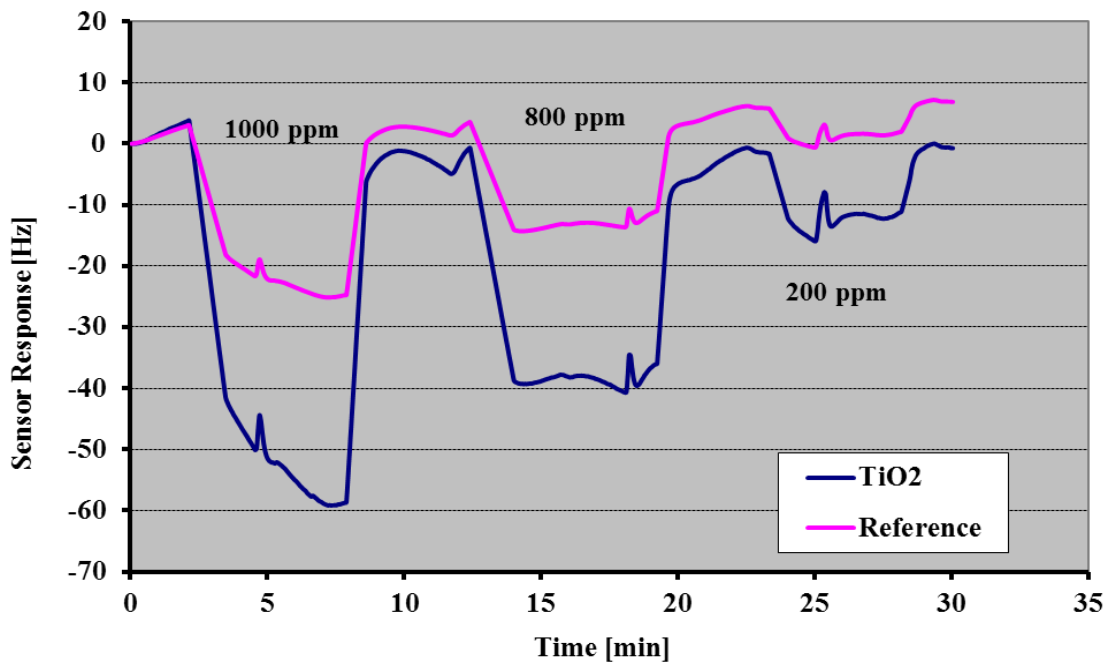


Figure 28 TiO₂ nanoparticles sensor signal against n-octane

In the case of butanol the response of the reference electrode is comparably high (about 40 % of titania response), which is of course also due to the rather low analyte concentrations. However one can observe a stable base line for the working electrode as well as reversible sensor responses that depend on concentration. The detection limit is impressive: 4 ppm of analyte gives rise to 15 Hz frequency shift.

First preliminary measurement depicted in **Figure 23** revealed sensor responses only for concentrations as high as 800 ppm n-octane. The repeated measurements on the new sensors resulted in more information as presented in **Figure 28**. Again, there is some minor interfering signal, observed also during previous n-octane measurements. Furthermore the reference electrode yields comparably large signals.

As there are data of at least 2 different QCMs with the same analytes (1-butanol, n-octane and 1-octanol), one can compare them taking into account the difference between layer heights (see the table on the bottom of this page and **Figure 29**). In such a way, one gains information on the reproducibility of the system: the effects with the second QCM are 3-4 times higher than the first QCM. This can be explained by the respective layer heights (QCM 1 120 nm, QCM 2 460 nm). Overall 1-octanol is strongly preferred by the TiO₂ layer, whereas n-octane only leads to minor effects. The results indicate efficient reproducibility of titania nanoparticles and QCM measurements. **Figure 29** directly compares the signals obtained for the two QCM towards the analytes in question. Overall selectivity remains of course unchanged, so the differences are mainly determined by the different sensitivities due to layer height.

Analyte	QCM 1 response, Hz/ppm	QCM 2 response, Hz/ppm	Improvement factor
1-Butanol	0,02358333	0,06976	2,9580212
n-Octane	0,01095	0,038	3,47031963
1-Octanol	1,21657407	4,807	3,95125961

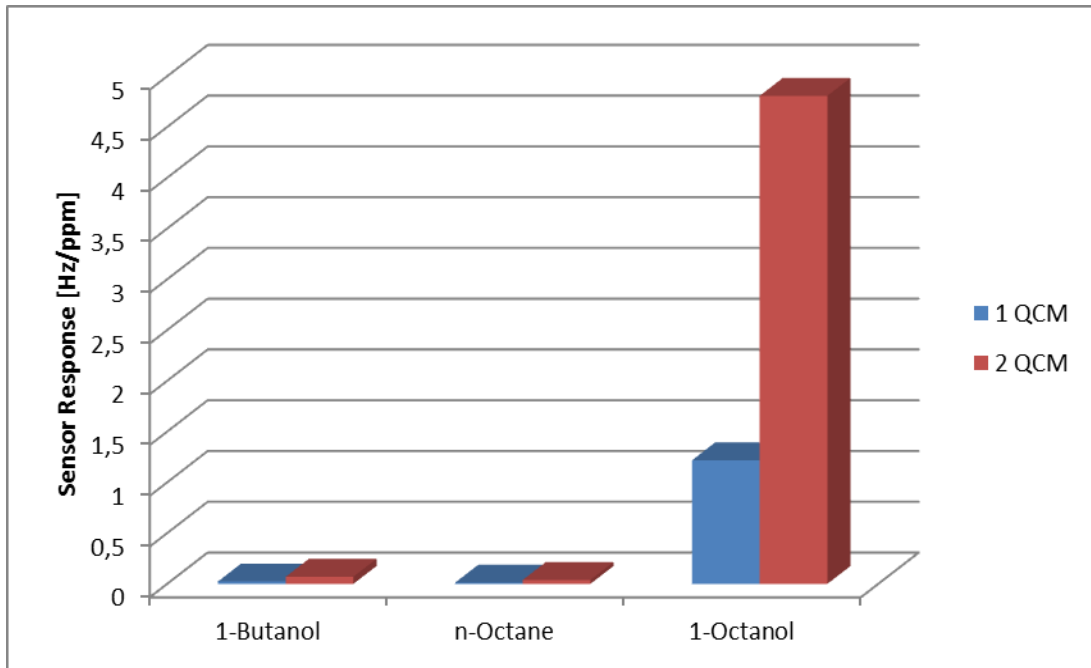


Figure 29 Selectivity pattern for two QCM with different layer height of TiO₂ NP

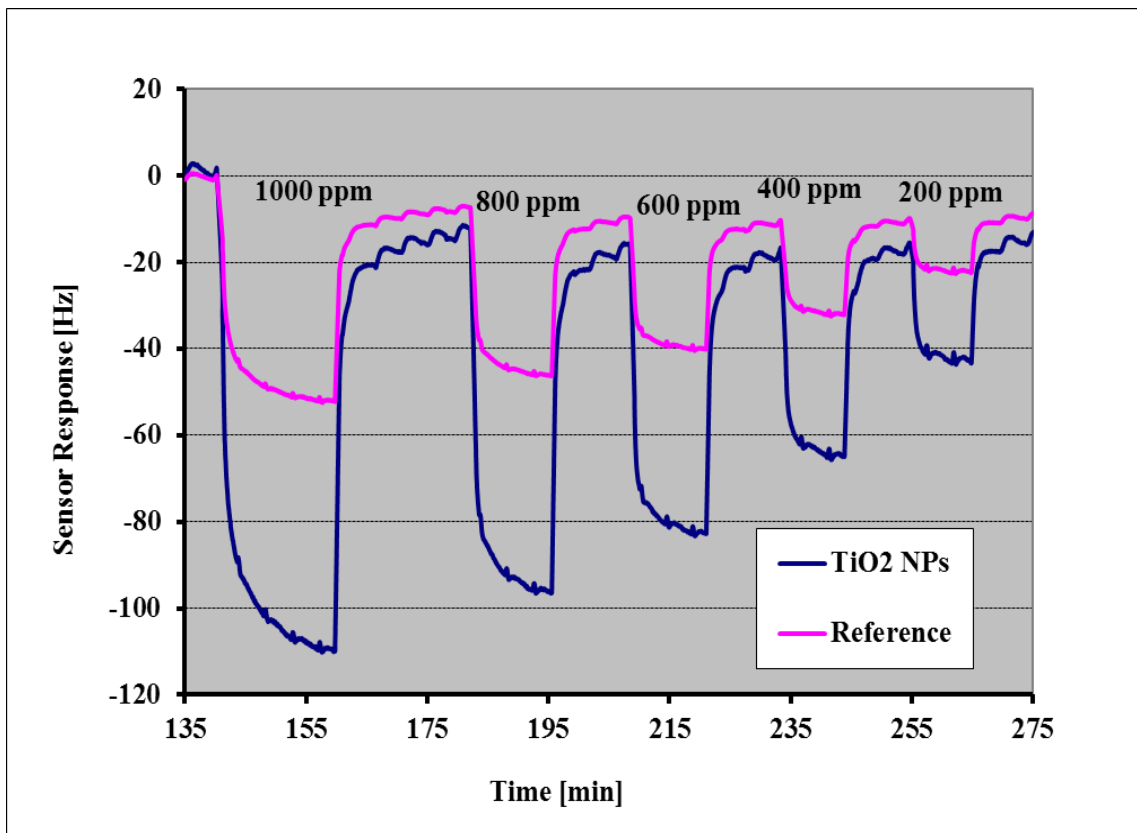


Figure 30 Sensing of triethylamine with TiO₂ nanoparticles

A further analyte of interest in this case is triethylamine due to its strong alkaline properties, which is suitable for testing possible acidic behavior of the layers. A typical example of the resulting sensor responses can be seen in **Figure 30**. When triethylamine molecules pass into measuring cell with the QCM they show affinity to titania nanoparticles. As a result one can observe reversible frequency shifts based on Sauerbrey effect that again depend on analyte concentration. Furthermore one can observe remarkably stable base line in this case. Ethylenediamine was used as a second analyte to further characterize TiO₂ NP. (**Figure 31**)

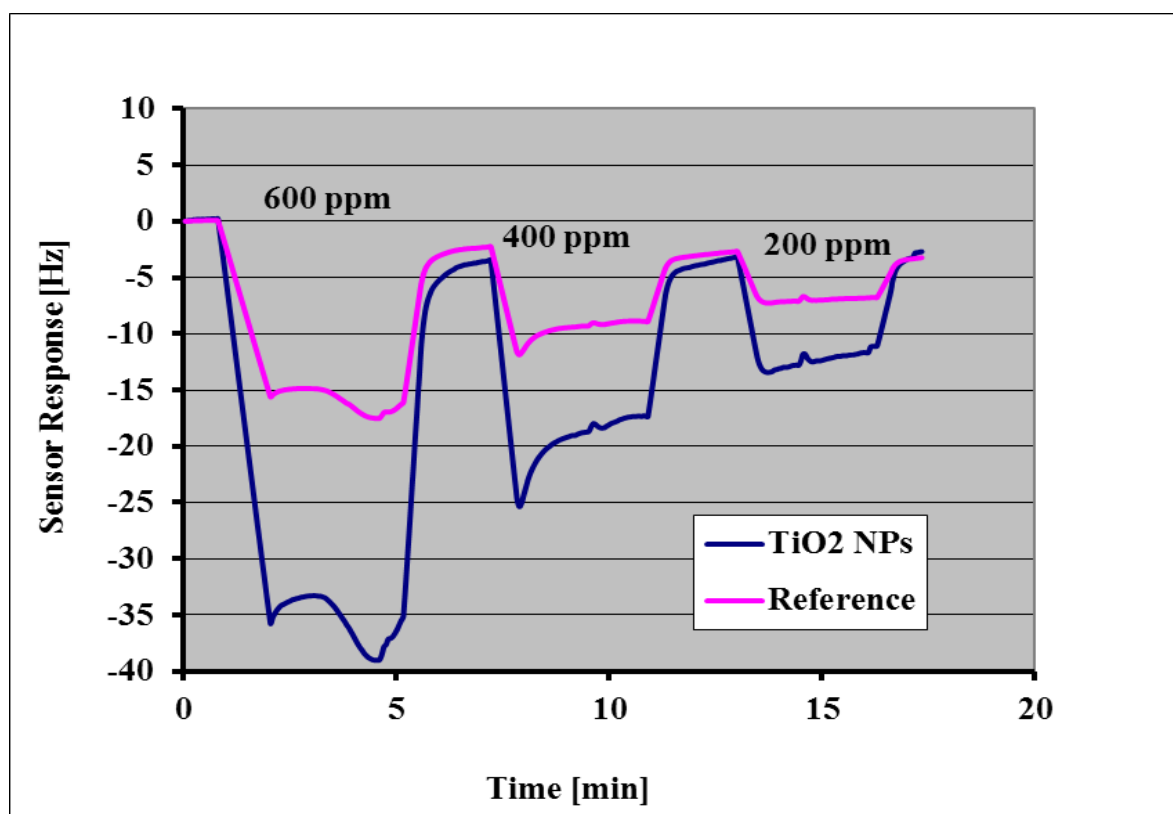


Figure 31 Sensor response of TiO₂ towards 1% ethylenediamine in 1-butanol

In order to directly compare the results of the two strong bases, they are summarized in the tables below. What one can clearly see from them, is that triethylamine yields 2 times higher effects than ethylenediamine. Two reasons for this are that tertiary amines show stronger alkaline reactions,

than primary ones and the larger molar mass of triethyl amine in comparison to ethylenediamine.

1% Ethylenediamine in 1-Butanol	Sensor Response		Triethylamine	Sensor Response
C, ppm	Hz		C, ppm	Hz
200	6,42		200	16,08
400	13,15		400	26,58
600	20,12		600	35,82
			800	45,44
			1000	59,45

Analyte	S.R. Hz/ppm
Ethylenediamine	0,0328
Triethylamine	0,0645

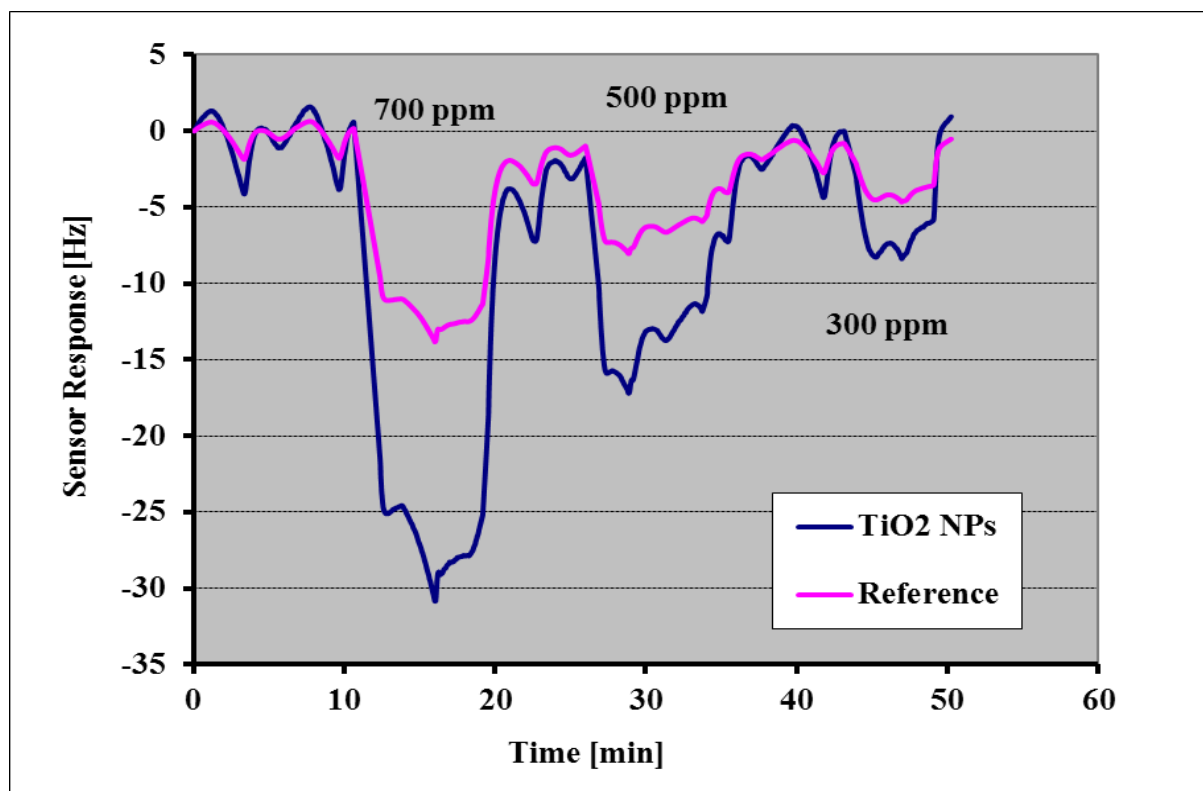


Figure 32 Sensor response of TiO₂ nanoparticles against acetic acid vapors

To obtain the complete picture of the interaction properties of the materials, the sensors were also exposed to an acidic compound, namely acetic acid. The results are summarized in **Figure 32**. Again some minor interfering signals can be observed, most probably resulting from the gas supply, because they occur on both channels. From the result one can see no substantial affinity between the comparably strong organic acid and titania nanoparticles. Results are summarized in **Figure 33** and the table below.

Acetic acid	S.R.	1% Ethylenediamine in 1-Butanol	S.R.	Triethylamin	S.R.
ppm	Hz/ppm	ppm	Hz/ppm	ppm	Hz/ppm
300	0,01803333	200	0,0321	200	0,0804
500	0,01782	400	0,032875	400	0,066275
700	0,02794286	600	0,03353333	600	0,05973333
				800	0,0568
				1000	0,05945

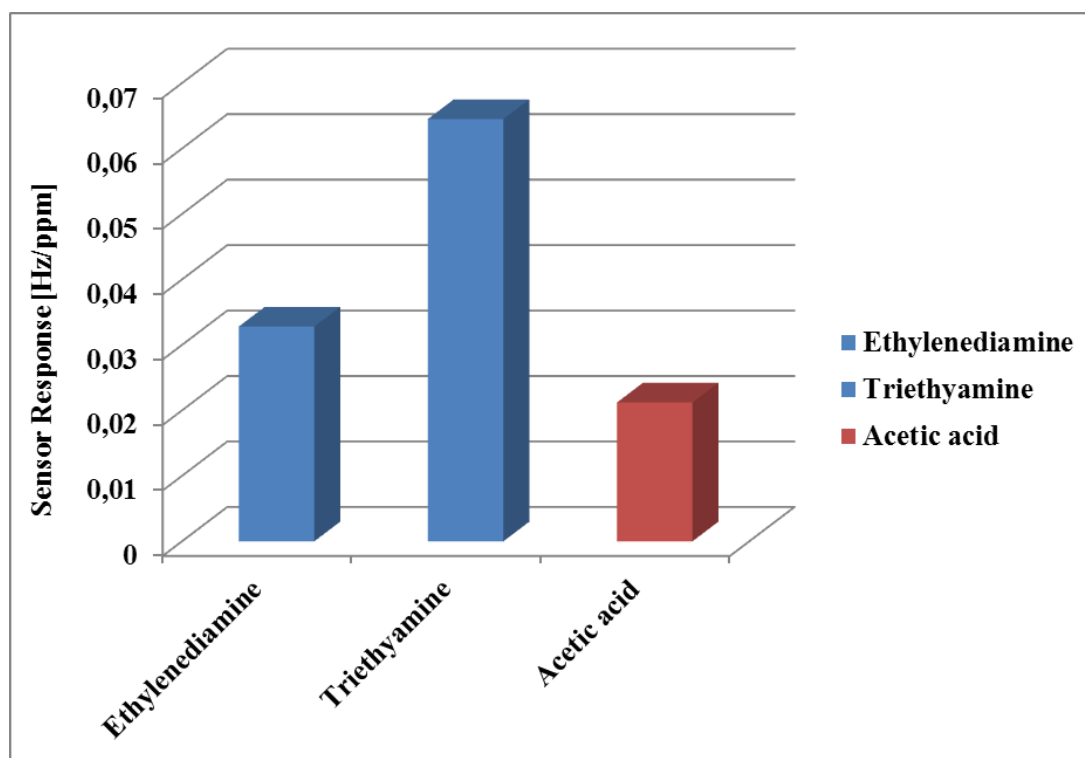


Figure 33 Selectivity pattern of TiO₂

Summarizing the acid-base results of TiO_2 , it is obvious that the acid is the least preferred compound. However, the ethylenediamine leads to signals that are only 50% higher. The material thus shows its amphiphilic behavior, although the sensor results indicate slightly acidic behavior of the nanoparticles.

TiO_2 Selectivity

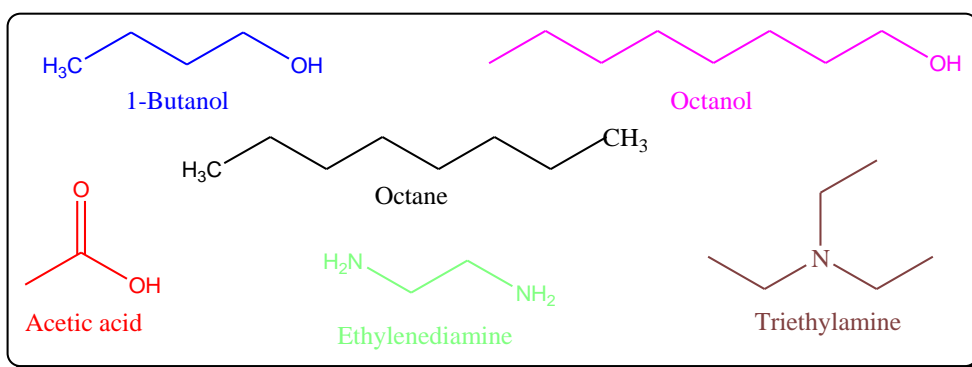


Figure 34 Analytes structures

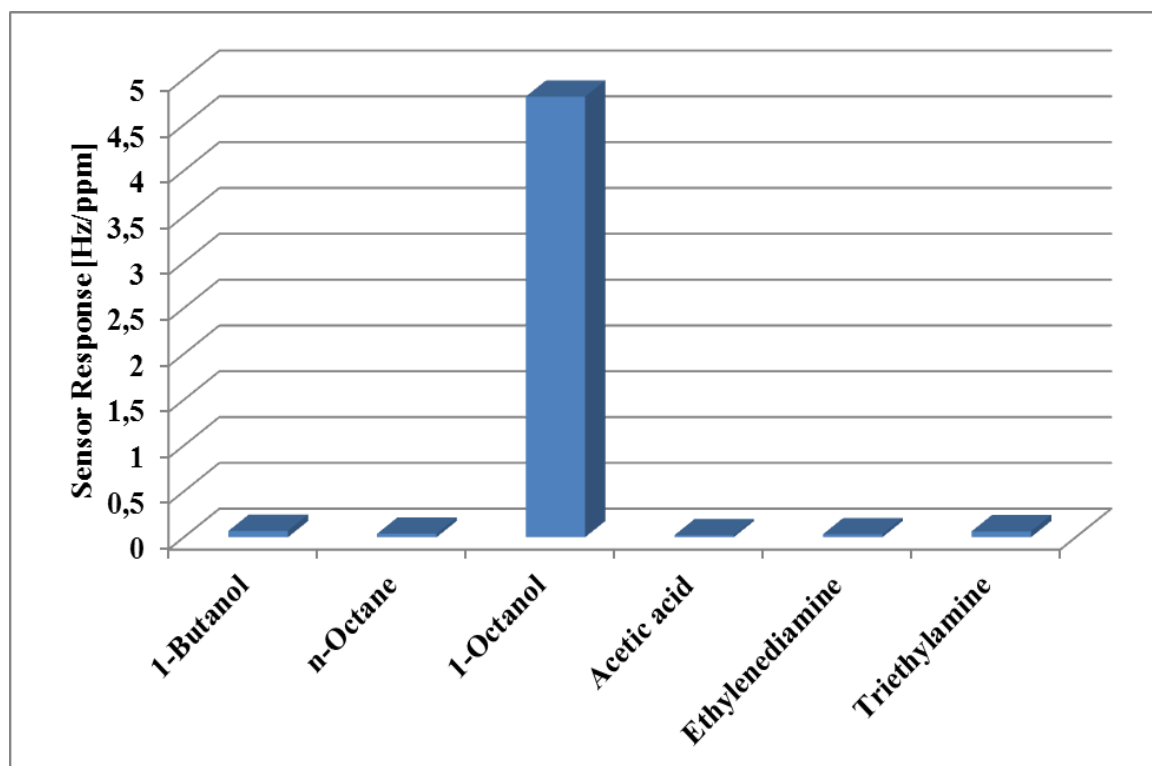


Figure 35 Extended selectivity pattern of TiO_2 nanoparticles

The complete selectivity pattern of titania nanoparticles (**Figure 35**; all analyte structures are summarized in **Figure 34**) once again reveals the amphoteric character of TiO₂ because neither acids nor bases are strongly preferred by NPs despite the slightly higher sensor responses for the alkaline compounds. In the same way hydrophobic interactions can be excluded, because also n-octane hardly shows any sensor response. Therefore the driving force for recognition in this case is governed by the vapor pressure of the analyte compound as long as it is slightly hydrophilic: Table below on the bottom of this page summarizes that data: 1-Octanol with the lowest vapor pressure leads to the largest results indicating condensation on the NP surfaces. The vapor pressures for n-octane, acetic acid and ethylenediamine are almost the same. Nonetheless their sensor responses substantially differ. Especially the alkane leads to much lower sensor responses than expected once more emphasizing the slightly hydrophilic character of the particles. When comparing the two amines, one can see that the more alkaline and heavier one again leads to somewhat larger sensor responses.

Analyte	Vapor pressure, mmHg 20°C
1-Butanol	5,5
n-Octane	11
1-Octanol	0,14
Acetic acid	11,4
Ethylenediamine	10
Triethylamine	51,75

Molecularly imprinted polyurethane

In previous investigations the electrodes of QCM were coated with pure titania nanoparticles. We also tested polymer composites on QCM for mass-sensitive measurements to assess both sensitivity behavior as well as potential changes in selectivity. As a base for such composite materials we chose polyurethane-based molecularly imprinted polymers from previous

work [51], imprinted with 1-butanol. The respective monomers are summarized in **Figure 36**. The synthesis of the respective polymer followed the procedures in that paper. The working electrode was coated with 1-butanol MIP, and the reference- with non-imprinted polymer.

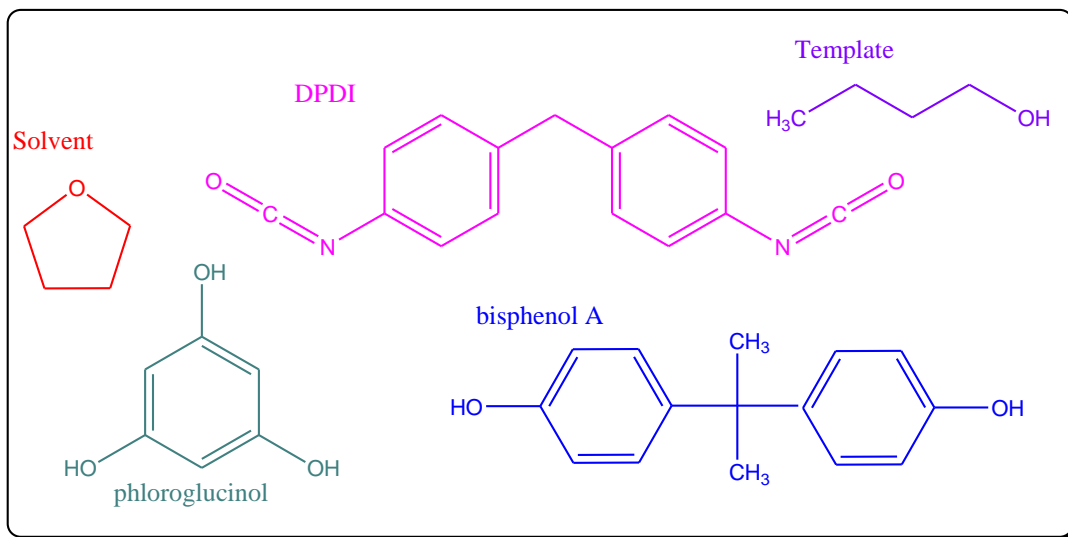


Figure 36 Compounds used for MIP PUR synthesis

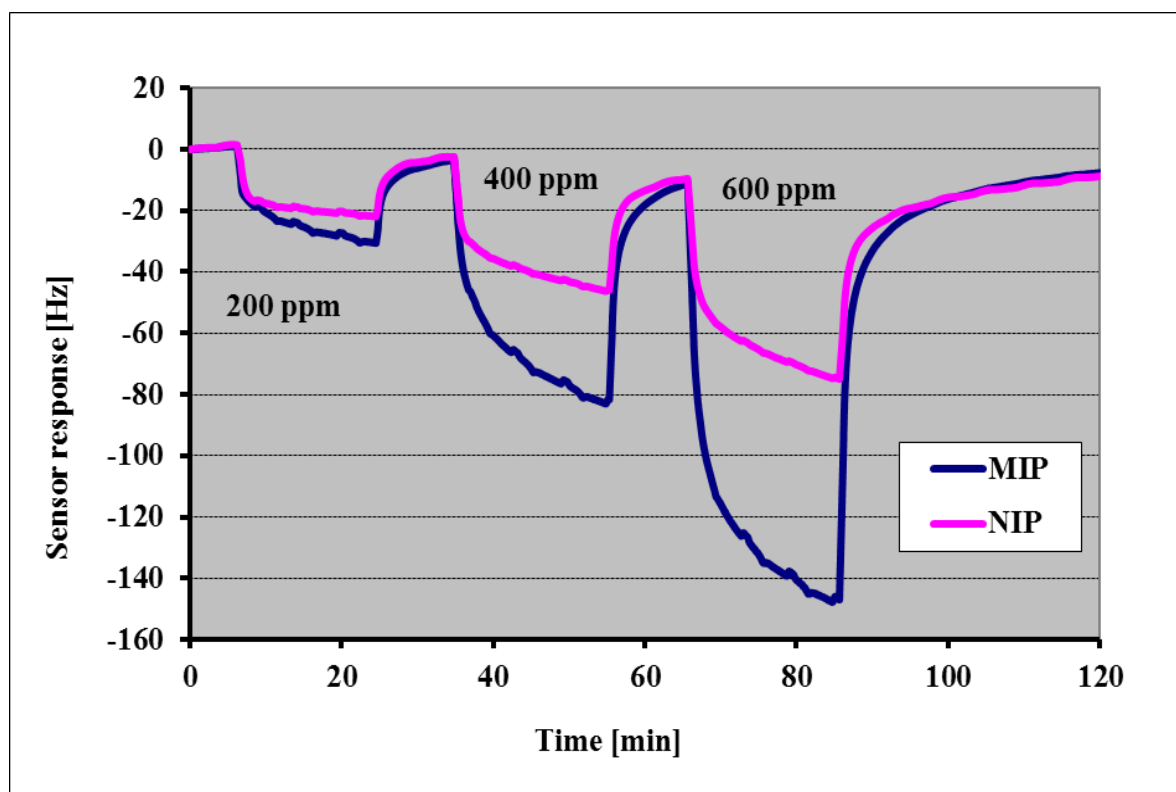


Figure 37 Sensor response of 1-butanol imprinted PUR towards 1-butanol

The sensor characteristic of a sensor towards 1-butanol, when exposed to the following vapor concentration: 200, 400 and 600 ppm, respectively, is shown in **Figure 37**. Obviously, there the base line is stable without discernible noise and only slight fluctuation when the system is exposed to 1-butanol. Those fluctuations are again caused by the gas supply, because both channels are concerned. When the sensor is exposed to the analyte the frequency changes on both electrodes. The sensor response of the working electrode is noticeably larger than sensor response of reference electrode, namely by a factor of 2. The sensor characteristic represents a reversible signal, which depends on 1-butanol vapor concentration.

Following this experiment, the sensor responses towards 1-octanol are of course of special interest, because this compound lead to the highest sensor responses with titania nanoparticle sensors. **Figure 38** shows the outcome of this:

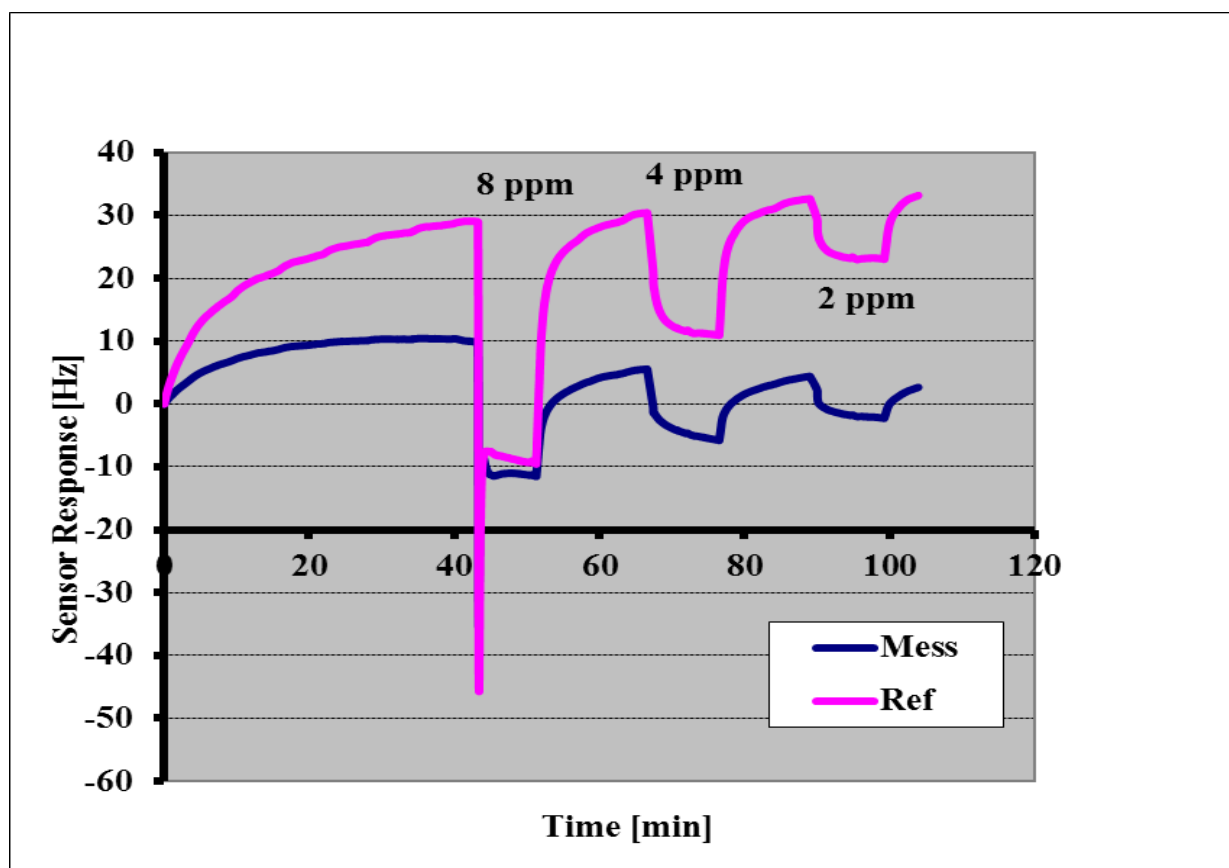


Figure 38 Sensor response of 1-butanol imprinted polyurethane against 1-octanol

Surprisingly the reference electrode yields larger response towards the analyte than the working electrode. There are two possible explanations of this phenomenon. First, the behavior of the NIP signifies the affinity between the surface and the analyte without geometrical constraints. Secondly, the pores in the MIP as well as diffusion pathways are obviously too narrow or small for the long 1-octanol molecules to pass. Therefore efficient exclusion of the analyte from the polymer matrix occurs. As a result exposing the sensor towards 1-octanol vapors yields smaller sensor effects on the working electrode, coated with the imprinted polymer. The phenomenon presented in Figure also clearly proves the consistency of the molecular imprinting approach for the polymer system under investigation.

MIP selectivity

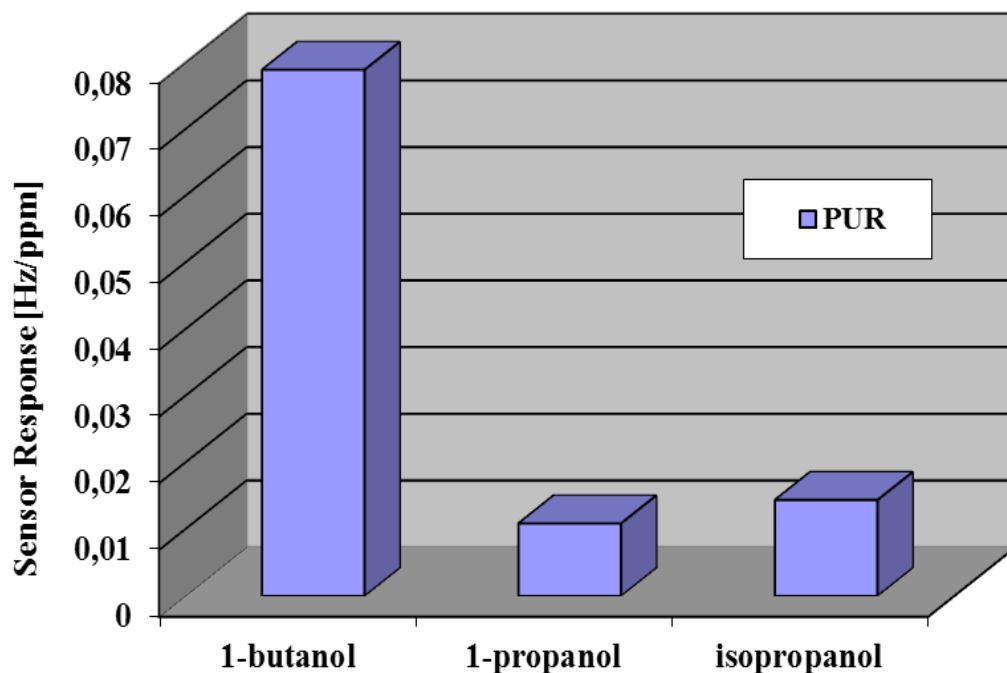


Figure 39 Selectivity pattern of 1-butanol imprinted polyurethane PUR

Figure 39 summarizes the selectivity of the MIP-based sensor. As can be seen, 1-butanol is preferred by the sensor, as expected. The sensor

response towards 1-butanol is 7 times higher than towards 1-propanol and about 6 times higher than for isopropanol, which means that the sensor shows minute interactions with these compounds proving the selectivity towards 1-butanol. It is somewhat surprising, however, that the response towards isopropanol is larger than for 1-propanol, because the respective molecular configurations (linear against branched) would suggest differently. However, the differences in sensor response are very low (isopropanol-0.014 Hz/ppm and 1-propanol 0.01 Hz/ppm), so they cannot be regarded statistically significant.

PUR+TiO₂ Nanocomposite material

Finally, the titania NP and the MIP were combined to form a nanocomposite containing 50% (m/m) titania nanoparticles plus 50% (m/m) 1-butanol imprinted polymer PUR.

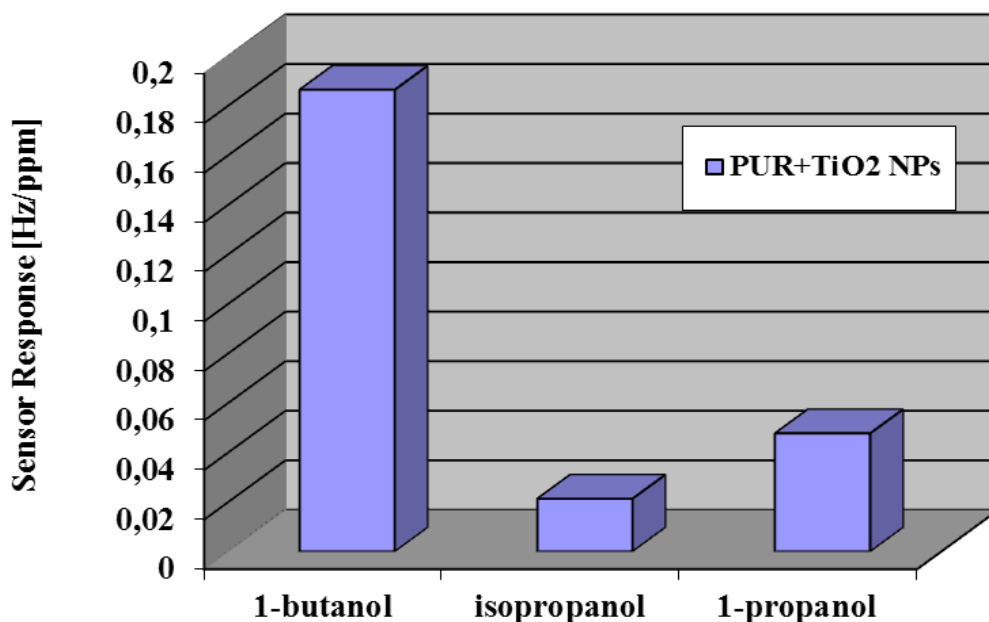


Figure 40 Selectivity pattern of composite material PUR+TiO₂ NPs

It was coated onto the surface of the working electrode, whereas the reference electrode was left uncoated. In principle again the same measurement strategy was applied. As can be seen in **Figure 40** 1-butanol is still preferred by the sensor. In this system one can observe 2.35 times higher sensor response towards 1-butanol, than the similar response in the MIP system (0.186 Hz/ppm against 0.079 Hz/ppm). Therefore combination of nanoparticles and polymer MIP leads to substantial interaction. Isopropanol yields the smallest effect (8.8 times lower than for 1-butanol) because of its branched structure. One reason for the better selectivity between the two propanol isomers can be the fact that the templating procedure lead to more well-defined cavities in this case.

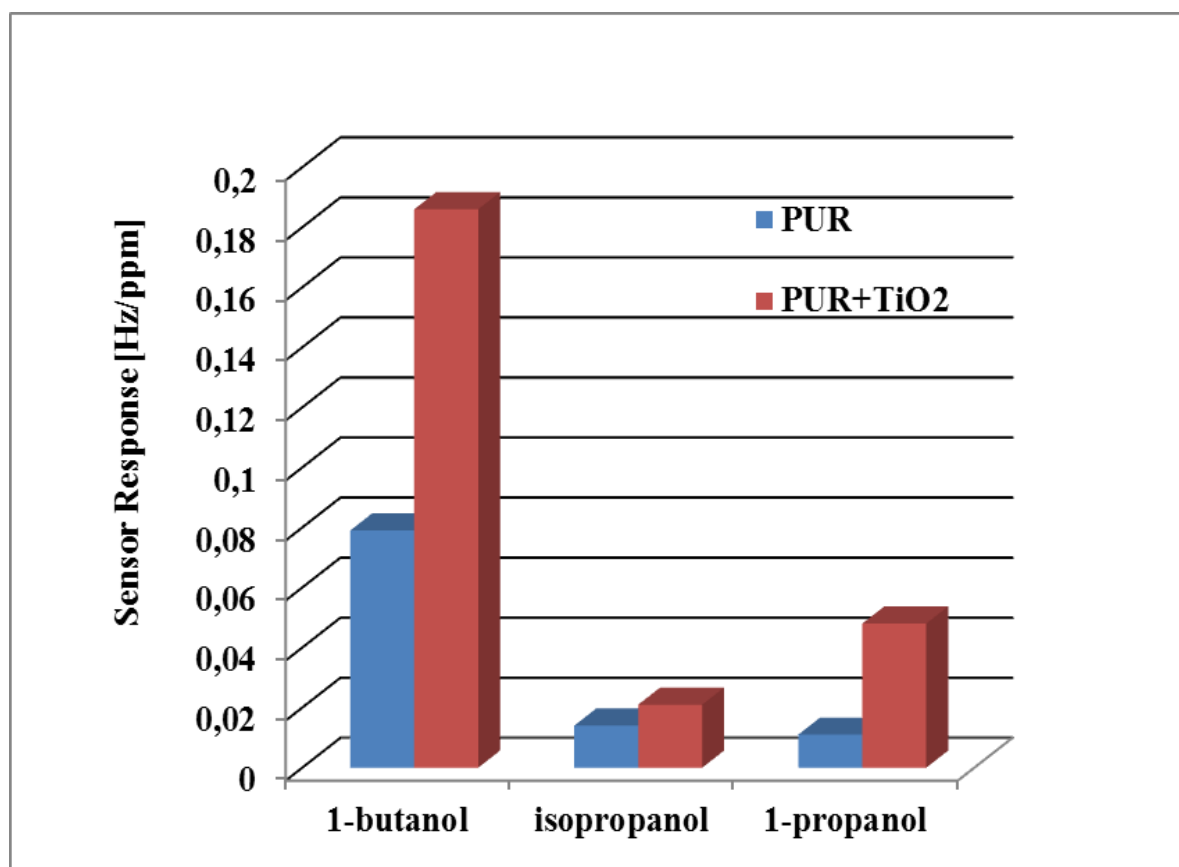


Figure 41 Comparison of sensitivities of imprinted PUR and the MIP-NP composite material.

Figure 41 compares the sensitivities obtained by the two materials, i.e. the PUR, imprinted with 1-butanol, and the nanocomposite (MIP PUR+NP). The data are normalized by layer height. Here, it can be seen that the effects of the nanocomposite exceed the effects of the polymeric system not only in case of 1-butanol (2.35 times higher), but also with isopropanol (1.5) and 1-propanol (4.36). This is the more surprising given the fact that in the case of purely additive effects, the polymer composite should show the average sensor responses of the two different systems. However, the signals are more than two times higher in this case.

PUR (non-imprinted) +TiO₂ Nanocomposite material

Further evidence proving the successful MIP approach is shown in **Figure 42**. There one can see sensor responses of a QCM, whose working electrode is coated with a composite, consisting of 50 mass percent non-imprinted polyurethane and 50 mass percent titania nanoparticles. The reference material is the respective NIP. The sensor is exposed to 200, 400 and 600 ppm of 1-butanol in dry air, respectively. The responses of both channels are identical when the sensor is exposed to mentioned concentrations of the analyte. The NIP hence shows some interaction, but the nanoparticles do not yield any additional signal. Therefore possible affinity interaction between the butanol and the nanoparticles – as observed with the pure nanoparticles – is blocked by the non-porous NIP. This is a somewhat expected result (**Figure 35** Selectivity pattern of TiO₂ nanoparticles, where normalized sensor response of TiO₂ towards 1-butanol is about 0.07 Hz/ppm). This strongly suggests that the NIP is not porous and hence does not offer substantial diffusion pathways into the material.

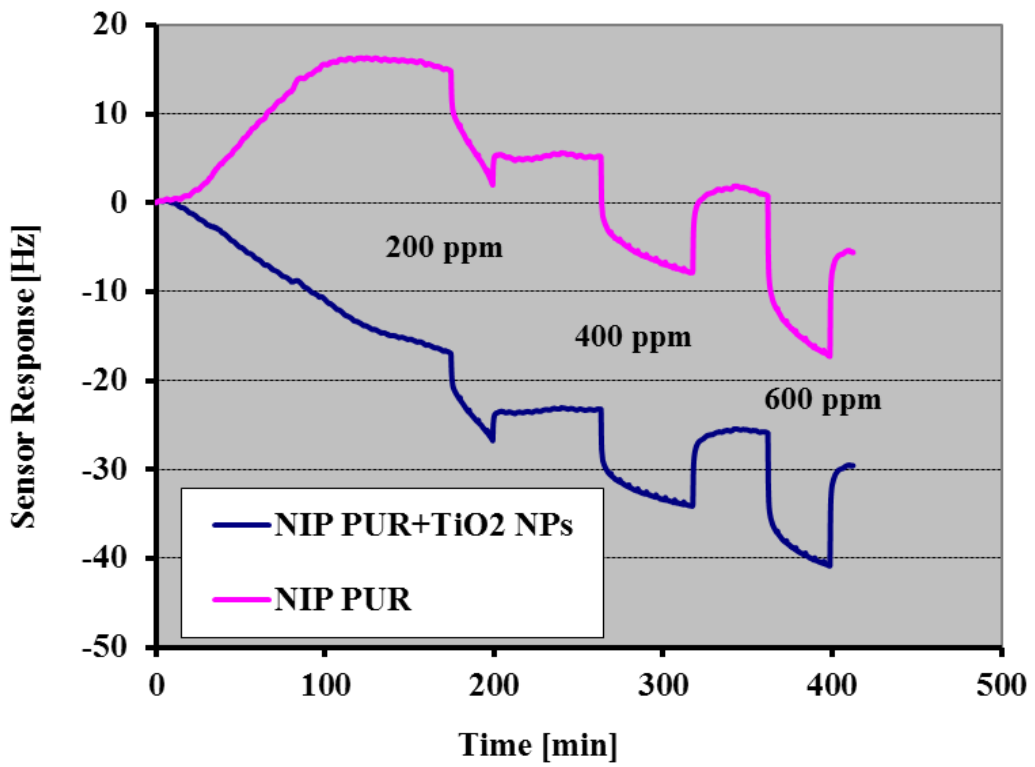


Figure 42 Sensing of 1-butanol with nanocomposite on the base of non-imprinted PUR

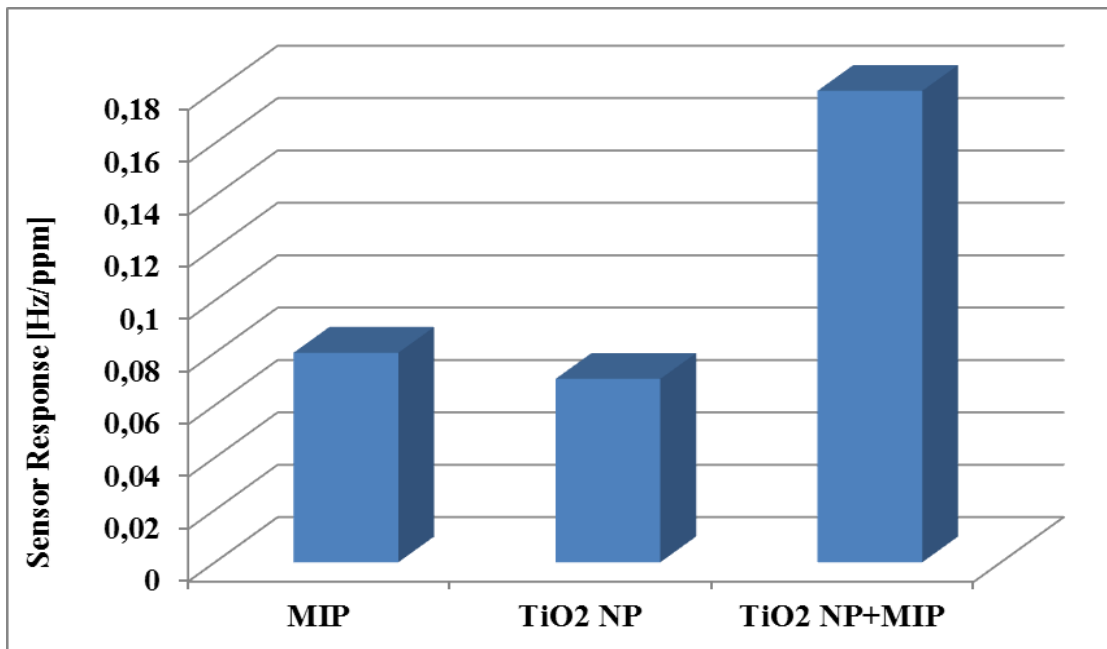


Figure 43 Sensitivity comparison of PUR MIP with TiO₂ NPs and nanocomposite on the base of imprinted PUR

In **Figure 43** “MIP” denotes the normalized sensor response of the polymer system towards 1-butanol, “TiO₂” - the sensor response of titania nanoparticles towards the analyte and “TiO₂ + MIP PUR” the response of nanocomposite, when exposed to 1-butanol. One can see, that nanocomposite material gives more than 2 times larger responses (2.25 times higher than polymer system and 2.57 times greater than titania NP). This phenomenon can be explained as a preconcentration effect (50-50): interaction takes place both in the MIP and on the particle surfaces. The fact that the sum signal is larger than its parts indicates that the MIP increases the analyte concentration in the immediate vicinity of the nanoparticles thus leading to higher affine effects. This overcompensates for less affine recognition sites within the MIP (high affine ones are expected to be occupied anyway).

SiO₂ NPs

In addition to the titania nanoparticles a silica material was studied, also to gain some insight into the sensor behavior of them and compare the effects with the TiO₂ system. Some aspects leading to this interest are possible minor differences in hydrophilic properties between the two matrices as well as slight differences in acid/base behavior.

In the same way as in the case of titania nanoparticles, also the silica material obviously interacts with organic solvent vapors (see **Figure 44**). Again the working electrode of sensor is covered with silica nanoparticles, which is measured against “naked” gold electrode. The silica NP sensor was exposed to the same analytes, as their titania counterparts: 1-butanol, n-octane, 1-octanol, acetic acid and triethylamine.

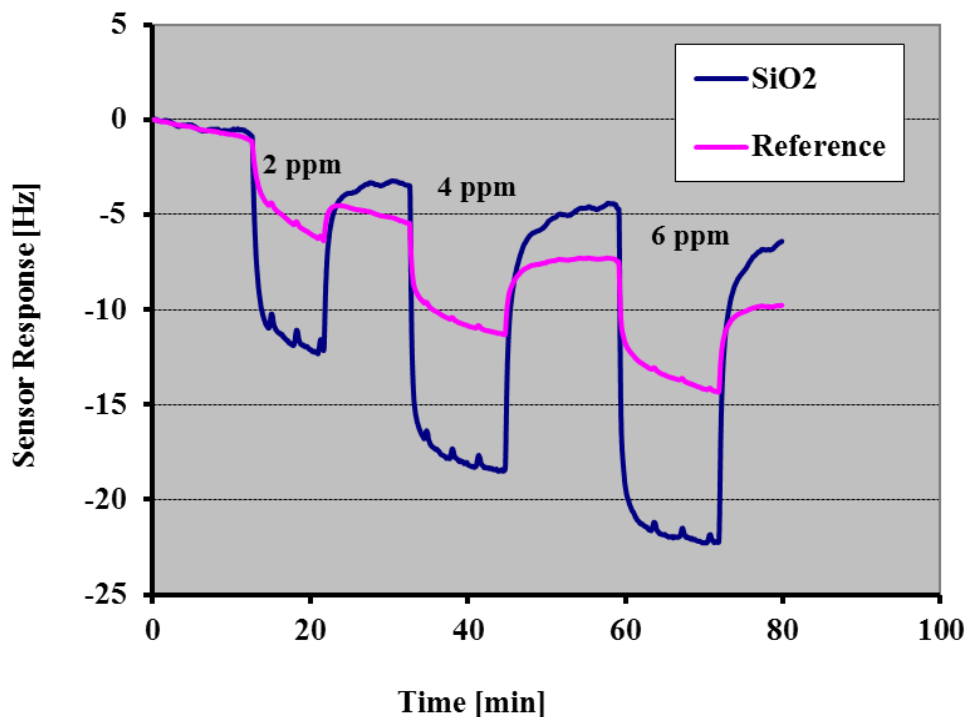


Figure 44 SiO₂ nanoparticles sensor signal against 1-octanol

Figure 44 again shows the responses towards 1-octanol: this alcohol was chosen as the analyte, because the effects towards 1-octanol were the highest in the TiO₂ system. Again, comparably low detection limits can be reached (in the range of 1 ppm or even slightly below that) and the sensor responses depend on concentration and are reversible.

Comparing the silica material with titania nanoparticles in **Figure 45** (all sensor effects are normalized against layer height), one can see that again 1-octanol gives highest effect, but affinity of silica material is only about 60% as compared to TiO₂. This can be explained the low vapor pressure of 1-octanol (the table on page 37). Furthermore, **Figure 45** clearly reveals that the sensor response towards 1-octanol again stands out enormously from the signal of the other analytes leveling out their differences. So for further assessing the interaction mechanism, this column is left out and only the sensor responses towards the other analytes, i.e. butanol, octane, acetic acid and triethylamine are considered in more detail. (**Figure 46**)

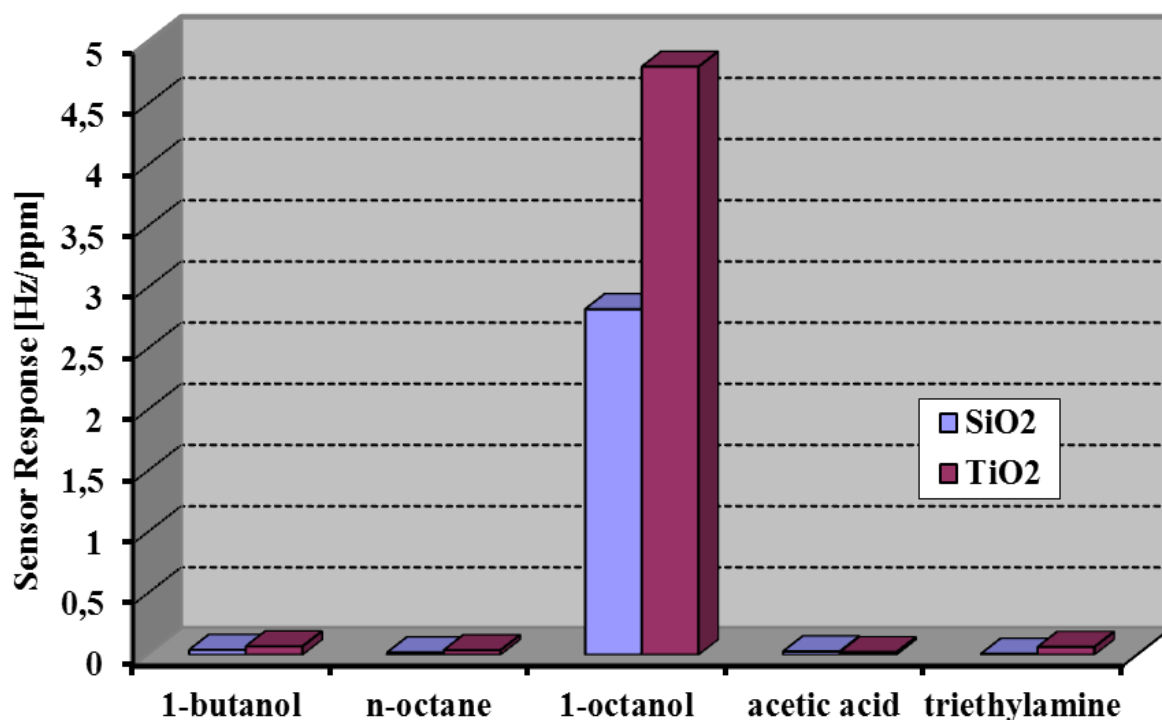


Figure 45 Comparison of sensor responses of SiO₂ with TiO₂ NPs

Overall both systems show amphiphilic properties, but titania nanoparticles seem slightly sour in gas reactions, which is indicated by the larger effects for the amine (sensor response of TiO₂ is about 7.3 times higher than the same parameter for SiO₂). Silica nanoparticles are slightly more basic, what can be seen by the effects for acetic acid (SiO₂ effect is 0.028 Hz/ppm, TiO₂ effect is 0.021 Hz/ppm) and triethylamine. Summarizing the effects of both systems, one sees that 4 analytes (1-octanol, n-octane, 1-butanol and triethylamine) out from 5 yield higher sensor signals in TiO₂ system. Speaking of 1-butanol (potentially interesting candidate for nanocomposite material), the analyte response is 0.069 Hz/ppm with titania and 0.04 Hz/ppm with silica. Therefore, it was decided not to prepare a nanocomposite material on the base of SiO₂ nanoparticles.

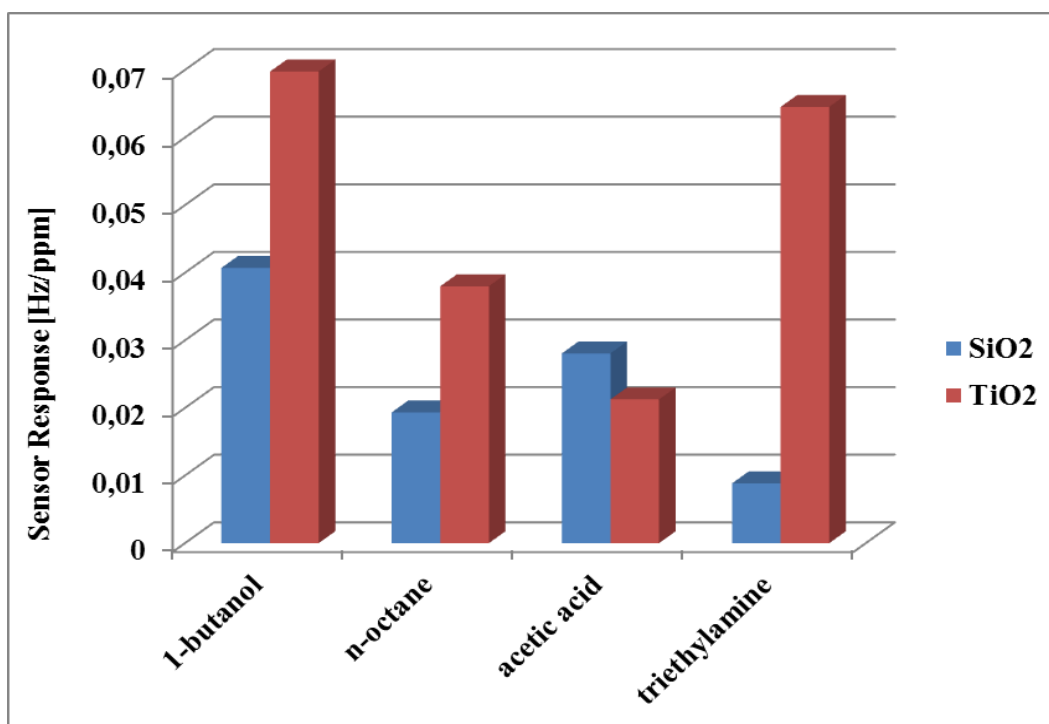


Figure 46 Selectivity pattern SiO₂ and TiO₂ NPs, respectively, without 1-octanol

3 Formaldehyde Sensing with MIP Nanoparticles

3.1 Introduction

Formaldehyde (CH_2O ; molar mass 30.03 g mol^{-1}) is the simplest aldehyde (**Figure 47**), gaseous at room temperature (boiling point -21°C); colorless, with strong smell, soluble in water (400 g dm^{-3}). The solution containing 37% (m/m) formaldehyde in water is called formalin. Normally about 10-12% of methanol is added to formalin solutions as a stabilizer.

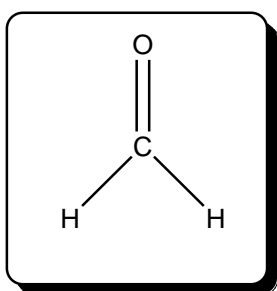


Figure 47 Formaldehyde structure

The planar formaldehyde molecule is highly reactive. In aqueous solution formaldehyde forms the hydrate methanediol (**Figure 48**):

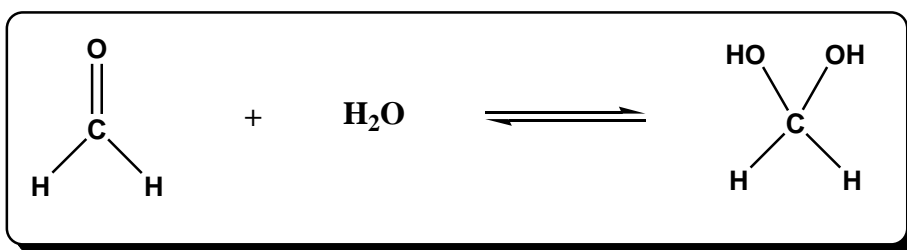


Figure 48 Reaction of formaldehyde with water

Formaldehyde was discovered by the Russian chemist Aleksandr Butlerov in 1855 and after 14 years first synthesized by the German August Wilhelm von Hofmann.^[53] In industry formaldehyde is produced by catalytic oxidation of methanol (mostly on metallic silver) (**Figure 49**):

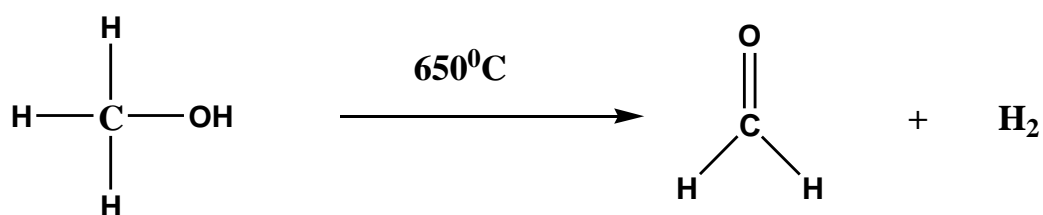


Figure 49 Oxidation of methanol

There are also natural sources of formaldehyde: it is produced in the atmosphere from alkanes and by all living organisms endogenously,[54] as depicted in **Figure 50**.

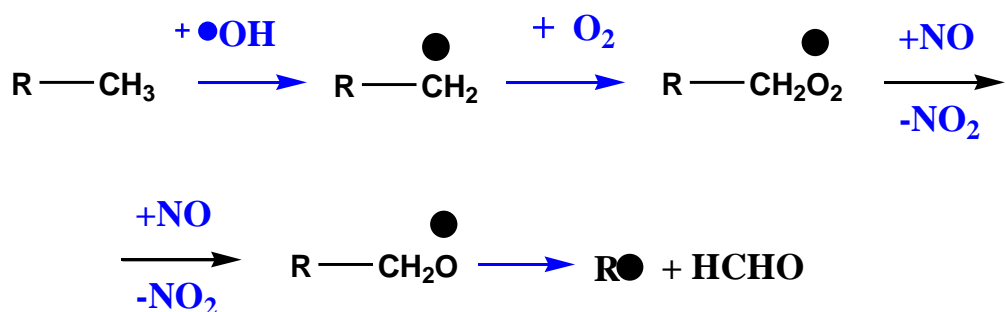


Figure 50 Formaldehyde synthesis from alkane in the atmosphere, adapted from [53]

In 1931 formaldehyde- and urea-based Kaurit glue appeared and immediately attracted interest in wood-processing industry. Due to its low cost this new product thus initiated the broad use of such materials as veneers, plywood and flake boards. Formaldehyde found its application not only in building materials industry, but also in producing household products such as paper, napkins, furniture, carpets, leather products [55] etc. One of the interesting properties of formaldehyde is its ability to kill viruses and bacteria, which explains its wide application as an industrial disinfectant and - sometimes in the form of derivatives - in medicine and cosmetics [56, 57] **Figure 51** shows dimethyloldimethyl hydantoin: this substance is a representative of the family of formaldehyde releasers, commonly used in cosmetics products to prevent the growth of microorganisms.

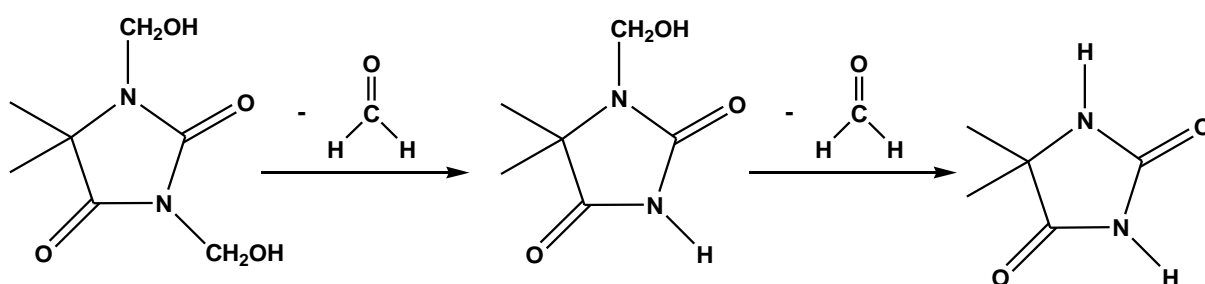


Figure 51 The release of formaldehyde from dimethyldimethyl hydantoin (DMDMH)

Due to its numerous types of application, formaldehyde is one of the most important and widely produced industrial organic chemicals with annual world production reaching over 30 million tons. [53]

3.1.1 Toxicity

In the beginning of the 1960s, formaldehyde attracted attention as an indoor pollutant. Household products made of press-wood materials release toxic formaldehyde vapor [58, 59, 60, 61], which plays a contributory role in sick building syndrome (SBS) [62, 63, 64]. SBS is characterized by symptoms occurring when humans spend extended periods of time in contaminated and unventilated indoor environments and hence suffer prolonged low-level formaldehyde exposure, thereby increasing the risk of related health issues.

As a highly reactive and water-soluble compound, formaldehyde is absorbed by the respiratory system, causing nasal, throat and especially eye irritation (watery eyes). To avoid the last one, the concentration of formaldehyde should not exceed 0.3 ppm in indoor environments. Formaldehyde can also be a reason for allergic reactions and cancer. [53] Although it is considered a typical indoor air pollutant, formaldehyde is increasingly becoming a serious problem of outdoor air pollution in large industrial cities. Nonetheless, taking into account the fact that people inhale most formaldehyde in-

doors, simply because of spending more time in closed rooms than outdoors, it is still very important to exclude using formaldehyde-emitting materials, or at least to minimize them and develop energy-efficient home ventilation systems. [53]

3.1.2 Formaldehyde Sensing: few examples

Formaldehyde, being on the one hand a widely used chemical compound, but on the other hand a hazardous air pollutant and human carcinogen, has hence to be effectively detected and monitored in both indoor and outdoor environments, ideally by the means of inexpensive, stable and portable low-power devices that allow for straightforward operation. Instrumental analytical methods including gas and high-performance liquid chromatography, spectrophotometry and polarography are hardly suitable for real-time formaldehyde measurements, because these methods require both off-line laboratory and trained staff.

Already in the mid-1980s it was possible to detect some pollutant gases with commercialized electrochemical sensors reacting with the gas of interest and providing a concentration-dependent signal. The main disadvantage of those systems was their limited lifetime, defined as the sum amount of target gas the sensor could be exposed to. [65] Furthermore, as detecting formaldehyde is an essential part of health care, also some other progress in formaldehyde sensing has been achieved, mainly in the field of receptor-based and transducer-based sensors. In 1996 for instance a potentiometric sensor for formaldehyde detection was developed (**Figure 52**). This system required to expose the surface of an ion-selective field effect transistor (ISFET) to formaldehyde dissolved in water. There the formaldehyde was catalytically decomposed by aldehyde dehydrogenase followed by detecting the changing proton concentration by the ISFET. The detection limit of the sensor was about 0.1 ppm and its lifetime up to several months.

However, detection includes at least two steps, namely which makes the operation of the system rather complicated.

Other small-scale formaldehyde receptors or transducers are presented in the Table below (adapted from [65])

Year	Authors	Functional Principle	Sensing materials	Sensitivity Measurement Range
2003	Suzuki	Receptor	Colorimetric reagents	0.13 a.u./ppm 0-1.0 ppm
2007	Seo	Receptor	Mercaptophenol	0.37 mV/ppm 0.027-2.7 ppm
2007	Lee	Transducer	NiO	0.33 Ω /ppm 0-30 ppm
2008	Achmann	Transducer	Enzyme	390 nA/ppm 0.5-15 ppm
2008	Lv	Transducer	SnO ₂ -NiO	0.53 ppm ⁻¹ (R _a /R _g) 0.06-0.3 ppm
2008	Bai	Transducer	ZnO	10.6 a.u./100 ppm 0-100 ppm
2008	Wang	Transducer	NiO-Al ₂ O ₃	70 Ω /ppm 0-15 ppm
2009	Chu	Transducer	ZnO	2.11 ppm ⁻¹ (R _a /R _g) 1-10 ppm
2009	Peng	Transducer	ZnO	0.04 μ A/ppm 0-50 ppm
2010	Xie C	Transducer	ZnO-MnO ₂	1.02 a.u./ppm 10-300 ppm
2011	Han	Transducer	ZnO	10 a.u./ppm 0-200 ppm
2011	Castro-Hurtado	Transducer	NiO	2.53*10 ³ Ω /ppm
2011	Zhang	Transducer	ZnO	0.564 ppm ⁻¹ (R _a /R _g) 1-1000 ppm

2011	Descamps	Transducer	Fluoaal-P	$1.2 \cdot 10^{-5} \text{ Vs}^{-1}/\text{ppb}$ 0-200 ppb
2012	Castro-Hurtado	Transducer	SnO_2	10 M Ω/ppm 0.5-15 ppm
2012	Deng L	Transducer	WO_3	$3.7 \cdot 10^{-10} (\Omega\text{s})^{-1}/\text{ppm}$ 10-100 ppm
2012	Deng B	Receptor	$(\text{NH}_3)_2\text{SO}_4$	0.48-96.000 mg/m^3
2012	Xie H	Transducer	Carbon nanotube	$0.4 \text{ ppm}^{-1} (R_a/R_g)$ 0-50 ppb

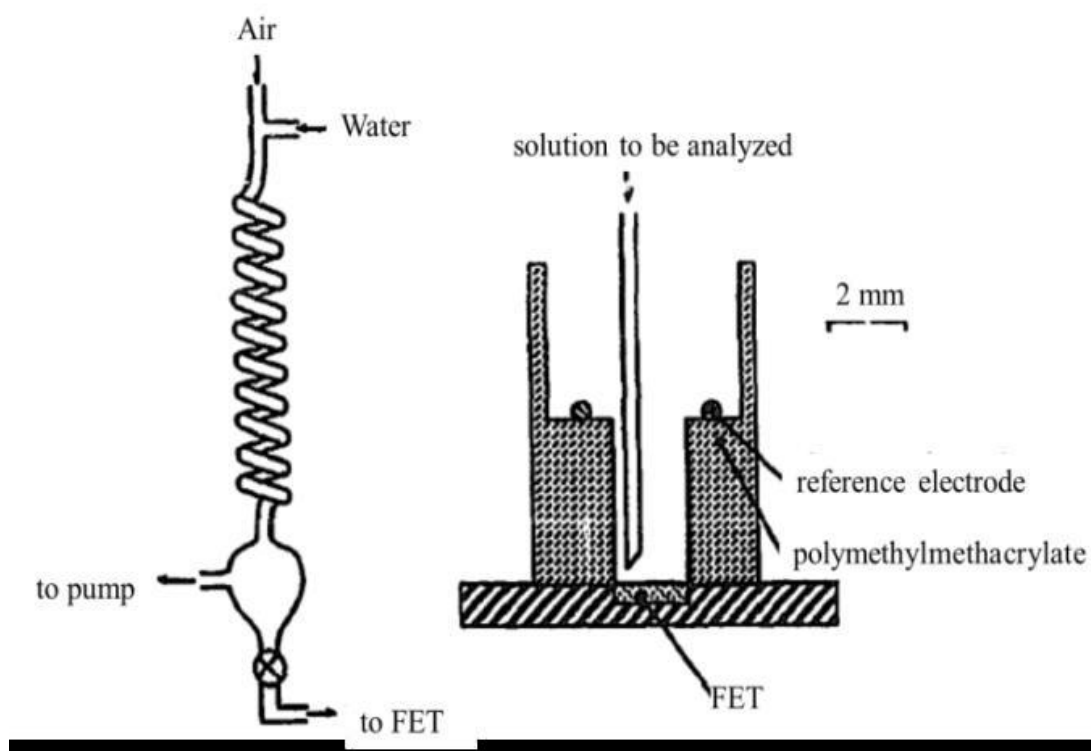


Figure 52 Schematic illustration of FET-based detection of gaseous formaldehyde. Reproduced from [65]

3.2 Experimental

3.2.1 Materials

Styrene, methacrylic acid, ethylene glycol dimethacrylate EGDMA, allylamine, methanol, dimethylformamide, AIBN, acetonitrile and formaldehyde (36.5 % puriss. p. a.) were purchased from Merck and Sigma-Aldrich with the highest available purity and used as received. QCM were produced exactly the same way like already described in chapter 2.2.2.

For synthesis of all MIP and NIP we used UV-initiated polymerization at room temperature, because this approach turned out more suitable for these systems than thermal polymerization. When polymerizing by UV irradiation one can control the exact polymerization time by changing the distance between the reaction tube and the UV source. The smaller it is, the faster the reaction proceeds. [66]

3.2.2 Synthesis of Molecularly Imprinted Polymer

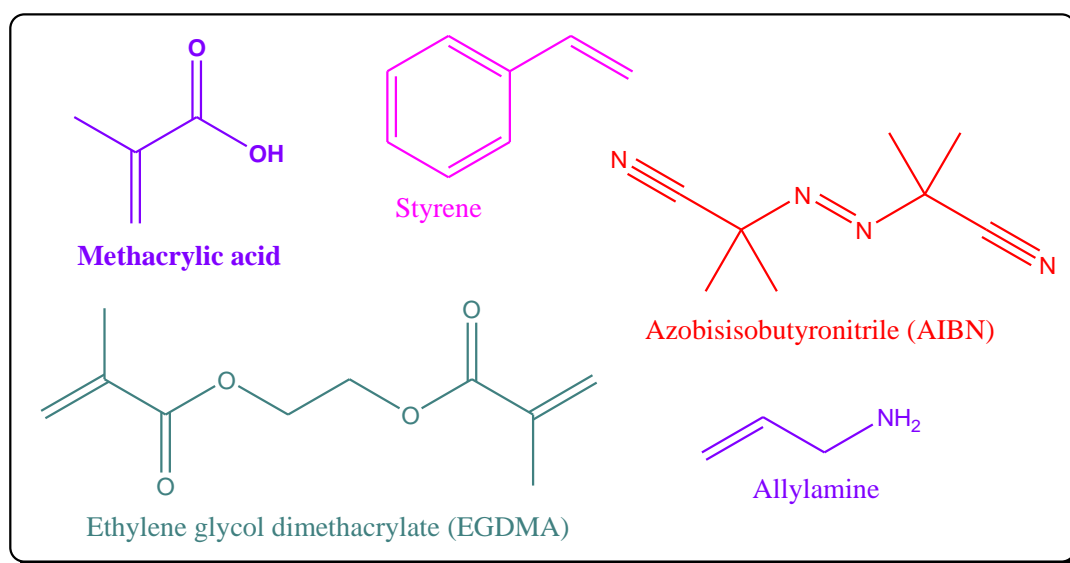


Figure 53 Chemicals used for MIP synthesis including monomers cross-linker and radical initiator

13 mg each of methacrylic acid, styrene and allylamine (Figure 53), respectively, lead to the monomer mixture, to which we added 60 mg of cross-linker EGDMA (ethylene glycol dimethacrylate). The mixture was stirred for ~15 minutes. Then 15 μ L of formalin solution was added to the

mixture followed by 500 μL of a mixture containing 200 μL methanol +300 μL dimethylformamide. After adding each component the mixture was stirred until forming a homogeneous solution. Finally, 6 mg AIBN we added to the reaction mixture followed by polymerizing under UV (λ_{max} 360 nm; 210 W) for 1 hour until just prior to the gel point. These oligomer batches were used for generating nanoparticles by precipitation techniques. For that purpose the prepolymer resulting from the previous steps was added to 10 mL acetonitrile and the suspension was stirred overnight at room temperature. Afterwards the suspension of NPs in solvent was centrifuged at 4000 rpm 10 min. After that the initial solvent was removed and NPs were washed two times with the fresh acetonitrile by consecutive steps of resuspension and centrifugation For QCM coating first the cleaned NP were suspended in 4 ml acetonitrile. Then, we added 4 ml AcCN to 1 ml of this suspension to reach the final coating solution.

3.2.3 Optimization of formalin measurements

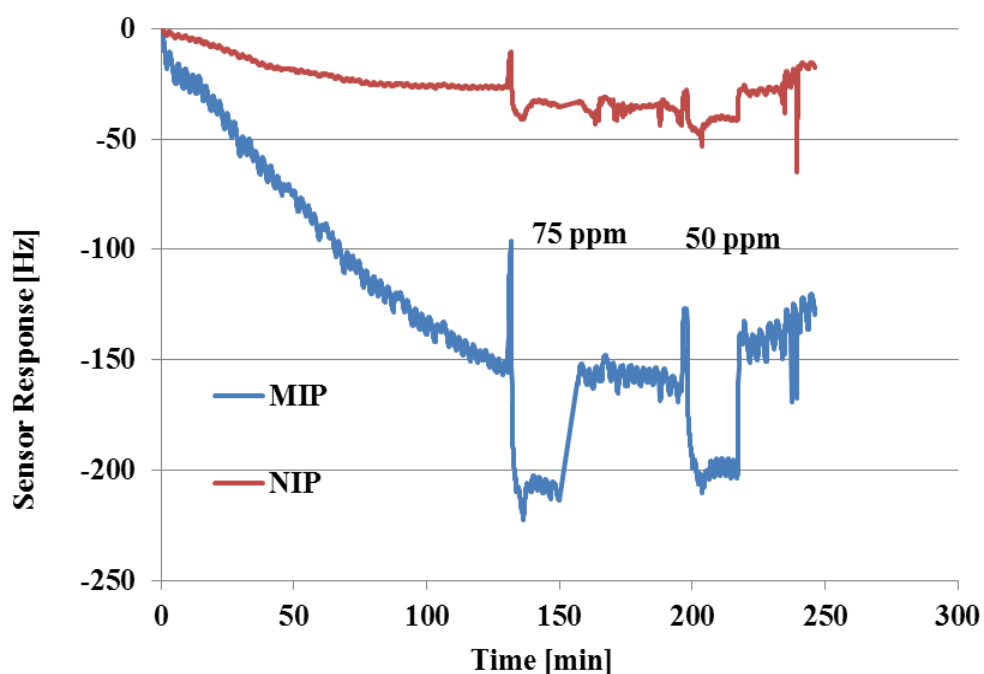


Figure 54 Sensor Responses of MIP NP sensor towards formalin with base line obtained in air with 100% humidity

The main limitation of formalin measurements is that formaldehyde is available only in aqueous solution, the abovementioned formalin (37%). So it is not possible to use the pure compound under these circumstances. Therefore preliminary screening experiments were performed in order to assess the most suitable measuring protocol in this case. This included choosing the correct background. In principle, there are two options for that, namely: base line against 100% humidity and against dry air. However, before such first actual measurements it was of course unclear, how large the influence of humidity is. Hence this was assessed on one QCM. The nanoparticle-coated sensor was exposed to two concentrations of formaldehyde vapours: 75 and 50 ppm. For screening purposes, this is sufficient, because it immediately yields information on whether sensors react at all, are reversible and show dynamic behavior in that concentration range.

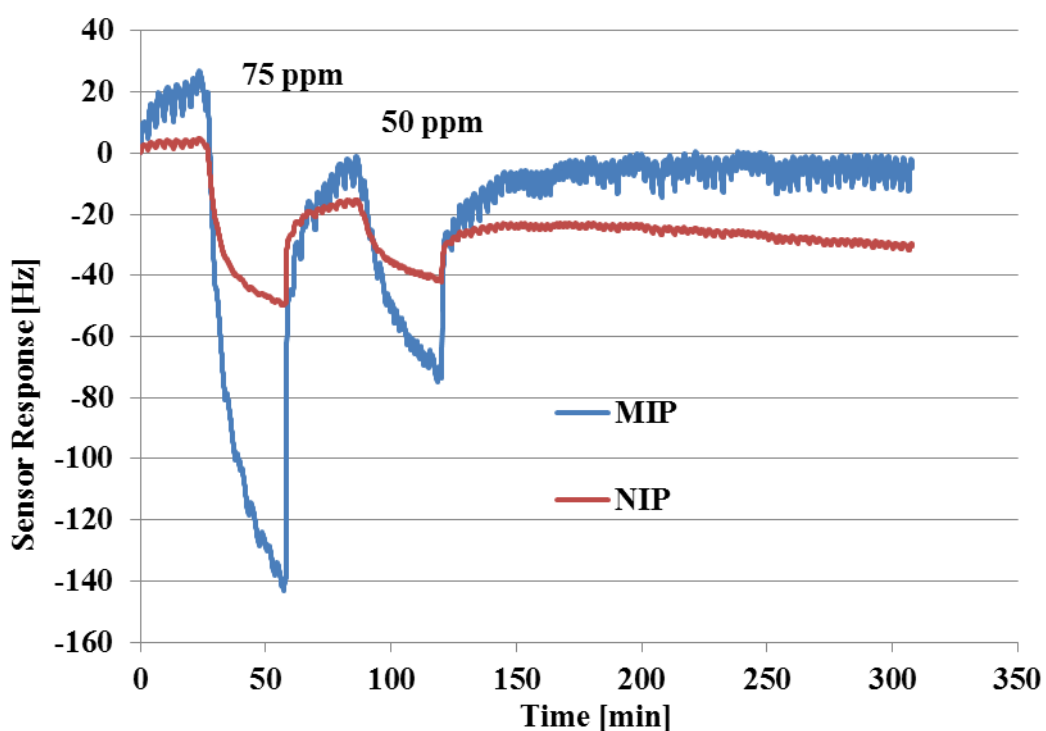


Figure 55 Sensor Responses of the NP sensors towards formalin with base line obtained in dry air

Figure 54 and **Figure 55** show the outcome of such measurement, **Figure 54** with 100% rH as the background and **Figure 55** with dry air. Afterward the resulting sensor responses were compared in the table below:

C, ppm	SR in Water,Hz	SR in Air, Hz	Δ , Hz
50	35	49	14
75	47	111	64

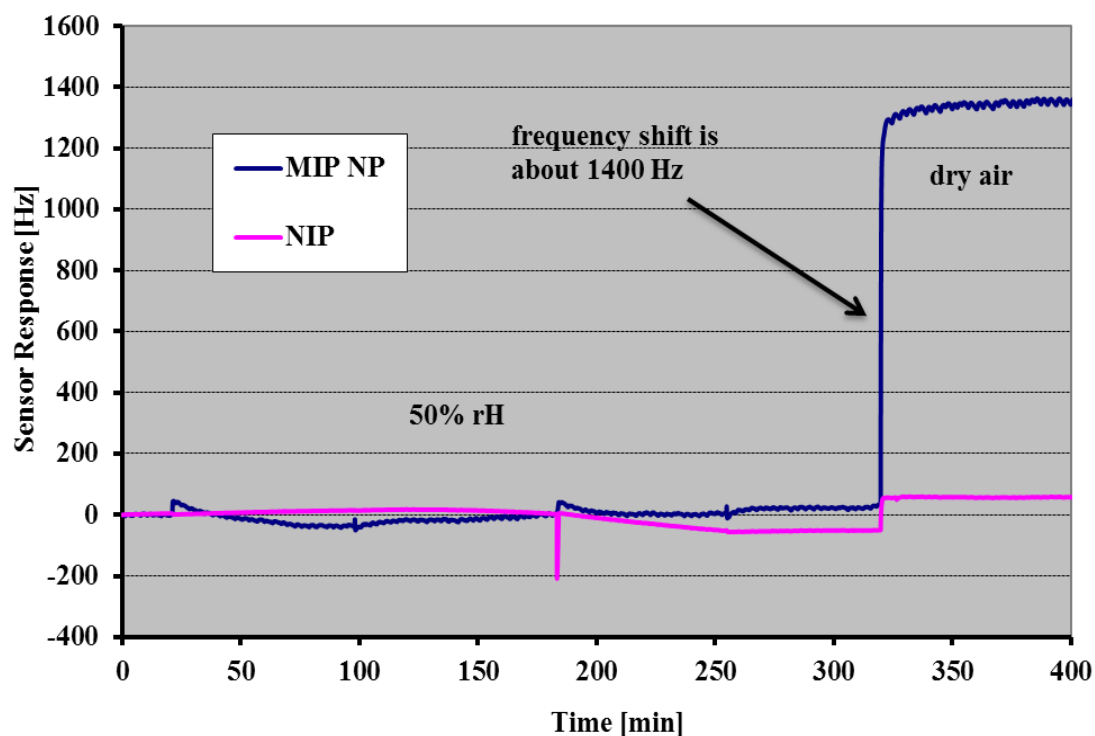


Figure 56 Frequency shift caused by the switching the system from 50% rH to dry air

Comparing the results one can see the difference between the sensor responses at the first glance: for 75 ppm the sensor response against dry air is twice as high as the sensor response with 100% humidity. This clearly indicates that the sensor layers do not only interact with formaldehyde, but also with water. Hence – expectedly - realistic sensor responses towards formaldehyde can only be obtained when measured against humid air. Therefore, all further measurements were obtained in an air stream mixing 1 liter of water-saturated air plus 1 liter of dry air per minute resulting in air streams containing 50% relative humidity. The substantial effect of water is further emphasized in **Figure 56**, which shows the large frequency shift about 1400 Hz when the system is switched from 50 % humidity to dry air.

The table below summarizes the setting on the gas mixing apparatus to generate samples with 25, 50 and 75 ppm formaldehyde in air at 50% rH. For reasons of simplification, it is assumed that the components of the formalin mixture evaporate proportionally to their content in liquid phase, i.e. disregarding any deviations from Henry's law. However, for first proof of concept such an approach is valid. Of course, final calibration of a possible commercial sensor would require a different approach.

C of Analyte, ppm	Air, L/min	Water, L/min	Analyte (Formalin), mL/min
25	1	0,96	29,2
50	1	0,94	58,4
75	1	0,91	87,59

3.3 Results and Discussion

3.3.1 Nanoparticle Characterization

Before evaluating the synthesized nanoparticles in sensing measurements, they were characterized via AFM. For that purpose 7 μL of the suspension was spin-coated onto a glass substrate. Afterwards the NP layer was dried at 60°C for 3 hours. The AFM image shows homogeneous distribution of particles. Particles show a mean diameter of 100-150 nm with some distribution of the particles (**Figure 57**). No substantial clusters can be found very clearly proving the feasibility of the preferred procedure to obtain homogeneous NP coatings on transducer surfaces.

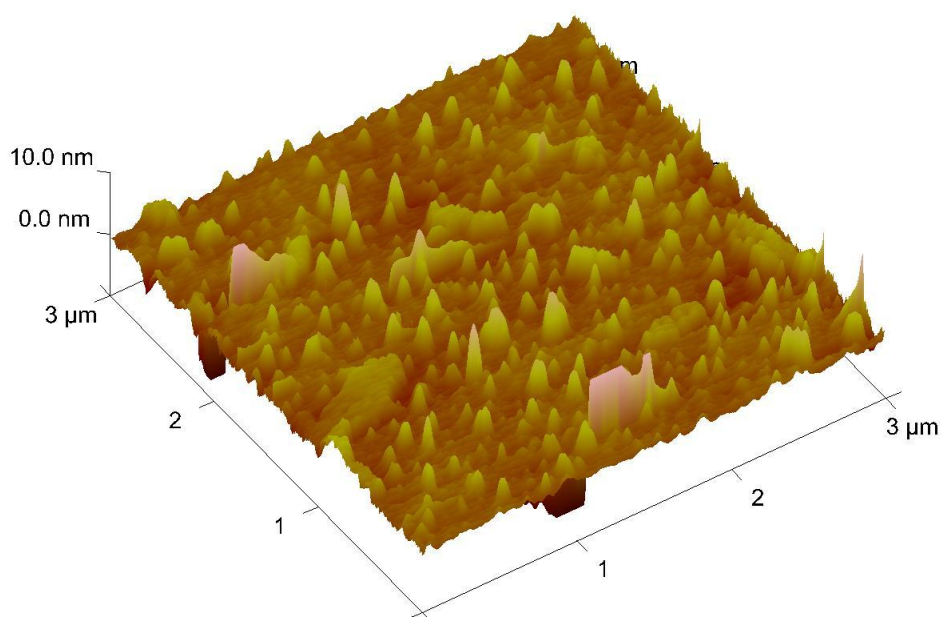


Figure 57 AFM image of MIP NP on a glass substrate

3.3.2 Mass sensitive measurements

Polymer thin film

First measurements with formaldehyde-imprinted polymer on QCM were performed with spin-coated thin films in order to assess the imprinting

effect (i.e. not with nanoparticle layers). A representative example is shown in **Figure 58** based on a copolymer of methacrylic acid, styrene and allylamine. In such a system one can expect hydrogen bond formation between formaldehyde molecules and the functional groups of these monomers.

One can clearly see that such an approach indeed leads to a receptor layer that can both reversibly bind formaldehyde and results in signals depending on the vapor concentration of this analyte. Furthermore, the MIP leads to substantially larger sensor effects, than the NIP, namely on average by a factor of 5.

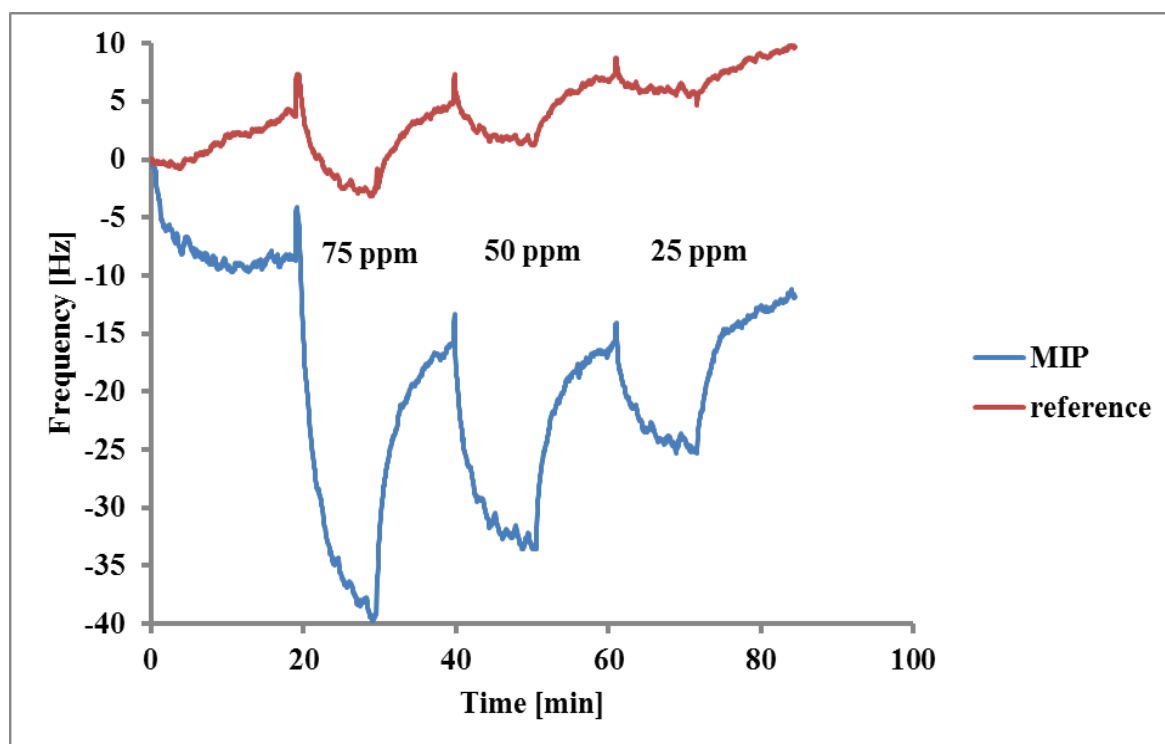


Figure 58 QCM sensor responses of MIP and NIP towards 75, 50 and 25 ppm respectively vapor concentrations of Formaldehyde (75 ppm-26 Hz)

Such a result is even more astonishing taking into account the fact that the formaldehyde molecule is a very small analyte and all monomers used are substantially bulkier. Nonetheless, self-organization in this case leads to sufficient structure-directing effects. Despite these promising results,

project requirements lead to abandoning the thin-film approach, because it is less suitable for mass production, than nanoparticle-based materials. All further measurements are therefore based on MIP NP. As for unclear reasons it turned out impossible to synthesize NIP nanoparticles, NIP thin films served as the references during further measurements.

Nanoparticles

Figure 59 summarizes the sensor responses for a nanoparticle sensor exposed to the same formaldehyde vapor concentrations as for the thin film.

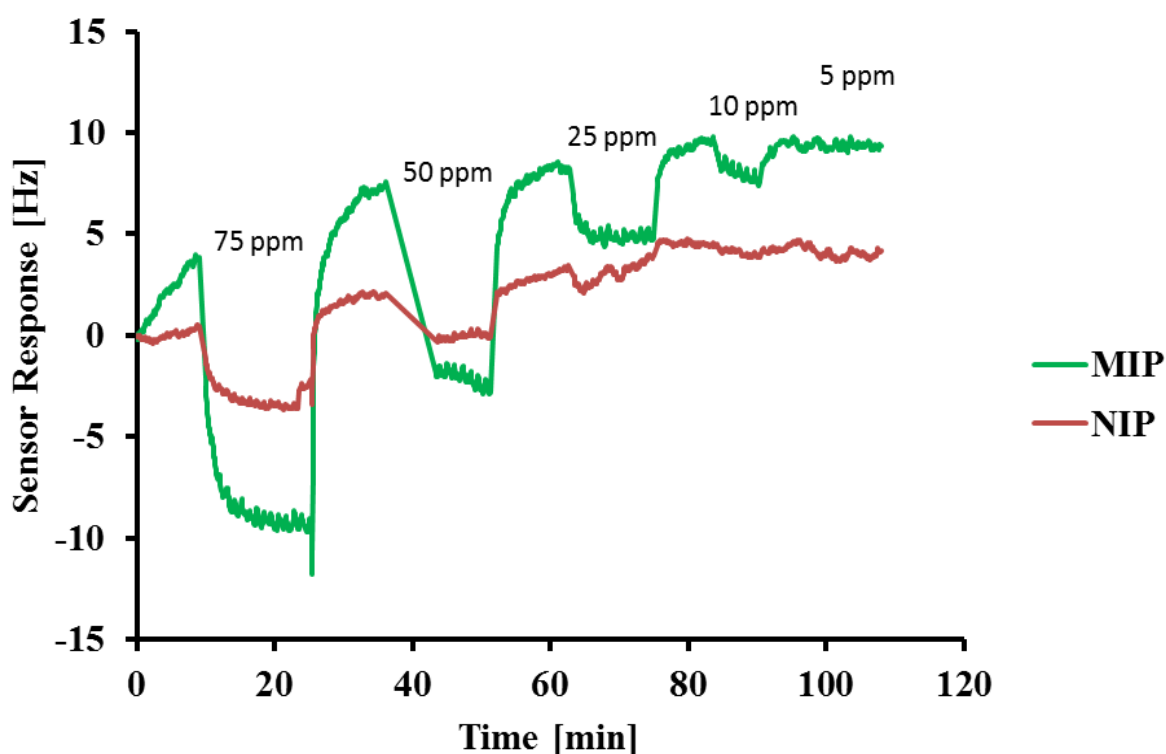


Figure 59 QCM sensor responses of MIP NP and NIP (polymer) towards 75, 50, 25, 10 and 5 ppm respectively vapour concentrations of Formaldehyde

Again, we observed mass effects, i.e. decreasing frequencies, namely -13 Hz at the MIP NP-coated electrode at 75 ppm. The reference electrode shows a frequency shift of -3 Hz, which means 23% from NPs electrode signal resulting in an overall sensor response of 10 Hz towards 75 ppm. To obtain the sensor characteristic, we hence exposed these sensors to air streams containing five different formaldehyde concentrations, ranging from 75 ppm to 5 ppm. At the lowest concentration, no sensor effect can be seen. However, at 10 ppm the MIP NP already lead to measurable frequency shifts (some 2 Hz). As the noise within the measurements is below 1 Hz, this shift is statistically significant. Overall, the detection limit of this measurement is hence ~10 ppm, following the regression parameters of the sensor characteristic as shown in **Figure 60**. This limit seems comparable high. However, taking into consideration the usual sensitivity of QCM and the small size of the formaldehyde molecule, it is a very appreciable result.

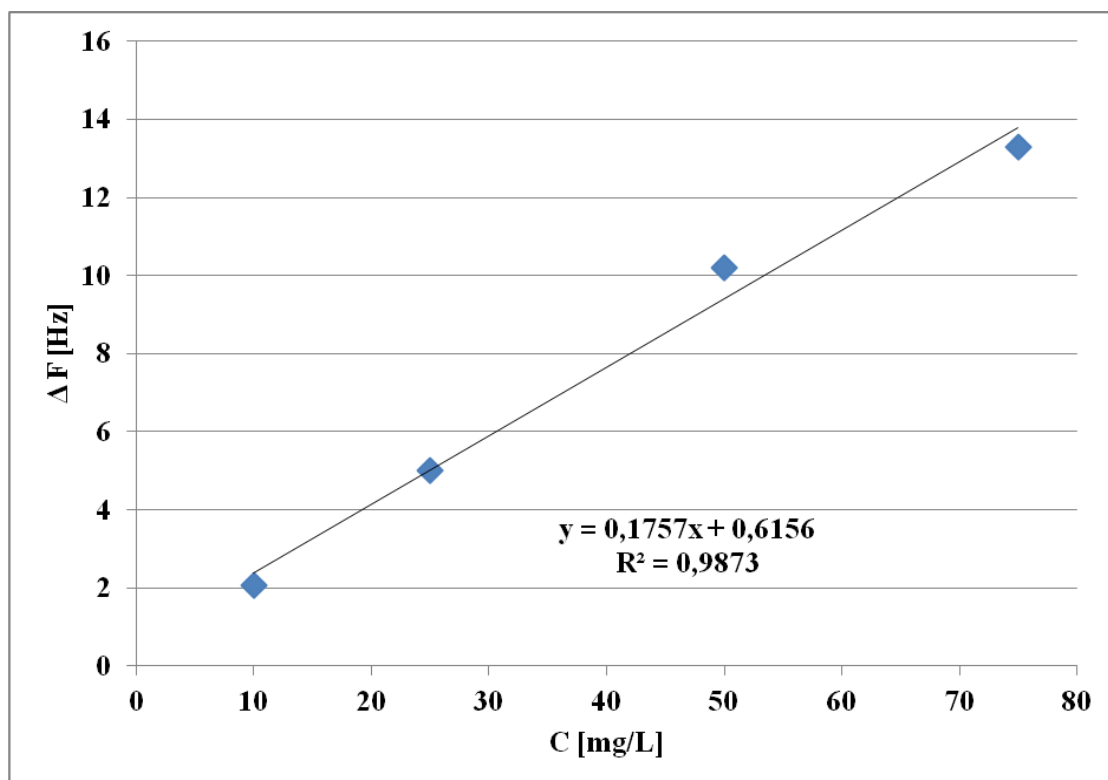


Figure 60 Sensor characteristic of Formaldehyde NP sensor

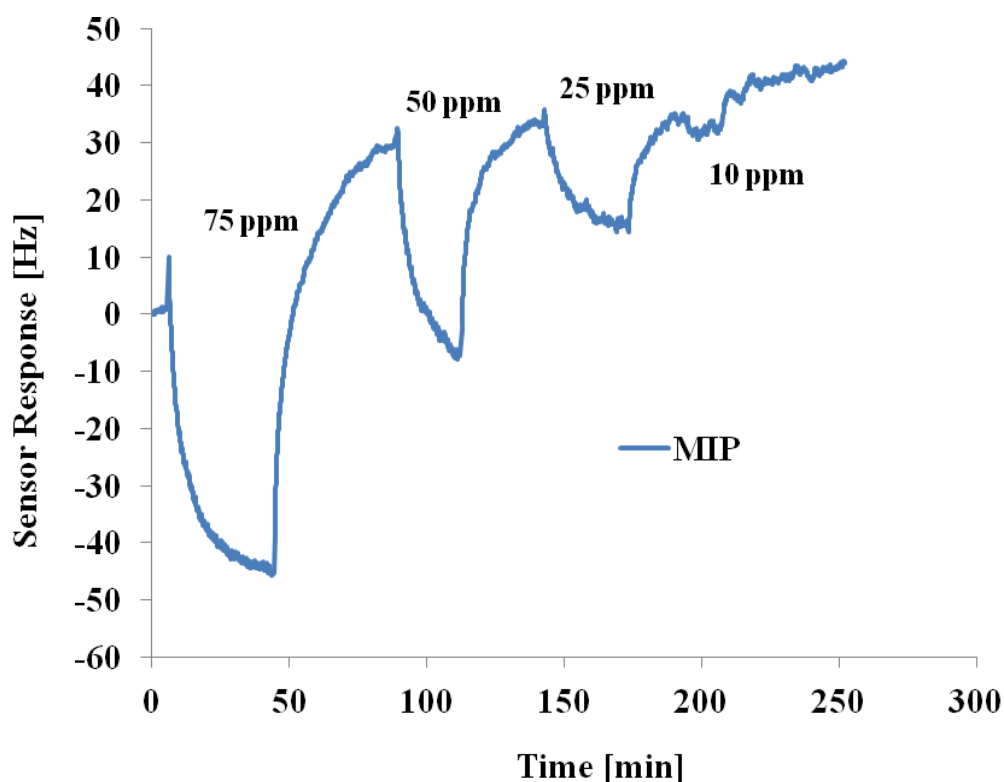


Figure 61 QCM sensor responses of MIP NP towards 75, 50, 25 and 10 ppm respectively vapour concentrations of Formaldehyde

For testing reproducibility, **Figure 61** shows the outcome of measuring the same nanoparticles on a different QCM at the same formaldehyde concentrations except for the one at 5 ppm, which did not show any responses. Comparing this result with **Figure 59**, one can see 3 times higher sensor responses: for 75 ppm the sensor response is about 70 Hz, for 50 ppm- 30 Hz and for 25 ppm 15 Hz. At the lowest concentration (10 ppm), no sensor signal can be observed. Such significant difference in sensor responses, obtained with the same sensing material, can be explained by different layer heights. The frequency data presented in **Figure 59** was obtained with the layer height of about 100 nm, whereas the second response was obtained with a nanoparticle layer height of about 300 nm. In **Figure 61** the reference channel showed no signals and was deleted due high drift.

Summarizingly, all these measurements impressively show that the MIP approach is in principle highly suitable to generate sensor layers to-

wards formaldehyde despite the small size of the molecule. To the best of our knowledge, formaldehyde hence represents the second smallest analyte after metal ions. [67] Selectivity, however, also has to be determined to assess sensor quality. The outcome of this can be seen in **Figure 62** collecting the mass effects obtained for both chemically related/similar compounds, such as acetone or formic acid, and compounds that can be expected in real-life samples, such as ethanol, methanol and dichloromethane.

Surprisingly, the sensors turned out to be basically specific. None of the competing compounds yields any measurable sensor signals. For the two alcohols this can be explained by their larger molecular structure. The formic acid molecule is only somewhat larger than formaldehyde. However, primary amines, such as the allylamine in the monomer mixture, react with the carbonyl groups of aldehydes, but not with those of carboxy groups. Obviously, no acid-base interactions take place, because otherwise formic acid would have to yield frequency shifts. Acetone is obviously too large and dichloromethane contains the wrong functional groups. Therefore, the formaldehyde MIP shows both acceptable sensitivity and outstanding selectivity, which makes them interesting candidates for actual sensor applications.

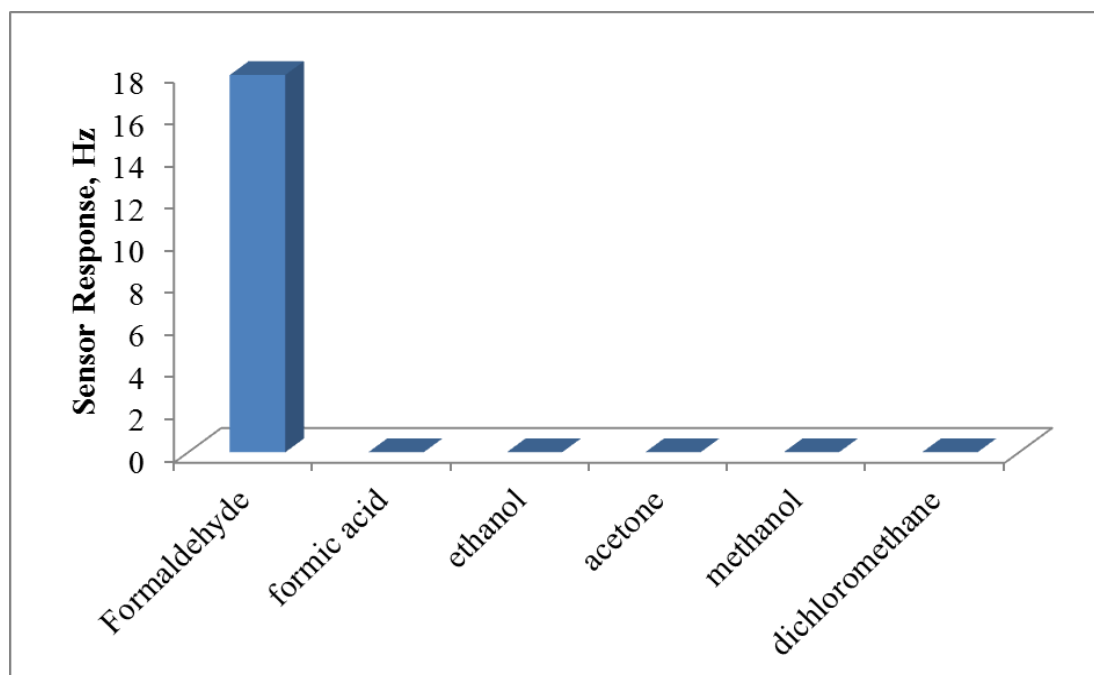


Figure 62 Selectivity pattern of formaldehyde sensor

4. Ephedrine MIP

4.1 Introduction

Increasing mobility on the one hand and hidden threats on the other hand demand continuous control of luggage and persons e.g. in large railway stations and airports. Not only dangerous substances (for example highly explosive ones), but also drugs have been becoming important topics for control. Because of the high number of necessary analyses screening methods are of substantial interest. Chemical sensors are one possibility to achieve them.

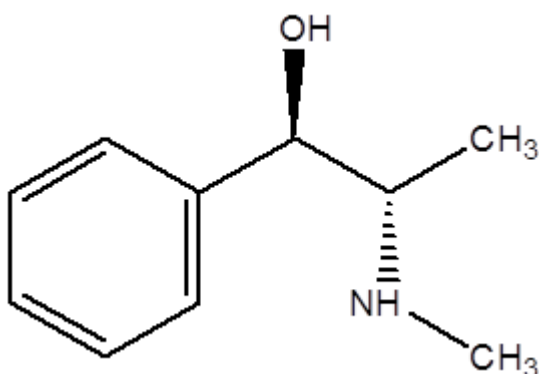


Figure 63 Ephedrine structure

Ephedrine (2-methylamino-1-phenylpropan-1-ol **Figure 63**) is one example for a restricted compound that is used both as an appetite suppressant and a precursor of illegal drugs. Due to its ability to stimulate the central nervous system, it is also used in special food products for athletes. [68]

The natural source of Ephedrine is a herb called Ephedrae Herba (Ephedra, Ma-huang), which is used as the most important component of the Chinese drug Ma-xing-gan-shi decoction. This drug has been used for treating flu, bronchitis, bronchial asthma, bronchopneumonia etc. for millennia.

[69] A large variety of products containing ephedrine can easily be purchased in drug stores in the United States over the counter, i.e. without prescription. Among others, such products are popular to treat asthma. The use of ephedrine and ephedra products as a remedy is a serious problem in the US “due to misuse and adverse events” and need to be regulated. Having a short look at history, it is worth mentioning, that the “career” of ephedrine as a drug in the US started in 1926, when it was put on the market. The reason for that was a finding in the early 1020s, namely that Ephedrine can successfully treat symptoms such as flu and bronchial disorders. [70] The table below adapted from that paper shows the timeline of the use of ephedrine in the US:

Early 1920s	Ephedrine introduced to the US to treat ailments such as asthma.
Late 1930s	False product claims began and Ephedrine was included into the Food, Drug and Cosmetics Act as a “safe” drug.
1950s	Stimulant misuse became prevalent in the US and has continued.
1960s	Ephedrine abuse was first documented. Ephedrine use was under-recognized due to over-reporting of amphetamine use.
1970	Ephedrine was not included in the schedules of the newly introduced Controlled Substances Act. The amphetamine “look-alike” phenomenon begins.
1980	Ephedrine became the new key ingredient to manufacture illicit methamphetamine.
Early 1980s	Federal agencies struggled to ban unapproved Ephedrine-containing “look-alikes”.
1994	The Dietary Supplement Health and Education Act of 1994 (DSHEA) classified Ephedra, the herbal source of Ephedrine, a “dietary supplement”, and thus was not regulated.
1995	The Federal Drug Administration (FDA) proposed to limit

	Ephedrine availability to prescription, but withdrew proposal. Medical benefits were said to outweigh risks.
1998	The FDA proposed a ban on ephedra products after receiving over 800 adverse event reports (AERs), but the rule was not passed due to lack of evidence.
2003	Steve Bechler, a well-known baseball player dies after ingesting an ephedra product. Ephedra becomes demonized by the media.
2004	After receiving over 18,000 AERs, the FDA banned ephedra products. Over-the-counter Ephedrine products remained available to the public without a prescription.
Late 2000s	Federal regulations allow Ephedrine to be available “behind the counter”, but it continues to be used to produce methamphetamine. New herbal stimulants have replaced ephedra.

There are three main ways to produce Ephedrine commercially for legal and illicit markets [71]: by biosynthesis, where the ephedra plant is the raw material (this option used to be the traditional way to produce Ephedrine, it is still used in illegal synthesis of the compound) (see **Figure 64**).

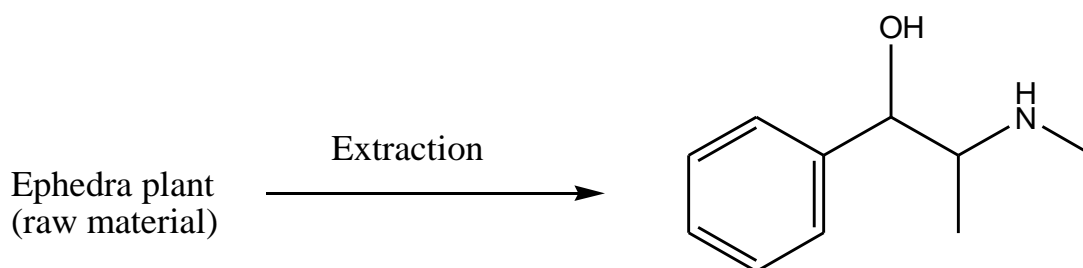


Figure 64 Biosynthesis of Ephedrine

The second possibility is chemical synthesis starting from Phenylethylketone and subsequent buildup of the aminic structure (see **Figure 65**).

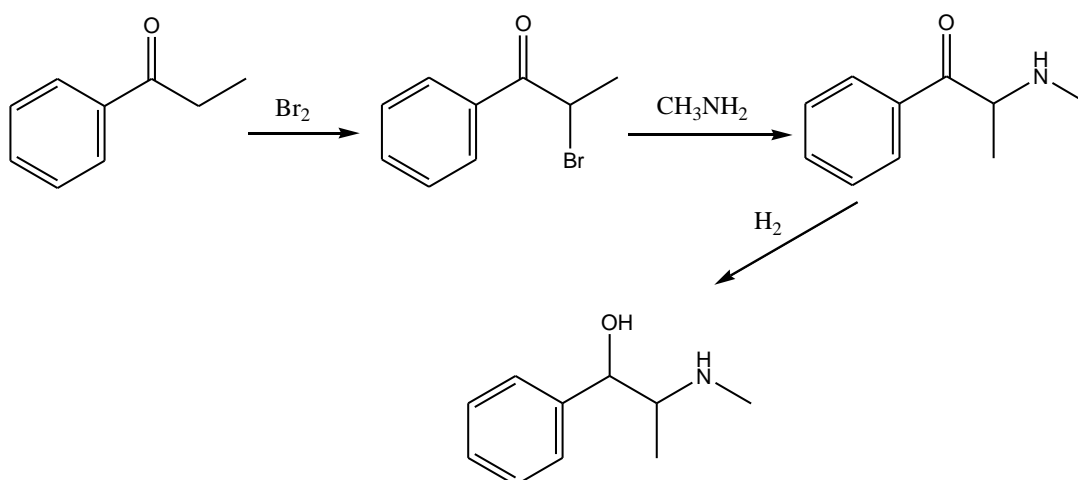


Figure 65 Chemical synthesis of Ephedrine from Phenylethyketone

Finally, semisynthesis can be done. This consists of sugar fermentation followed by amination. (see **Figure 66**)

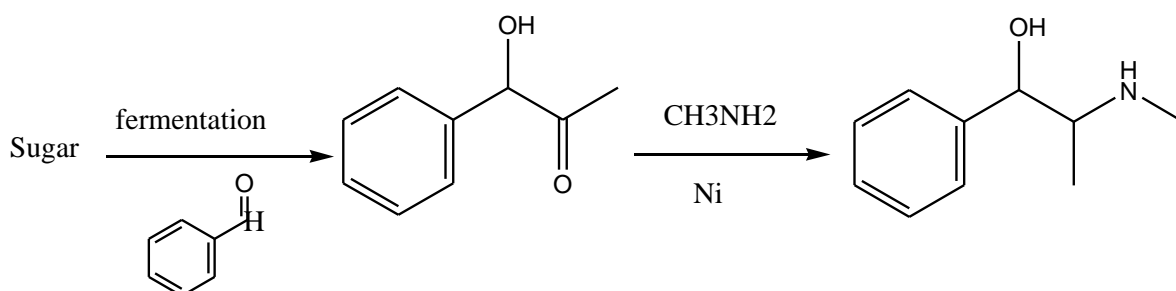


Figure 66 Semisynthesis of Ephedrine

Ephedrine has become a highly interesting compound for chemical analysis due to its illegal application as an amphetamine and methamphetamine precursor: both compounds are drugs, which stimulate the central nervous system. [72] Ephedrine is used as a precursor for methamphetamine synthesis along with 1-phenyl-2-propanone and Ephedra plants. [73] **Figure 67** shows the principal synthetic pathway from Ephedrine to metamphetamine. It basically consists of reductively removing the hydroxyl group from the molecular structure.

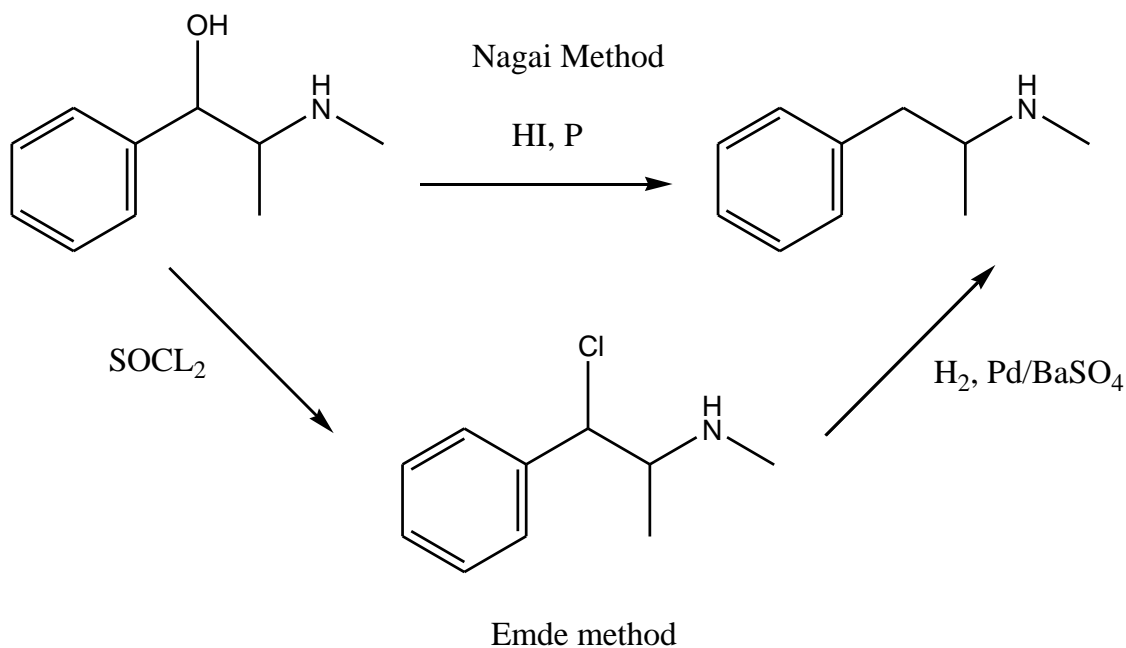


Figure 67 Methamphetamine synthesis from ephedrine

The main aim of this thesis thus was to design a possible sensor system for detecting ephedrine rapidly and straightforwardly. This is in line with the goals of the EU-FP6 IP NMP3-CT-2007-026549 “NANOSECURE”, in course of which this part of the thesis was carried out. The challenge of the present study has been to develop selective receptor layers for Ephedrine, which consists of an aromatic ring, a carbonyl group and an aliphatic part (see **Figure 63**), and apply them in chemical sensors. For developing such Ephedrine sensors [74] molecular imprinting was chosen, because it assures fast synthesis and adequate selectivity [75].

A special challenge in European projects comes from the combination of research and development. In the concrete case this means that even if the materials scientist succeeds in designing sensitive polymer materials towards Ephedrine, there is still a challenge to indeed implement such MIP into industry: research therefore should keep the actual application in mind right from the beginning by especially keeping in mind the ruggedness and reproducibility of such systems.[76] Both for application and for sensor re-

search, also the binding mechanism between Ephedrine and polymer as well as the selectivity of MIP have to receive special attention.

Polystyrene and polymethacrylate were chosen as two potential candidates for the basis of the recognition material. The polystyrene system was selected because of its aromatic rings. This idea to apply the polymethacrylate system was based mainly on the ability of –NH functional groups of Ephedrine to bind with the -COOH groups of the polymer matrix. In such cases one can expect to use non-covalent imprinting. The respective functional monomers (methacrylic acid and methyl methacrylate) and the crosslinker ethylene glycol dimethacrylate (EGDMA) were mixed with Ephedrine as the template molecule to form highly cross-linked (70% crosslinker) polymers.

Therefore, this section of the PhD thesis is based on the following logic: firstly, selection of polymer system and optimization; secondly sensor characterization of candidate polymers taking into special consideration selectivity towards substances containing similar functional groups, such as ethylamine, toluene, 2-butanol and 1-propanol; finally, developing a synthetic procedure for preparing nanoparticles on the base of the selected polymers and their characterization as sensor material.

4.2 Experimental strategies and polymer screening

4.2.1 Materials

Dual electrode structures were deposited onto the front and the rear faces of quartz crystal sheets with 15.5 mm in diameter by screen-printing, when the gold paste was distributed through special sieves manufactured in our laboratory. Front side electrodes are 5 mm in diameter and connected with one another (electrode design for QCM in liquid phase). These electrodes face the sample side and are connected to electrical ground. The diameter of the rear electrodes on the phase side of the oscillator is 4 mm.

These electrodes of course are not connected to one another, because this would obviously lead to short-circuit.

4.2.2. Selection of polymer system and optimization

Initially, polystyrene was chosen because of its aromatic rings and the fact that it is rather straightforward to handle (polymerization and coating). However, it proved not successful: MIP could by no means be obtained, because the monomers did not react in the presence of the template, neither in toluene, nor in tetrahydrofuran as a solvent, be it under UV or at elevated temperature. The problem could only be overcome by leaving out the solvent from the polymerization mixture altogether. Samples in that case were only diluted just before reaching the gel point, but this strategy did not result in sensor effects. Whether no imprinted sites were generated or whether adding the solvent at such a late stage prevented the formation of sufficient diffusion pathways could not be distinguished. **table 1** summarizes the process parameters assessed for styrene/divinyl benzene copolymers. However, the polymer system was abandoned after having proven not useful for the application. Therefore further work focused on the acrylic system, which can interact with OH- and NH-group of ephedrine via H-bonds and acid-base affinity. The experimental details on how polymers were actually synthesized can be found for the selected candidate polymer in chapter 4.2.5 of this thesis. All other compositions were prepared following the same steps, but of course using the amounts of reactants as shown in the **table 2**.

Table 1 styrene/divinyl benzene copolymers

N	DVB, mg	STY, mg	Ephedrine, mg	AIBN, mg	Toluene, μL
1	70	30	10	5	0
2	70	30	10	5	100

3	70	30	10	5	200
4	70	30	10	5	300
5	70	30	10	5	500
6	60	40	10	5	0
7	60	40	10	5	100
8	60	40	10	5	200
9	60	40	10	5	300
10	60	40	10	5	500
11	70	30	5	5	0
12	70	30	5	5	100
13	70	30	5	5	200
14	70	30	5	5	300
15	70	30	5	5	500
16	60	40	5	5	0
17	60	40	5	5	100
18	60	40	5	5	200
19	60	40	5	5	300

20	60	40	5	5	500
----	----	----	---	---	-----

Table 2 acrylic system

N	EGDMA, mg	MMA, mg	MAA, mg	Ephedrine, mg	AIBN, mg	Solvent, μ L
1	70	0	30	10	2	50 THF
2	70	10	20	10	2	50 THF
3	70	20	10	10	2	50 THF
4	70	0	30	5	2	50 THF
5	70	10	20	5	2	50 THF
6	70	20	10	5	2	50 THF
7	70	30	0	5	2	50 THF
8	60	0	40	5	2	50 THF
9	60	20	20	5	2	50 THF
10	60	40	0	5	2	50 THF
11	70	20	10	5	2	200 THF
12	70	20	10	5	2	100 ACN
13	70	20	10	5	2	100 Toluene

14	70	20	10	5	2	100 DMF
15	70	20	10	3	2	100 ACN
16	70	20	10	3	2	100 Toluene
17	70	20	10	3	2	100 DMF
18	70	20	10	5	2	50 ACN
19	70	20	10	5	2	50 Toluene
20	70	20	10	5	2	50 DMF
21	70	20	10	5	2	50 THF

As one can see from polymer optimization **table 2**, 21 different acrylic polymers were synthesized (all of them were stable in water). Optimization parameters were the monomer, cross-linker, analyte, solvent and porogen, which were varied in order to find an optimal ratio leading to recognition sites resulting in a molecular imprinting effect. [77].

The majority of polymers presented in **table 2**, namely 18 compositions, contain 70 mass percent of the cross-linker ethylene glycol dimethacrylate (EGDMA). This percentage refers to the mass of polymer matrix without the analyte and the solvent. Such high cross linking has also proven useful in other polymer systems aiming at the detection of volatile organic compounds (VOC) previously assessed by the group, such as for instance in compost sensing [78] Furthermore, the amount of template was varied in the range between 10 - 3 mg (for “70-30” polymers), i.e. between ten and three percent (m/m), which is a rather typical range in MIP. Different solvents were assessed, including tetrahydrofuran (THF), acetonitrile (ACN), toluene and dimethylformamide (DMF). As it can be seen in the **table 2**, 10

μL of diphenylmethane were added as a porogen to the respective polymerization batches.

4.2.3 FT-IR Screening

Taking into account the considerable number of candidate polymers, it was necessary to apply spectrometry to screen them and to hence clarify, if binding takes place. Such a spectrometric approach allows faster screening for larger amounts of samples than mass-sensitive measurements, so it makes sense to only test the most promising candidate. For this purpose FT-IR was chosen.

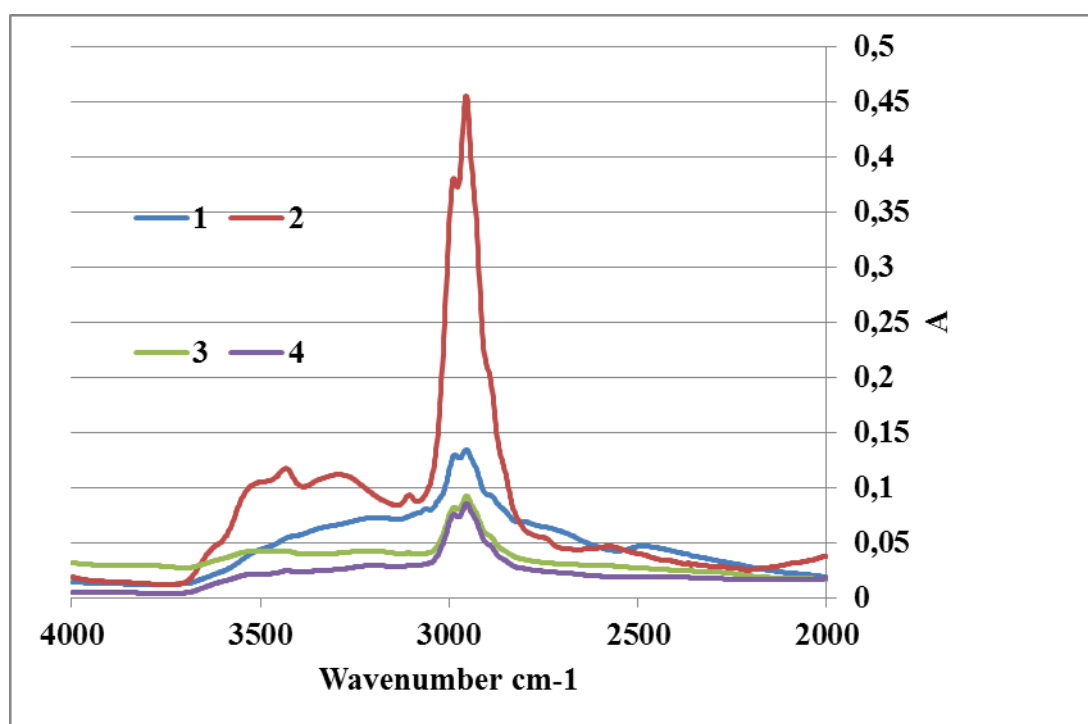


Figure 68 (MIP and NIP spectra, peak at 3057 cm-1)

1 NIP

2 MIP

3 Template removal

4 Re-inclusion

Before template removal and re-inclusion were checked (both manipulations were performed on MIP), spectra of MIP and NIP were recorded (in **Figure 68** 1 and 2). In **Figure 68** one can clearly see the weak spectral band at 3057 cm^{-1} , which can be used as differentiating parameter for MIP and NIP spectra. It corresponds to symmetric C-H stretching vibrations of the aromatic systems. This is of course caused by the fact that ephedrine is the only aromatic molecule in the system.

Template removal

All spectra were recorded on a Perkin Elmer Spectrum 100 FT-IR Spectrophotometer. During the first step, template removal from the MIP was tested. For that purpose $7\mu\text{l}$ of the MIP pre-polymer solution were spin-coated onto a glass substrate at 3500 rpm. In that way layer heights were achieved that were similar to the respective thin films on QCM. In order to finish polymerization of the pre-polymer, the glass substrate was placed under a UV lamp (λ_{max} 360 nm; 210 W) overnight. On the next day the glass substrate carrying the hardened polymer was placed in a Petri dish with water, so that the polymer film was covered with water and stirred overnight at room temperature. Then the glass substrate was mounted in the solid sample holder and the respective IR spectra were recorded.

Result

The respective IR spectra (3 in **Figure 68**) after washing did not reveal any spectral band at 3057 cm^{-1} . Logically, it was concluded that the template had successfully been washed out from the polymeric matrix. Similarly, the template removal step was successful for all tested polymers.

Re-inclusion

After successful template removal, the next step was to confirm if the generated cavities are able to re-include template molecules from aqueous Ephedrine solution. For that purpose, the washed glass substrate carrying

the MIP were exposed to a concentrated solution of Ephedrine (0.5 mass. %) for a few minutes at room temperature and afterwards analyzed by IR.

Result

For the 21st polymer the peak at 3057 cm^{-1} reappeared hence proving successful re-inclusion (**Figure 68**). Therefore all further experiments were carried out with this material having the following composition: 70 mass percent of the cross-linker ethylene glycol dimethacrylate (EGDMA), 10 mass percent of methacrylic acid, 20 mass percent of methyl methacrylate (MMA), 5 mass percent of Ephedrine, 2 mass percent of AIBN.

4.2.4 Synthesis of the final ephedrine MIP for sensor coatings.

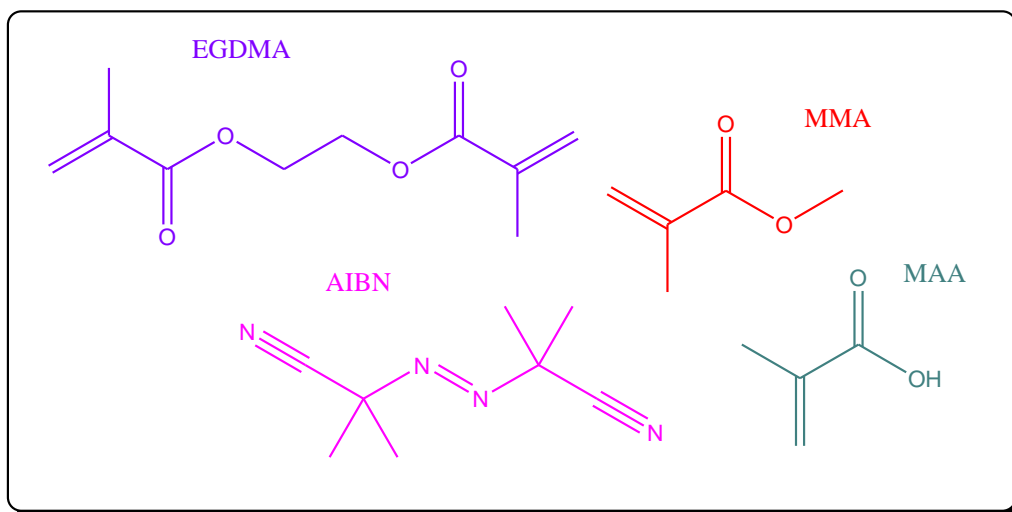


Figure 69 Initial components for polymer synthesis

We dissolved 5 mg ephedrine in 50 μL tetrahydrofuran (THF) in an Eppendorf reaction tube. Then we added 70 mg ethylene glycol dimethacrylate (EGDMA), 10 mg methacrylic acid, 20 mg methyl methacrylate (MMA) and 10 mg of diphenylmethane (DPM) as a porogen to the solution and sonicated the resulting mixture for 10 minutes (**Figure 69**). Diphenylmethane was added in order to make recognition sites more accessible and the resulting polymeric matrix more porous. As a polymerization initiator we used 5 mg azobisisobutyronitrile (AIBN). The Eppendorf reaction

tube was placed under a UV lamp for polymerization (λ_{\max} 360 nm and 210 W), which lasted 20 min just before the solution turned gel-like.

To generate recognition layers, we spin-coated 5 μ l of the respective oligomer solution at 3500 rpm onto the electrode with lower frequency of a 10 MHz-QCM, which was later used as the measuring electrode. The second electrode was spin coated with NIP. Afterwards, the coated QCM were left overnight at room temperature for polymer hardening. Usually on the next day the final polymer layers were washed with water overnight in a Petri dish or already mounted in measuring cell to extract the template molecules. When washing the polymer directly in the measuring cell, water was pumped through. Recording the respective frequency shifts allowed to follow the washing procedure in situ. This is a reliable, but time-consuming method. After successful washing we determined the resulting layer heights by the frequency shifts observed on the quartzes (according to year-long experience of the group, 1 kHz frequency change on a 10 MHz QCM corresponds to roughly 40 nm layer height). Following all these steps the resulting layers were about 160 nm thick, which - as mentioned before - corresponds to frequency shifts of 4 kHz.

4.2.5 Synthesis of MIP nanoparticle and coatings

For generating suitable MIP nanoparticles, the freshly synthesized optimized oligomer mixture was added to 20 times its own volume of acetonitrile, and then stirred overnight for homogeneous precipitation. The particles were then washed and collected by centrifugation at 4400 rpm. Following the same procedure, the template molecule was left out during NIP synthesis.

To generate nanoparticle layers, a suspension of 5 mg of synthesized nanoparticles in 500 μ l of ethylenediamine was prepared. We spin-coated 7 μ l of the respective suspension at 3500 rpm onto the measuring electrode. The second electrode was spin coated with NIP nanoparticles. After the coating procedure the QCMs were left to harden and dry overnight. Usually

on the next day the final nanoparticle layers were washed with water overnight in a Petri dish or straight in measuring cell to extract the template molecules. After successful washing we determined the resulting layer heights by the frequency shifts observed on the quartzes. The resulting nanoparticle layers were about 160 nm thick. This information contradicts with the average nanoparticle size, what can be explained by the interstitial gap between particles; in the case of nanoparticles the frequency shift can therefore not directly be transformed to a layer height, because the coating is of course not massive.

4.2.6 Nanoparticles Characterization

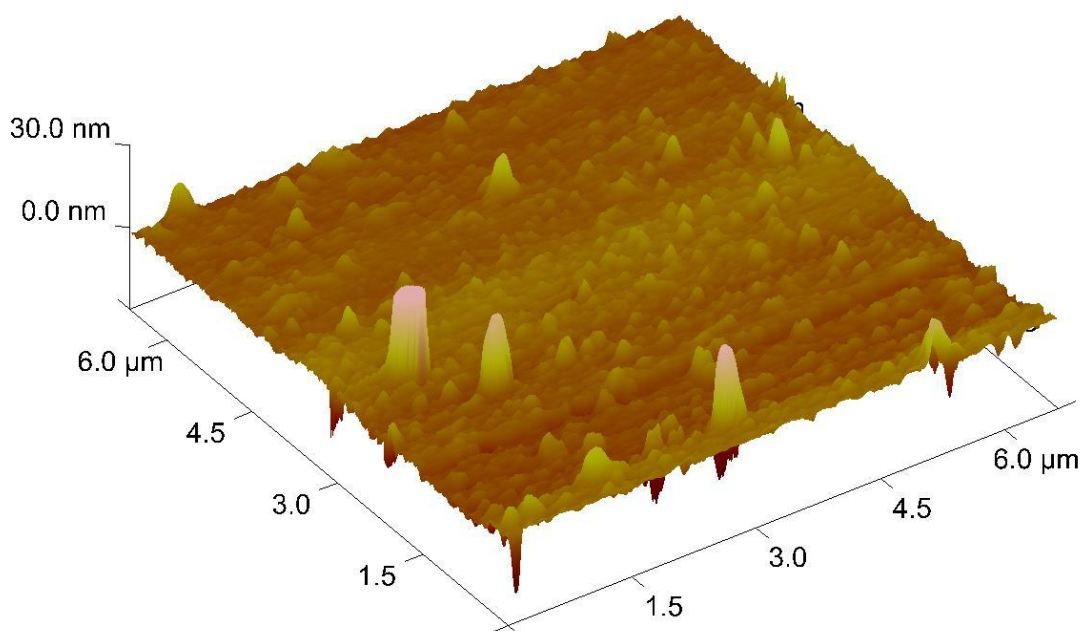


Figure 70 AFM image of nanoparticles

For nanoparticle characterization AFM was used. A VEECO Nanoscope IVa AFM/STM system in contact mode was applied to record AFM images and thereby to prove the feasibility of the nanoparticle synthe-

sis. In order to obtain nanoparticle images, their suspension was deposited onto glass substrates. For coating we prepared a suspension of 5 μg of nanoparticles in 500 μL of ethylenediamine. 5 μL of the suspension were drop-coated onto the glass substrate and then dried in oven overnight at 40 degrees centigrade.

Results

Figure 70 shows typical AFM images of the resulting layers. One can clearly see that the majority of nanoparticles is of globular shape. Furthermore, nanoparticle diameters are distributed over the range from 150-200 nm. Also a few larger agglomerates are visible. Their presence shows that stirring during nanoparticle synthesis does not necessarily guarantee fully uniform distribution of nanoparticles.

4.2.7 Sensing Apparatus

The quality of QCM was checked by a network analyzer (Agilent Technologies E5062A). In order to perform mass sensitive measurements the quartz sheets were mounted into a custom-made measuring cell (**Figure 71**) comprising of PMMA (polymethylmethacrylate) with 80 μl volume with four electrical connections and a sandwich cell fixing the quartz, made from PDMS (polydimethylsiloxane). This PDMS cell also contained sample inlet and outlet. The QCM is placed into the cell so that the recognition material – be it polymer layers or nanoparticles - deposited onto the electrodes with larger diameter faces the liquid phase. The rear side of the QCM with smaller uncoated electrodes faces the cell base filled with air. The measuring cell is operated in flow mode at room temperature. Such a setup minimizes the influence of sample conductivity. The QCM electrodes were connected to a homemade oscillator circuit and this was connected to a frequency counter (Agilent 53131A) read out by a custom-made LabView routine via a GPIB

USB interface. Liquid samples were delivered by the means of a peristaltic pump.

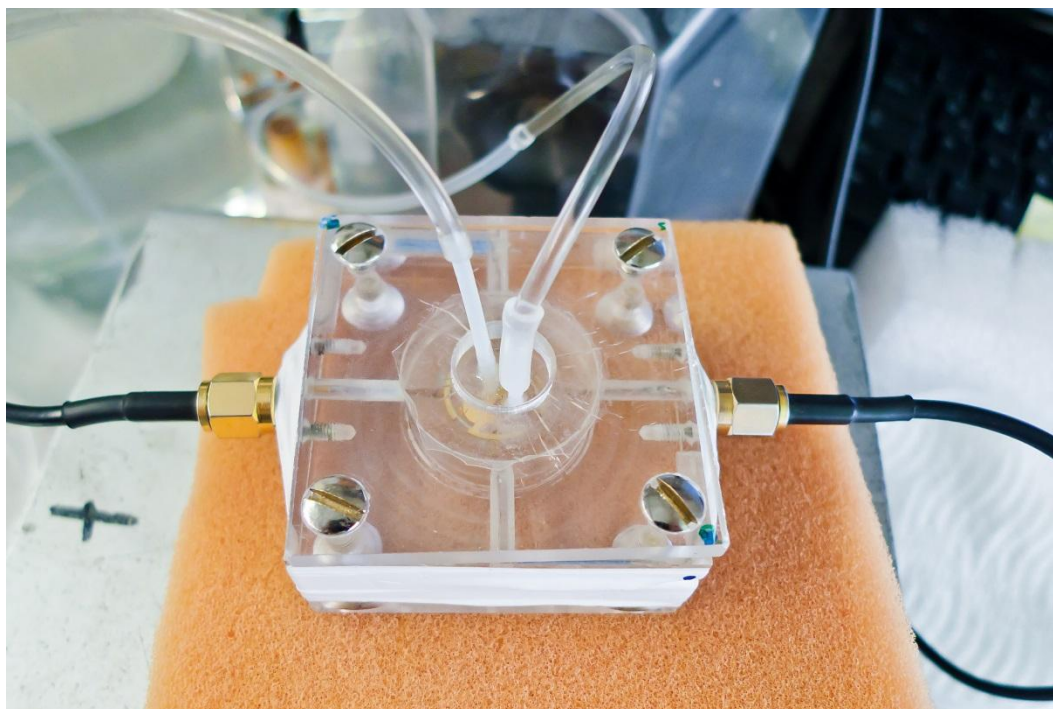


Figure 71 The measuring cell for liquid phase

4.2.8 QCM Sensor results and Discussion

Polymer films

Before discussing the mass-sensitive experiments, it is important to mention that QCM measurements in liquid phase with the Ephedrine sensors are possible due to the solubility of Ephedrine in water. (2.8 g /100 mL)

Figure 72 shows one of the first QCM measurements with the optimal recognition polymer layer. The blue curve represents the frequency changes obtained by the MIP-coated electrode, and the red one the signal changes of the NIP-coated channel. As previously discussed, measurements took place in a flow system. The constant base line represents the frequency obtained in distilled water, which serves as a reference point and thus is set to zero.

After having reached equilibrium, an aqueous solution containing 400 mg/l Ephedrine is pumped into the cell. When the template molecules reach the polymer surface, they are incorporated into the imprinted cavities. As the result of this process, the frequency of the MIP-coated measuring electrode gradually decreases. The response of reference electrode is also significant in this case, as it reaches about 150 Hz, which is almost 40% of MIP-electrode response. After reaching the maximum sensor response towards 400 mg/l, we switched back the system to de-ionized water. The next analyte concentration was 200 mg/l. For that, the response of the MIP-coated electrode is about 200 Hz, which is two times less than the MIP response towards 400 mg/l. Whereas the sensor response of MIP-electrode is fully reversible, the reference electrode in this case yielded some signal drift. Nonetheless, this result already proves the presence of adapted interaction sites in the matrix of the MIP.

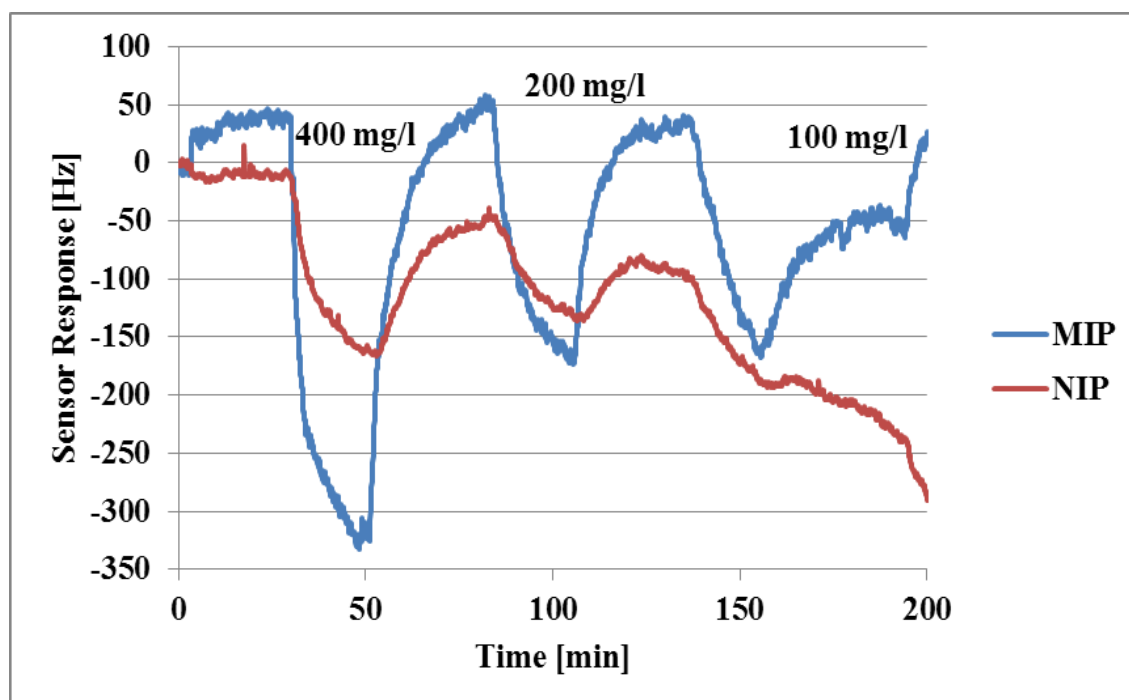


Figure 72 QCM sensor responses of MIP and NIP towards 100,200 and 400 mg/l Ephedrine, respectively

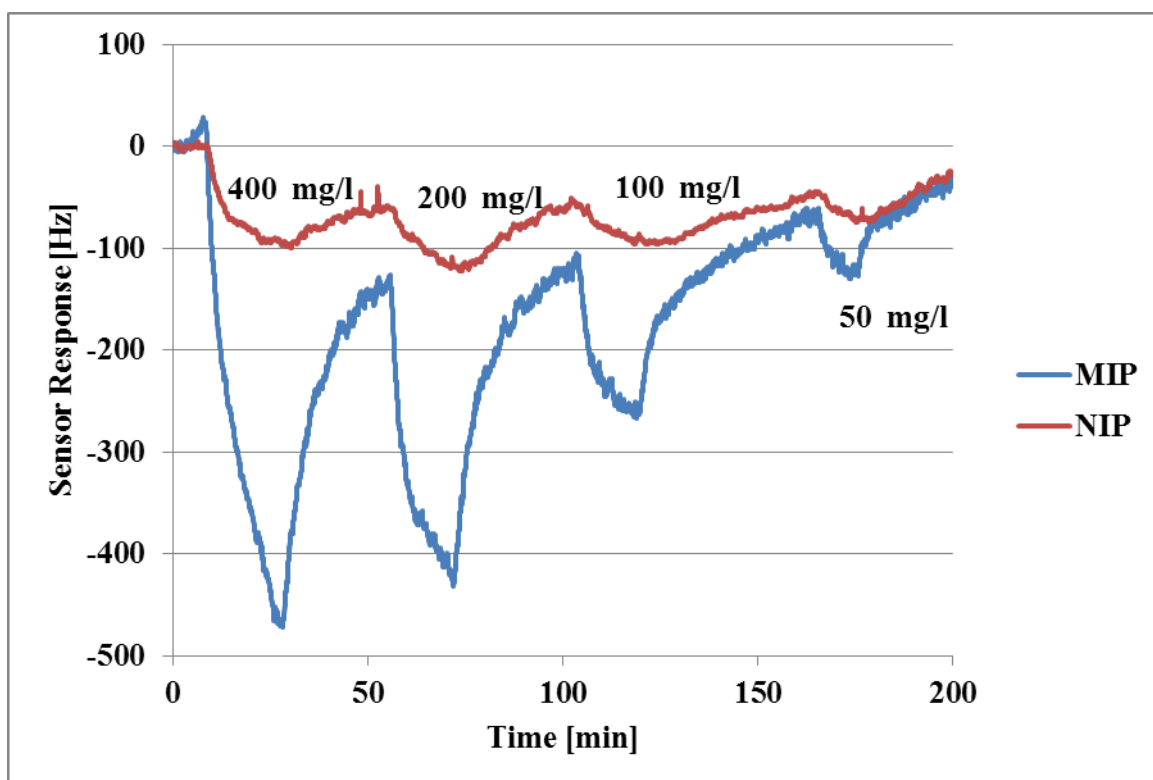


Figure 73 QCM sensor responses of MIP and NIP towards different concentrations of Ephedrine

A single measurement does of course not give statistically significant information. In order to ensure reproducibility of the MIP a different QCM was coated with the same polymer batch. The sensor was exposed to 400, 200, 100 and 50 mg/l Ephedrine in aqueous solution and it yielded reversible and reproducible signals also for reference electrode (**Figure 73**). When the sensor is exposed to 400 mg/l, the imprinted polymer yields frequency shifts up to 470 ± 3 Hz. The non-imprinted reference electrode also delivers a considerable response towards analyte i.e. 100 ± 3 Hz. Thus is a pure mass effect towards 400 mg/l of $370 \text{ Hz} \pm 6 \text{ Hz}$ is observed. After that the system is washed with water. As Ephedrine molecules are removed from the cavities of the polymer matrix, the frequency of both channels increases. Usually the system is flushed with water until the frequency has reverted to base line value. As **Figure 73** shows, the frequency shifts on both channels are re-

versible when switching back to water. Concerning a possible binding mechanism, one can suppose that COOH groups of the polymer backbone bind to the NH group of Ephedrine molecules, thereby generating cavities for reversible recognition. For 400, 200, 100 and 50 mg/l the sensor shows responses of 370, 241, 110 and 55 Hz, respectively. The noise in the measurement system is maximum 10 Hz; that means that limit of detection is about 25 mg/l. Comparing the sensor response characteristic with the previous one (**Figure 72**) we can mark larger sensor responses and a more stable reference signal.

As a conclusion to polymer film measurements, one can state that the chosen acrylic MIP system fulfills several necessary prerequisites of a sensitive layer: the measurements prove the interaction between Ephedrine molecules and the corresponding MIP layers, the sensor signals are reversible and stable. In spite of the fact that the sensitive polymer layer hence accomplishes essential parameters required from a sensor, the resulting QCM sensor characteristic reveals that sensitivity and limit of detection (25 mg/l) need some improvement. Therefore a nanoparticle approach was applied, because one can expect higher internal surfaces and better accessibility of binding sites there. [79]

Nanoparticles

Synthesizing nanoparticles on the basis of the optimized polymer system and coating them on QCM sensors, means that in principle the same experimental approach was explored, as for thin films. The main idea behind the experiment was to establish whether the larger surface area of nanoparticles affects the obtained sensor signals.

In **Figure 74** one cannot observe proper and stable base line both for working and reference electrode. The signals of the latter three concentrations (400, 200 and 100 mg/l) are reversible. Reproducibility of the frequency shifts when repeating the measurement 400 mg/l results in two different sensor responses (for the first time 1120 Hz and for the second time is 870

Hz). Nonetheless, it is evident that the nanoparticles in principle can also serve as a sensor material for Ephedrine recognition.

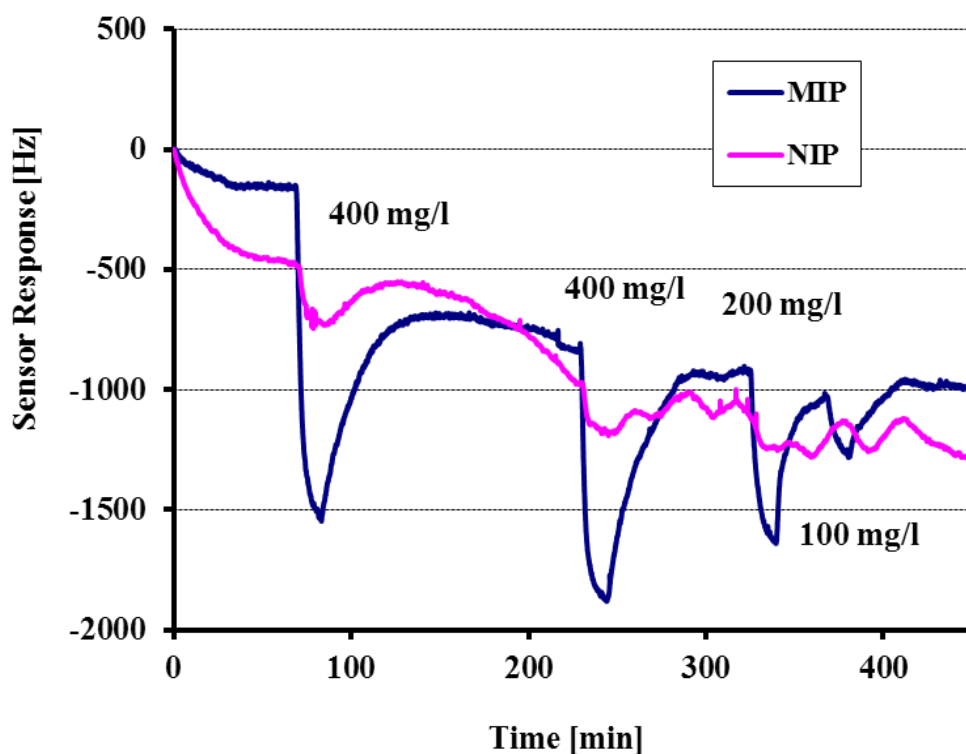


Figure 74 QCM sensor signal of molecularly imprinted polymer nanoparticles (MIP-NPs) toward different concentrations of ephedrine (400-100 ppm)

Assessing other QCM coated with Ephedrine MIP nanoparticles leads to reversible and sensitive sensor characteristics in the concentration range between 200mg/l and 10mg/l, namely at the following ephedrine levels: 200, 150, 100, 50, 35, 20 and 10 mg/l (see **Figure 75**). The data reveals that even 10 mg/l ephedrine in water can be detected without any problems, as they lead to a frequency shift of 72 Hz. Taking into consideration the noise level of 19 Hz, this means that the lower limit of detection is 6 mg/l. Furthermore, all sensor signals are reversible. When comparing these data with the results obtained from MIP thin films, one can clearly see that the NP sensor is still fully operational in the concentration range 50 mg/l - 5 mg/l. At such

low concentrations, MIP thin-films are already not usable due to limited sensitivity. Comparing these data with the outcome of the first nanoparticle measurement, one can see substantially increased sensitivity (for 200 mg/l the MIP channel in **Figure 74** shows approximately 700 Hz and **Figure 75** shows almost 1000 Hz). The two layers leading to the results in **Figure 74** and **Figure 75** had the same height, namely 4 kHz/160 nm. Nonetheless, the difference in sensor response between them can be explained by their different kinetic behavior. Obviously, the responses in **Figure 74** are slower. As being a screening measurement, analyte exposure had been stopped before the sensor reached equilibrium. This has been taken into consideration in the further measurements. Additionally, diffusion of the analyte within the second polymer batch seems better than for the first batch.

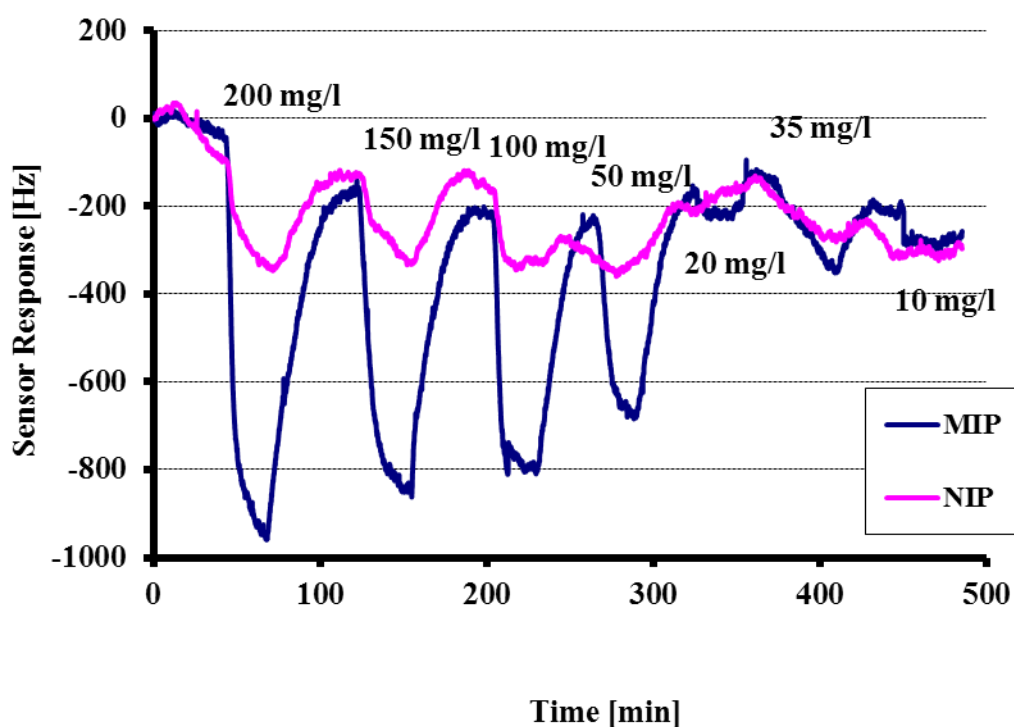


Figure 75 QCM sensor signal of molecularly imprinted polymer nanoparticles (MIP-NPs) toward different concentrations of ephedrine (200-10 ppm)

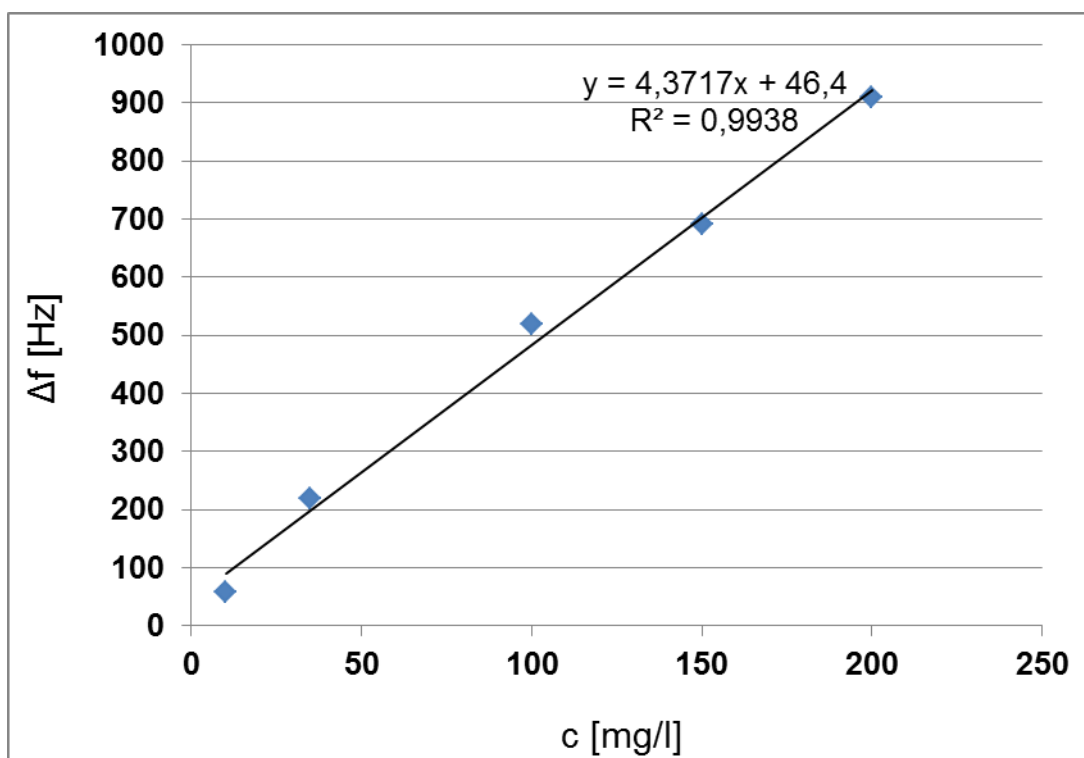


Figure 76 Regression analysis of the sensor characteristics of nanoparticles, showing linear behavior in the concentration range of 10-200 mg/l of Ephedrine

Figure 76 summarizes the same sensor responses for assessing the respective sensor characteristic. One can see roughly linear response behavior with Ephedrine. As the aim of this sensor system was to establish an ephedrine sensor system for law enforcement authorities, especially the lower limit of detection is of interest. However, this is not the case for the upper limit of detection. After discussions with the responsible project partners, sensors were therefore not calibrated above 200 mg/l.

Nanoparticles: selectivity

Nevertheless, one successful sensitivity measurements does of course not explain the nature of binding between Ephedrine and the polymer. To obtain further insight into Ephedrine-MIP interactions, selectivity data are necessary. The interest here is fundamentally to test the systems with substructures of Ephedrine to yield information on the nature of binding. To

perform selectivity studies for assessing polymer sensitivities, 4 compounds were chosen (**Figure 77**), which represent “parts” of the ephedrine molecule, namely ethyl amine, 2-butanol, 1-propanol and toluene, respectively. **Figure 78** summarizes the selectivity data obtained at 200 mg/l of each analyte. When the nanoparticle sensor is exposed towards the two alcohols 1-propanol and 2-butanol, no signals are obtained on either channel. Such zero effects towards alcohols clearly show that recognition is not determined by the alcoholic OH functionality of the Ephedrine molecule. Applying the same logic, one can also exclude major influence of the aliphatic part of the template molecule.

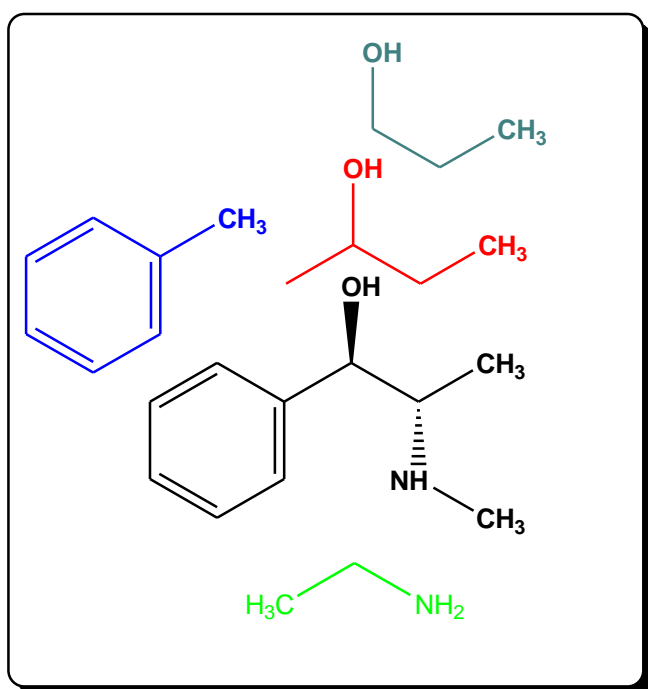


Figure 77 Ephedrine and substructure

Exposing the sensor towards toluene leads to rather low sensor responses of 100 Hz. Here it is important to remember the sensor response towards 200 mg/l Ephedrine (see **Figure 75**), which is six times higher. Nonetheless, a signal of about 100 Hz suggests a role of the aromatic ring during recognition. Hence the rigid aromatic ring in combination with aliphatic group interacts with polymeric matrix, which leads to the final recognition sites. Nonetheless the main driving force of the interaction is given by the

NH-group of the Ephedrine: This fact is strongly supported by the selectivity results with ethyl amine. The effect obtained by exposing the nanoparticle sensor towards this slightly basic amine ($pK_b = 3.367$ at 298 K) is unexpectedly large (almost 1900 Hz on the MIP minus 700 Hz on NIP, which means that the net sensor effect of the MIP is about 1200 Hz). Therefore acid-base interactions between the NH and the COOH groups of the polymer can be assumed being the reason of the comparably large sensor signals towards ethyl amine, namely two times higher than for Ephedrine.

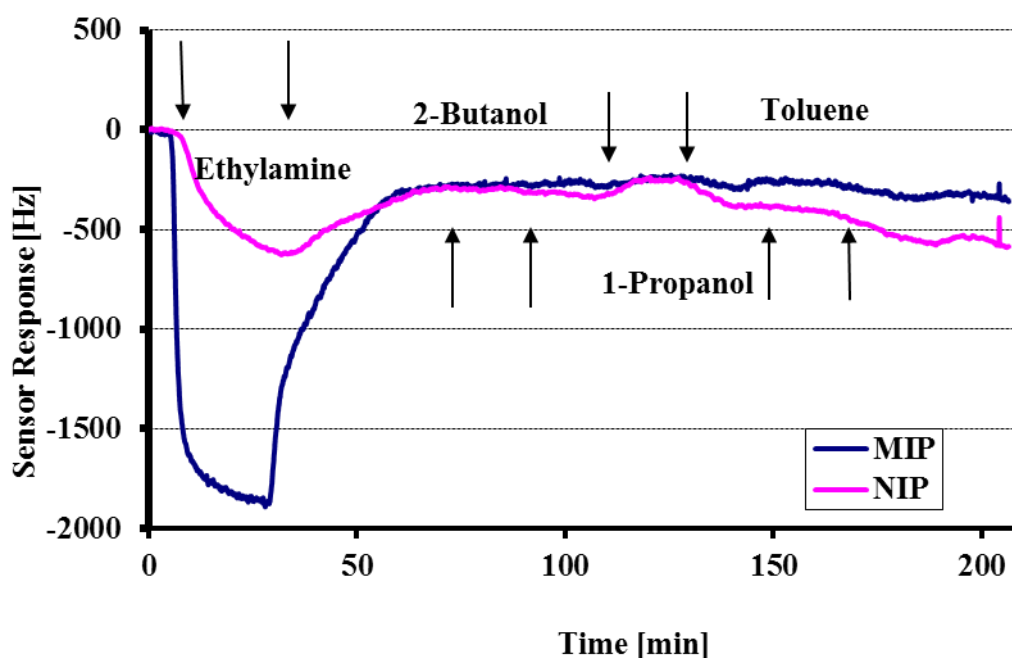


Figure 78 Selectivity behavior of ephedrine imprinted NP toward ephedrine and its analogs

On the other hand, the frequency on the NIP-coated channel also changes substantially, namely by 600 Hz. Basically, this means that a noticeable amount of non-specific adsorption of ethylamine occurs due to the functionality of the polymer. Taking into account that the MIP matrix usually possesses higher internal surfaces than NIP because of the selective cavities [80], one can suppose that small and reactive molecules of ethyl amine

can diffuse into the channels of the polymer bulk and bind to the polymer thus leading to substantial non-specific interaction.

Summarizingly, the nanoparticle approach turned out successful: Switching from polymer to nanoparticles results in increasing the sensor response more than twice. Mass-sensitive measurements with QCM reveal a detection limit of 6 mg/l, as can be seen in **Figure 76** resulting in linear sensor characteristic between x and y mg/l.

Preliminary tests in a real-life matrix

All previous measurements with the Ephedrine MIP (thin film and nanoparticles) were performed in water. Taking into account the pharmaceutical and physiological properties of Ephedrine, it can readily be assumed that the pharmaceutical industry is interested in such an Ephedrine sensor including diagnostics as a further potential application area. Therefore it was decided to perform measurements in a buffer system (phosphate buffered saline, pH=7.4), which is more similar to blood serum than pure water. The measurement is presented in **Figure 79**.

The first interesting effect worth mentioning is the huge frequency shift caused by switching the matrix from water to buffer solution. As the system is flushed with the buffer, the frequency of both electrodes decreases rapidly and reaches -50000 Hz. The reason of this phenomenon is the high ion concentration in the buffer. Whereas the signal on the MIP-coated channel stabilizes after 9 minutes, some drift remains on the NIP channel. Nonetheless, after 30 minutes, the QCM was exposed to a solution of Ethylamine in buffer with a concentration of 100 mg/l. The idea to use ethylamine for this purpose is based on the selectivity results (**Figure 78**), where it showed significant sensor responses in contrast to 2-butanol, 1-propanol and toluene exceeding even the Ephedrine sensor response by a factor of two. In buffer solutions ethyl amine yields substantial frequency shifts, reaching roughly 40000 Hz. Switching the system back to buffer leads to a fully reversible signal in the case of the measuring electrode. Exposing the sensor to Ephed-

rine dissolved in buffer leads to frequency shifts of about 20000 Hz, as it was expected. It can be concluded, that ethyl amine binds to the polymer specifically (as a base) and non-specifically because of the small size of molecules also in a buffer system. The comparably very large frequency shifts in this case cannot be described by mass effects alone, but also ionic conductivity. However, details still have to be evaluated in future experiments.

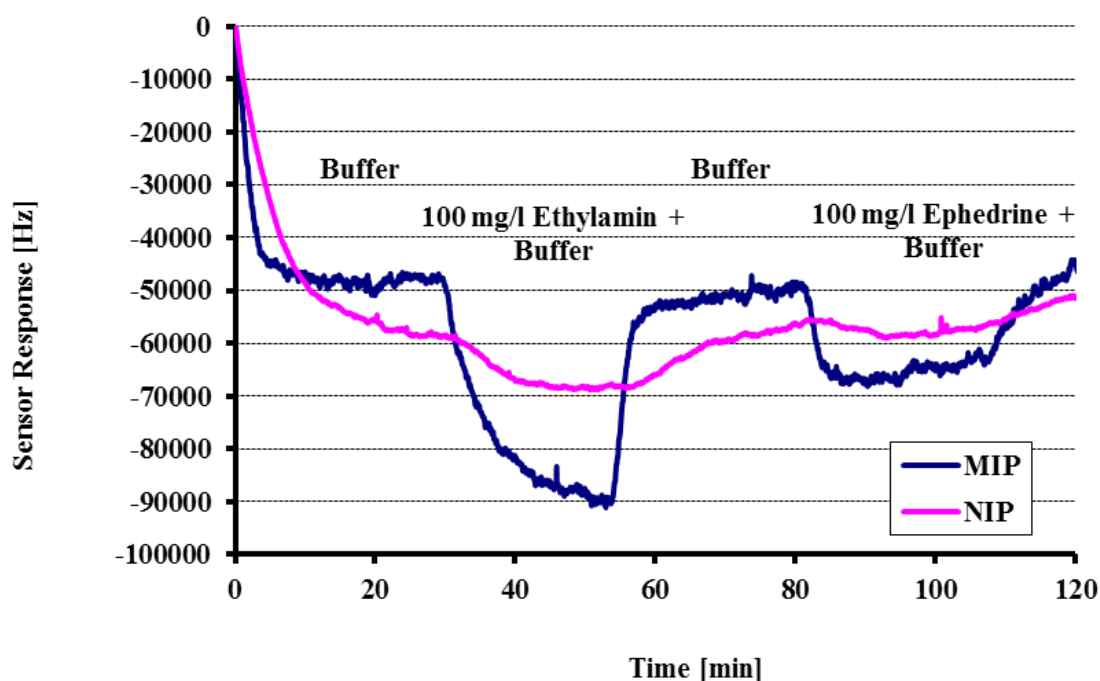


Figure 79 Selectivity behavior of ephedrine imprinted NP toward ephedrine and ethylamine

Finally, the selectivity of the sensor system towards 10 g/l acetic acid in water was tested (**Figure 80**). One can clearly see substantial effects on both MIP and NIP on both electrodes. However, compared to ephedrine and ethyl amine the normalized sensor responses are by a factor of 13 and 26, respectively, lower. This further supports the idea that acid-base interactions play a major role in recognition for this polymer system: the acidic compound despite the strong change in free protons in the solution shows by far lower sensor signals than the slightly alkaline analyte.

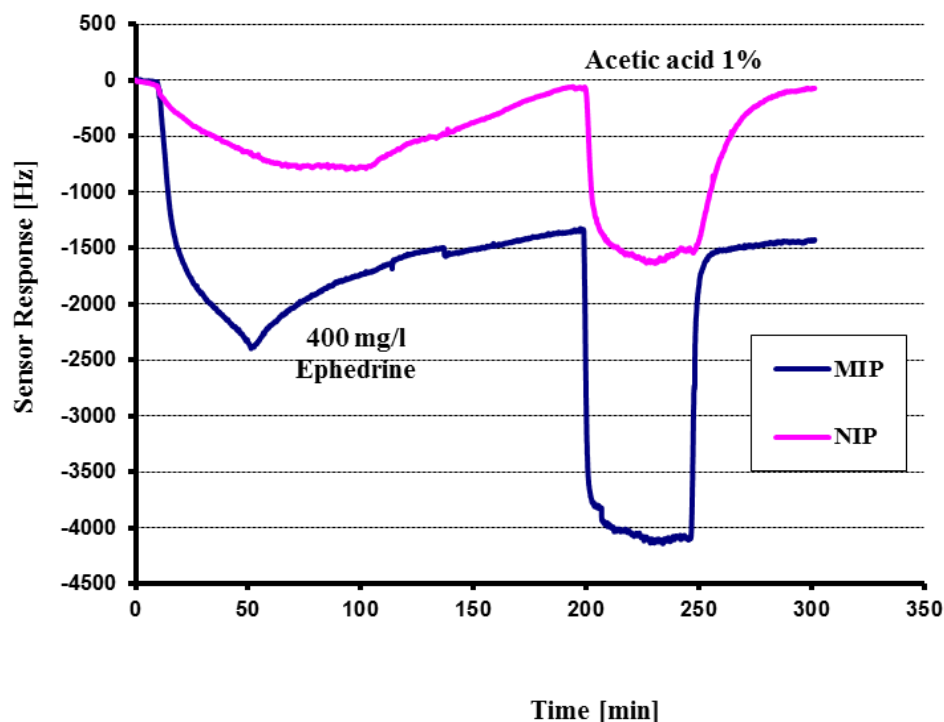


Figure 80 QCM sensor Responses of Ephedrine NP sensor towards Ephedrine and Acetic acid

4.2.9 Conclusion

Summarizingly, acrylic systems have proven most suitable for ephedrine MIP due to the free COOH groups in their backbone: selectivity measurements revealed only minor influence of the aromatic ring for recognition hence ruling out polystyrenes as suitable MIP. In the case of acrylate-based systems, the NH group of the Ephedrine molecule interacts with the -COOH group of the polymer backbone. Methacrylic acid increases the hydrophilicity of the polymers and hence improves recognition in aqueous buffers. Furthermore, comparing the data of thin films and nanoparticle MIP reveals that indeed bulk imprinting processes have occurred, i.e. that recognition sites are distributed within the entire polymer matrix: NP-based sensors show two

times larger sensor effects than thin film MIP. The reason for this is of course the increased accessibility of binding sites. Furthermore the average diffusion pathway within the polymer matrix can be expected to be much smaller in a nanoparticle with roughly 100nm in diameter than for a film of 400nm thickness and 5 mm diameter. Although sensitivities of the QCM-based sensor are somewhat too low for safety-related screening tests, MIP-based recognition has proven its high suitability to actually generate materials in a low-cost approach for inherently mass-producible sensors. The overall sensitivity and detection limit of such a system will then of course be not only determined by the sensor alone, but the entire unit consisting of sampling, pre-concentration and sensing.

Abstract (English)

The aim of this thesis has been to generate recognition materials based on polymer layers and nanoparticles as well as their composites for safety-relevant analytes, namely primary aliphatic alcohols, formaldehyde and ephedrine. Those recognition materials served as selective and sensitive layers on QCM sensors.

In a first step the suitability of titania nanoparticles to act as affinity material was tested towards several **vapors of volatile organic compounds**, namely 1-butanol, n-octane, 1-octanol, acetic acid, ethylene diamine and triethyl amine. Among these, 1-octanol yields the largest signals due its low vapor pressure (0.014 mmHg 20°C) with a detection limit of 3 ppm. n-Octane, acetic acid and ethylenediamine sharing almost the same vapour pressure among one another yield substantially different results: Especially octane leads to much lower sensor responses, namely two orders of magnitude less, revealing the slightly hydrophilic character of the NP. When comparing the two amines, one can see that the more alkaline and heavier one again leads to somewhat larger sensor responses: triethylamine yields two times larger effects than ethylenediamine. Carrying this affinity concept further, nanocomposite materials based on TiO₂ NP and polyurethane-based molecularly imprinted polymers (MIP) were developed. This approach resulted in substantial preconcentration effects towards 1-butanol leading to a twofold increase of the respective QCM sensor responses. Moreover, SiO₂ nanoparticles were synthesized and characterized to compare its sensing abilities for the same range of VOC with titania NP. Generally speaking the affinity of the two materials is similar, but titania leads to 2-3 times larger sensor responses.

Formaldehyde was chosen as analyte due to its toxic and carcinogenic features. A MIP copolymer system was developed for sensing formaldehyde vapor. On QCM, a detection limit of 10 ppm formaldehyde vapor in air could be reached despite the fact that the formaldehyde molecule is very

small. Furthermore, the MIP consisting of an acrylate-allylamine copolymer yielded excellent selectivity: the resulting sensors did not show any effects towards closely related and competing compounds including acetone, formic acid, methanol, ethanol and dichloromethane.

Ephedrine is an amphetamine and methamphetamine precursor. Polyacrylate-based systems were chosen by FT-IR screening to design MIP layers as well as MIP nanoparticles with 150-200 nm diameter. Both approaches were successful. Polymer film sensors yielded about 25 mg/l detection limit for ephedrine in water. Nanoparticles on the other hand allowed for a lower limit of detection of 6 mg/l. With a NP-sensor it is hence possible to work in the low concentration range 50 mg/l - 5 mg/l. Such sensors yield similar results in buffered ephedrine solutions as compared to distilled water as a solvent. The selectivity of the MIP NP was assessed with ethyl amine, 2-butanol, 1-propanol and toluene (at 200 mg/l of each analyte). Both alcohols did not yield sensor signals. Toluene yields low sensor responses of 100 Hz (six times lower than for 200 pmg/l Ephedrine) indicating some role of the aromatic moiety in recognition. The main driving force in interaction is played by the NH-group of the Ephedrine: the large ethyl amine signal (about two times higher than for Ephedrine) proves this fact. However, NIP measurements reveal that non-specific adsorption plays a major role. These selectivity studies do not only support the applicability of the system, but also allowed for structural considerations leading to possible template-MIP binding events.

Zusammenfassung (Deutsch)

Die vorliegende Dissertation befasste sich mit der Entwicklung neuartiger Erkennungsmaterialien auf der Basis von Polymeren und Nanopartikeln sowie deren Kompositen für Sensoren, die sicherheitsrelevante Analyte detektieren sollten. Diese waren primäre Alkohole, Formaldehyd und Ephedrin. Als Transducer dienten Quarzmikrowaagen (quartz crystal microbalance – QCM).

In einem ersten Schritt behandelt sie die Erforschung der Wechselwirkungen zwischen Titandioxid-Nanopartikeln und **flüchtigen organischen Verbindungen**, nämlich 1-Butanol, n-Oktan, 1-Oktanol, Essigsäure, Ethylendiamin und Triethylamin. Von allen diesen Verbindungen führt Oktanol aufgrund seines geringen Dampfdrucks (0.014 mmHg bei 20°C) zu den stärksten Sensorantworten, die ein unteres Detektionslimit von 3 ppm in Luft ermöglichen. N-Oktan, Essigsäure und Ethylendiamin, die alle ungefähr den selben Dampfdruck haben, zeigen untereinander stark verschiedene Resultate: insbesondere Oktan führt zu um zwei Zehnerpotenzen niedrigeren Sensorantworten als man erwarten würde, was den leicht hydrophilen Charakter der Nanopartikel zeigt. Vergleicht man die beiden Amine miteinander, stellt sich heraus, dass das schwerere und stärker alkalische Molekül – Triethylamin – zwei Mal größere Sensoreffekte verursacht, als Ethylendiamin. Dieses Affinitätskonzept konnte weiterentwickelt werden, indem Kompositmaterialien aus TiO_2 Nanopartikeln und molekular geprägten Polyurethanen synthetisiert wurden. Dieser Ansatz führte zur Vorkonzentration von Butanol in der Nähe der Partikel und letztlich zu zweifach erhöhten Sensorantworten. Um Vergleichsdaten zum Titanat zu haben, wurden Sensormessungen auch mit SiO_2 Nanopartikeln durchgeführt. Allgemein gesagt sind die Affinitäten der beiden Materialien ähnlich, allerdings sind die Sensoreffekte der TiO_2 Nanopartikel um einen Faktor 2-3 höher.

Formaldehyd ist aufgrund seiner Toxizität und Karzinogenität ein wichtiger Analyt für die Sensorik. Deswegen wurde ein molekular geprägtes

Polymer (MIP) für die Detektion von Formaldehyddämpfen in Luft entwickelt. Auf QCM konnte trotz der geringen Größe des Analytmoleküls auf diese Weise ein Detektionslimit von 10ppm in Luft erzielt werden. Außerdem zeigte das verwendete Copolymer aus Acrylaten und Allylamin erstaunliche Selektivität: die Sensoren zeigten keinerlei Antwort auf verwandte Verbindungen oder mögliche Störkomponenten, wie Azeton, Ameisensäure, Methanol, Ethanol und Dichlormethan.

Der dritte Analyt war **Ephedrin**, das eine Vorstufe für Amphetamine und Methamphetamine ist. Screening mittels FT-IR-Spektroskopie führte zu Polyacrylaten als für das Prägen geeigneten Polymeren. Diese konnten sowohl als Dünnschichten, als auch als Nanopartikel mit 150-200nm Durchmesser synthetisiert werden. Sensoren mit Dünnschichten erreichten ein Detektionslimit von 25 mg/l Ephedrin in wässriger Lösung. Nanopartikel dagegen erreichten sogar 6 mg/l und erlauben es daher in einem Konzentrationsbereich von 5-50 mg/l quantitative Sensormessungen durchzuführen. In Pufferlösungen ergeben sich sehr ähnliche Signale. Selektivitätsmessungen umfassten Ethylamin, 2-Butanol, 1-Propanol und Toluol (jeweils 200 mg/l), da diese Verbindungen Substrukturen des Ephedrinmoleküls darstellen. Die Alkohole führten zu keinen messbaren Frequenzsignalen. Toluol führt zu einer Sensorantwort von -100Hz, was einem Sechstel des Ephedrinsignals bei 200 mg/l entspricht. Das zeigt, dass der aromatische Ring in der Erkennung eine gewisse Rolle spielt. Offensichtlich ist die Hauptantriebskraft der Erkennung die NH-Gruppe im Ephedrinmolekül: Ethylamin führt zu doppelt so hohen Signalen auf dem Sensor, allerdings zeigen die Daten des ungeprägten Polymers, dass ein großer Teil dieses Effekts auf unspezifische Wechselwirkungen zurückzuführen ist. Diese Selektivitäten zeigen nicht nur Potential für tatsächliche Anwendung der Sensoren sondern erlauben auch Rückschlüsse auf die der Erkennung zugrundeliegenden Bindungsverhältnisse.

Literature List

- 1 M. Guenther, G. Gerlach, Springer Series on Chemical Sensors and Biosensors (Hydrogel Sensors and Actuators), Springer-Verlag Berlin Heidelberg (2009) 165
- 2 C.K. Ho, A. Robinson, D.R. Miller, M.J. Davis, Overview over sensors and needs for environmental monitoring, *Sensors* 5 (2005) 4–37
- 3 U. Lehmann, H. Plehn, O. Krusemark, J. Muller, A Miniaturized Gas Chromatograph for Autonomous and Longtime Measurements, in *Proc. Sensor*, Nuremberg, AMA Service, Wunstorf 1 (1999) 155-158
- 4 F.L. Dickert, P.A. Lieberzeit, Solid-State Sensors for Field Measurements of Gases and Vapours, in *Encyclopaedia of Analytical Chemistry*, R. A. Meyers (Ed.), John Wiley and Sons Ltd. Chichester, (2000) 3831-3855
- 5 G. Mustafa, P.A. Lieberzeit, MIP Sensors on the Way to Real-World Applications, in *Designing receptors for the next generation of Biosensor*, ed. S. A. Piletsky, M. J Whitcombe, 12 (2012) 167-188
- 6 O. Hayden, F.L. Dickert, Selective microorganism detection with cell surface imprinted polymers, *Adv Mater* 13 (2001) 1480–1483
- 7 A. Aherne, C. Alexander, M.J. Payne, Bacteria-mediated lithography of polymer surfaces, *J Am Chem Soc* 118 (1996) 8771–8772
- 8 Y. Wang, Z.Zhang, V. Jain, J.Yi, S. Mueller, J. Sokolov, Z. Liu, K. Levon, B. Rigas, M. H. Rafailovic, Potentiometric sensors based on surface molecular imprinting: Detection of cancer biomarkers and viruses, *Sens Actuators B* 146 (2010) 381-387

- 9 S. Yaqub, U. Latif, F.L. Dickert, Plastic antibodies as chemical sensor material for atrazine detection, *Sens Actuators B* 160 (2011) 227–233
- 10 R. Schirhagl, U. Latif, F.L. Dickert, Atrazine detection based on antibody replicas, *J Mater Chem* 21 (2011) 14594–14598
- 11 P.A. Lieberzeit, G. Glanznig, A. Leidl, F.L. Dickert, Ceramic materials for mass-sensitive sensors detection of VOCs and monitoring oil degradation, *Adv Sci Technol* 45 (2006) 1799–1802
- 12 F.L. Dickert, P. Forth, P.A. Lieberzeit, G. Voigt, Quality control of automotive engine oils with mass-sensitive chemical sensors-QCMs and molecularly imprinted polymers, *Fresenius J Anal Chem* 366 (2000) 802–806
- 13 W.S. Hughes, Potential difference between glass and electrolytes in contact with the glass, *J Am Chem Soc* 44 (1922) 2860-7
- 14 A. Hulanicki, S. Glab, F. Ingman, Chemical sensors: definitions and classification, *F Pure Appl Chem* 63 (1991) 1247-1250
- 15 P. Grüdler, *Chemical Sensors; An Introduction for Scientists and Engineers*, Springer-Verlag Berlin Heidelberg 7 (2007) 3-12
- 16 F.L. Dickert, A. Haunschild, Sensor materials for solvent vapor detection—donor–acceptor and host–guest interactions, *Adv Mater*, 5 (1993) 887–889
- 17 F.L. Dickert, U.P. Baumler, G. K. Zwissler, Supramolecular structures and chemical sensing, *Syn Met*, 61 (1993) 47-51

- 18 G. Mustafa, Soft Metal Sulfide Nanoparticles and Nanocomposite Based Sensors for Thiol and Alcohol Detection, Dissertation, University of Vienna (2011)
- 19 J. Janata, Principles of Chemical Sensors, Springer, Second Edition (2009)
- 20 M. Sys, B. Pecec, K. Kalcher, Amperometric enzyme carbon paste-based biosensor for quantification of hydroquinone and polyphenolic antioxidant capacity, Int J Electrochem Sci 8 (2013) 9030-9040
- 21 M. Stoces, K. Kalcher, I. Syancara, K. Vytras, A new biosensor for glucose based on carbon paste and enzyme immobilized onto the polyaniline film, Int J Electrochem Sci 6 (2011) 1917-1926
- 22 P. Curie, L. Curie, Développement, par pression, de l'électricité polaire dans les cristaux hémicédrés à faces inclinées, C.R.T. (1880) 91 294
- 23 A. Afzala, N. Iqbala, A. Mujahida, R. Schirhagl, Advanced vapor recognition materials for selective and fast responsive surface acoustic wave sensors: A review, Anal Chim Acta 787 (2013) 36– 49
- 24 M.G. Schweyer, J.A. Hilton, J.E. Munson, J.C. Andle, Ultrasonics Symposium Proceedings, IEEE, Toronto, Ont., Canada, (1997)
- 25 G. Sauerbrey, Verwendung von Schwingquarzen zur Wägung dünner Schichten und zur Mikrowägung, Zeitschr f Physik 155 (1959) 206-222
- 26 K.K. Kanazawa, J.G. Gordon, Frequency of a quartz microbalance in contact with liquid, Anal Chem 57 (1985) 1770-1771

- 27 R.J.T. Holford, F. Davis, S. P.J. Higson, Recent trends in antibody based sensors, *J Biosens Bioelectron* 34 (2012) 12–24
- 28 T. Wangchareansak, C. Sangma, P. Ngermmeesri, A. Thitithanyanont P.A. Lieberzeit, Self-assembled glucosamine monolayers as biomimetic receptors for detecting WGA lectin and influenza virus with a quartz crystal microbalance, *Anal Bioanal Chem* 405 (2013) 6471–6478
- 29 M. Komiyama ,T. Takeuchi , T. Mukawa ,H. Asanuma, *Molecular Imprinting: From Fundamentals to Applications*, (2003) Wiley Library
- 30 B. Sellergren, Molecularly imprinted polymers: Shaping enzyme inhibitors, *Nat Chem* 2 (2010) 7-8
- 31 N. Iqbal, P.A. Lieberzeit, *Artificial Receptors for Mass-Sensitive Sensors: Targeting Analytes from Surfaces, Nanoparticles, and Bioanalytes by Molecular Imprinting* (2012) 195-235
- 32 S.A. Piletsky, N.W. Turner, P. Laitenberger, Molecularly imprinted polymers in clinical diagnostics--future potential and existing problems, *Med Eng & Phy* 28 (2006) 971
- 33 G. Wulff, *Molecular Imprinting in Cross-Linked Materials with the Aid of Molecular Templates - A Way towards Artificial Antibodies*, *Angew Chem Int. Ed. Engl.* 34 (1995) 1812-1832
- 34 A.G. Mayes, K. Mosbach, Molecularly imprinted polymers: useful materials for analytical chemistry? *Trends Anal Chem* 16 (1997) 321-332
- 35 K. Mosbach, *Molecular Imprinting*, *Tren Biochem Scien* 19 (1994) 9-15

- 36 M. Yan, O. Ramstrom (Eds.), *Molecularly Imprinted Materials: Science and Technology*, CRC Press (2004)
- 37 N. Katada, M. Niwa, *The Re-Birth of Molecular Imprinting on Silica*, Chapter 3 in *Molecular Imprinting of Polymers*, S. Piletsky, A. Turner (2006) Landes Bioscience
- 38 L. Novakova, H. Vlckova, *A review of current trends and advances in modern bio-analytical methods: Chromatography and sample preparation*, *Anal Chim Acta* 656 (2009) 8-35
- 39 A. Martin-Esteban, *Molecularly-imprinted polymers as a versatile, highly selective tool in sample preparation*, *TrAC* 45 (2013)169-170
- 40 M. Zeilinger, *Molekular gepragte Materialien fur die Sensorik mittles oberflachenverstarker Raman-Spektroskopie sowie photonischen Kristallen*, Dissertation, University of Vienna (2013)
- 41 R. Zhanga, A.A. Elzatahry, S.S. Al-Deyabb, D. Zhao, *Mesoporous titania: From synthesis to application*, *Nano Today* 7 (2012) 344-366
- 42 D. Reyes-Coronado, G. Rodriguez-Gattorno, M. Espinosa-Pesqueira, C. Cab, R. De Coss, G. Oskam, *Phase-pure TiO₂ nanoparticles: anatase, brookite and rutile*, *Nanotechnology* 19 (2008) 1-10
- 43 A.S de Dios, M.E. Dıaz-Garcıa, *Multifunctional nanoparticles: Analytical prospects*, *Anal Chim Acta* 666 (2010) 1–22
- 44 A. Fujishima, K. Honda, *TiO₂ photocatalysis*, *Nature* 238 (1972) 37-38

- 45 K. Nakataa, A. Fujishima, TiO₂ photocatalysis: Design and applications, invited review, *J Photochem Photobiol C Photochem Rev* 13 (2012) 169–189
- 46 A. Menard, D. Drobne, A. Jemec, Ecotoxicity of nanosized TiO₂. Review of in vivo data, *EnvironPollut* 159 (2011) 677-684
- 47 R. Zhanga, Y. Baib, B. Zhanga, L. Chenc, B. Yan, The potential health risk of titania nanoparticles, Review, *J Hazard Mater* 211– 212 (2012) 404– 413
- 48 A.S de Dios, M.E. Díaz-García, Multifunctional nanoparticles: Analytical prospects, Review, *Anal Chim Acta* 666 (2010) 1–22
- 49 W. Wei, M. Weii, S. Liu, Silica nanoparticles as a carrier for signal amplification, *31* (2012) 3-4
- 50 M. Hussain, N. Iqbal, F.L. Dickert, P.A. Lieberzeit, Quartz crystal microbalance sensor based on affinity interactions between organic thiols and molybdenum disulfide nanoparticles, *Sens Actuators B* 162 (2012) 63– 67
- 51 F.L. Dickert, P.A. Lieberzeit, P. Achatz, C. Palfinger, M. Fassnauer, E. Schmid, W. Werthera, G. Hornerb ,QCM array for on-line-monitoring of composting procedures, *Analyst* 129 (2004) 432-437
- 52 J.C. Vickerman, I.S. Gilmore, *Surface analysis- The principal Techniques*, 2 Edition (2009)
- 53 T. Salthammer, Formaldehyde in the Ambient Atmosphere: From an Indoor Pollutant to an Outdoor Pollutant? *Angew Chem Int Ed* 52 (2013) 3320 – 3327

- 54 A. Duong, C. Steinmaus, C.M. McHale, C.P. Vaughan, L. Zhang, Reproductive and developmental toxicity of formaldehyde: A systematic review, *Mutation Research* 728 (2011) 118–138
- 55 E.E Bayramođlu, Hidden treasure of the nature: PAs. The effects of grape seeds on free formaldehyde of leather, *Ind Crop Prod* 41 (2013) 53– 56
- 56 G. Dhom, *Geschichte der Histopathologie*, Springer Wissenschaftsverlag, Heidelberg (2001) S. 744; W. Gerabek, B.D. Haage, G. Keil, W. Wegner, *Enzyklopädie Medizingeschichte*, W. de Gruyter, Berlin u. New York (2005) 410
- 57 J. Blum, Formaldehyd als Konservierungsmittel, *Zool Anz* 9 (1893) 229-231
- 58 Z. Que, T. Furuno, S. Katoh, Y. Nishino, Evaluation of three test methods in determination of formaldehyde emission from particleboard bonded with different mole ratio in the urea-formaldehyde resin, *Build Environ* 42 (2007) 1242–1249
- 59 J.Y. An, S. Kim, H.J. Kim, J. Seo, Emission behavior of formaldehyde and TVOC from engineered flooring in under heating and air circulation systems, *Build Environ* 45 (2010) 1826–1833
- 60 Z. He, Y. Zhang, W. Wei, Formaldehyde and VOC emissions at different manufacturing stages of wood-based panels, *Build Environ* 47 (2012) 197–204

- 61 M.Z.M Salem, M. Böhm, J. Srba, J. Beránková, Evaluation of formaldehyde emission from different types of wood-based panels and flooring materials using different standard test methods, *Build Environ* 49 (2012) 86–96
- 62 W.J. Kim, N. Terada, T. Nomura, R. Takahashi, S.D. Lee, J.H. Park, A. Konno, Effect on formaldehyde on the expression of adhesion molecule in nasal microvascular endothelial cells: The role of formaldehyde in the pathogenesis of sick building syndrome, *Clin Exp Allergy* 32 (2002) 287–295
- 63 R. Katakya, M.R. Bryce, L. Goldenberg, S. Hayes, A. Nowak, A biosensor for monitoring formaldehyde using a new lipophilic tetrathiafulvalene-tetracyanoquinodimethane salt and a polyurethane membrane, *Talanta* 56 (2002) 451–458
- 64 K. Kawamura, K. Kerman, M. Fujihara, N. Nagatani, T. Hashiba, E. Tamiya, Development of a novel hand-held formaldehyde gas sensor for the rapid detection of sick building syndrome, *Sens Actuators B Chem* 105 (2005) 495–501
- 65 P.R. Chung, C.T. Tzeng, M.T. Ke, C.Y. Lee, Formaldehyde Gas Sensors: A Review, *Sensors* 13 (2013) 4468-4484
- 66 M. Hussain, N. Iqbal, P.A. Lieberzeit, Acidic and basic polymers for molecularly imprinted folic acid sensors—QCM studies with thin films and nanoparticles, *Sens Actuators B* 176 (2013) 1090– 1095
- 67 S.Z. Bajwa, R. Dumler, P.A. Lieberzeit, Molecularly imprinted polymers for conductance sensing of Cu²⁺ in aqueous solutions, *Sens Actuators B* 192 (2014) 522-528

- 68 E. Mazzotta, R.A. Picca, C. Malitesta, S.A. Piletsky, E.V. Piletska, Development of a sensor prepared by entrapment of MIP particles in electrosynthesised polymer films for electrochemical detection of ephedrine, *J Biosens Bioelectron* 23 (2008) 1152–1156
- 69 F.J. Duan, *Formula of Traditional Chinese Medicine*, China Press of Traditional Chinese Medicine, Beijing (1999) 80–83
- 70 J. Palamar, How ephedrine escaped regulation in the United States: A historical review of misuse and associated policy, *Health Policy* 99 (2011) 1-9
- 71 N. Kurashima, Y. Makino, S. Sekita, Y. Urano, T. Nagano, Determination of Origin of Ephedrine Used as Precursor for Illicit Methamphetamine by Carbon and Nitrogen Stable Isotope Ratio Analysis, *Anal Chem* 76 (2004) 4233-4236
- 72 M.R. Wood R.A. Lalancette, Understanding the microcrystal tests of three related phenethylamines: the ortho-metallated (–)-amphetamine formed with gold(III) chloride, and the tetrachloridoaurate(III) salts of (+)-methamphetamine and (–)-ephedrine, *Acta Crystallographica C: Cryst Struct Comm* 69 (2013) 388-393
- 73 B.J. Ko, S. Suh, Y.J. Suh, M.K. In, S.H. Kim, J.H. Kim, (1S,2S)-1-Methylamino-1-phenyl-2-chloropropane: Route specific marker impurity of methamphetamine synthesized from ephedrine via chloroephedrine, *Forensic Sci Intl* 221 (2012) 92–97

- 74 S.Z. Bajwa, G. Mustafa, R. Samardzic, T. Wangchareansak, P.A. Lieberzeit, Nanostructured materials with biomimetic recognition abilities for chemical sensing, *Nanoscale Res Lett* 328 (2012) 7
- 75 H. Zhang, L. Ye, K. Mosbach, Non-covalent molecular imprinting with emphasis on its application in separation and drug development, *J Mol Recognit* 19 (2006) 248–259
- 76 K. Kotova, M. Hussain, G. Mustafa, P.A. Lieberzeit, MIP sensors on the way to biotech applications: Targeting selectivity, *Sens Actuators B: Chem* 189 (2013) 199-202
- 77 R.J. Ansell, D. Wang, J.K.L. Kuah, Imprinted polymers for chiral resolution of (\pm)-ephedrine. Part 2: probing pre-polymerisation equilibria in different solvents by NMR, *Analyst* 133 (2008) 1673-1683
- 78 P.A. Lieberzeit, A. Rehman, B. Najafi, F.L. Dickert, Real-life application of a QCM-based e-nose: quantitative characterization of different plant-degradation processes, *Anal Bioanal Chem* 391 (2008) 2897-2903
- 79 P.A. Lieberzeit, A. Adeel, G. Glanzing, F.L. Dickert, Molecularly imprinted sol-gel nanoparticles for mass-sensitive engine oil degradation sensing, *Anal Bioanal Chem* 389 (2007) 441–446
- 80 A. Findeisen, J. Wackerlig, R. Samardzic, J. Pitkänen, O. Anttalainen, F.L. Dickert, P.A. Lieberzeit, Artificial receptor layers for detecting chemical and biological agent mimics, *Sens Actuators B* 170 (2012) 196–200

Curriculum Vitae

Name: Kira Kotova

Date of Birth: 15th January, 1983

Education

PhD in Chemistry (ongoing since March 2010) Department of Analytical Chemistry, University of Vienna, Vienna, Austria

Master in Chemistry (Sep 2004-May 2006) Faculty of Chemistry, Saint Petersburg State University, Saint Petersburg, Russia.

Bachelor in Chemistry (Sep 2000-May 2004) Faculty of Chemistry, Saint Petersburg State University, Saint Petersburg, Russia

Secondary School (Sep 1989-June 2000) Smolensk Oblast, Russia

Publications and Conference Contributions

K. Kotova, M. Hussain, G. Mustafa, P.A. Lieberzeit, MIP sensors on the way to biotech applications: Targeting selectivity, **Sensors and Actuators B: Chemical** 189 (2013) 199-202

P.A. Lieberzeit, R. Samardzic, **K. Kotova**, M. Hussain, MIP sensors on the way to biotech applications: Targeting selectivity and ruggedness, *Procedia Engineering* 47 (2012) 534-537

Novel Nanostructured Sensor Materials for Pharmaceutically Active Compounds and Biospecies, P.A. Lieberzeit, M. Hussain, R. Samardzic, **K. Kotova**, N. Jongkon, 2nd Current Drug Development Conference CDD, Phuket, Thailand, May 2-4, 2012

Molecularly Imprinted Polymers for Ephedrine and Folic Acid: Thin Films vs. Nanoparticles, **K. Kotova**, M. Hussain, P.A. Lieberzeit, RSC Workshop "Biosensors- A Multidisciplinary Approach", Bangor, United Kingdom, June 26th, 2012

Nanopatterned Polymers for highly selective recognition of physiologically active compounds, M. Hussain, **K. Kotova**, G. Mustafa, P.A. Lieberzeit, XI International Conference on Nanostructured Materials. Phodos, Greece, August 26-31, 2012

MIP Sensors on the way to Biothech Application: selectivity and ruggedness, P.A. Lieberzeit, R. Samardzic, **K. Kotova**, M. Hussain, XXVI Eurosensors 2012, Krakow, Poland, September 9-12, 2012

Nanostructured materials and their composites: Novel materials for chemical sensing, **K. Kotova**, G. Mustafa, M. Zeilinger, P.A. Lieberzeit, The second International Congress on Advanced Materials (AM2013), Jiangsu University, Zhejiang, PR China, May 16-19, 2013

Professional Experience

2010-2013 Three years working experience in the laboratory as a tutor in Department of Analytical Chemistry, University of Vienna, Vienna, Austria